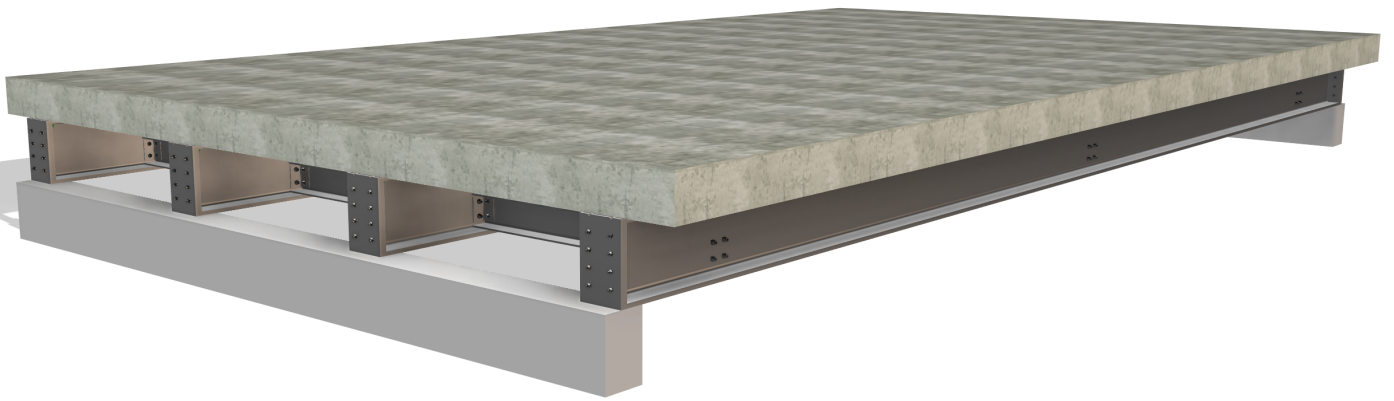


Pre-Design Assessment of Demountable Short Superstructures

Niels Buiting

Delft University of Technology



Pre-Design Assessment of Demountable Short Superstructures

by

Niels Buiting

in partial fulfilment of the requirements for the degree of

Master of Science
in Civil Engineering

at the Delft University of Technology,
to be defended publicly on March 1st, 2023 at 14:00.

Student Number:	4961706	
Project Duration:	Februari, 2022 - March, 2023	
Thesis Committee:	Prof.dr. M. Veljkovic	TU Delft, Chairman
	Dr. F. Kavoura	TU Delft
	Prof.dr. H. Jonkers	TU Delft
	Ir. A. Christoforidou	TU Delft
	Ir. N. Koeman	Dura Vermeer

An electronic version of this thesis is available at <http://repository.tudelft.nl/>

Preface

Ten years ago, I started with an HBO bachelor in Civil Engineering at Amsterdam University of Applied Sciences. Afterwards, I moved to Delft to start with the pre-master, which eventually led me to my final destination: a master's degree in Civil Engineering. Since my internship at the construction site of the Zandhazenbrug in 2016, my interest in steel structures has grown strongly, and from then on, I knew I wanted to design steel structures in my future career.

Firstly, I want to thank Dura Vermeer, where I was supervised by Ir. Nico Koeman. Together, the combination of circular principles with small superstructures was created and resulted in this research topic. I would like to express my gratitude towards Nico and all the other people at Dura Vermeer for their time, effort and knowledge. During the past year, I have enjoyed working on this topic and I have gained a lot of knowledge. For the steel part of my research, I would like to thank ASK Romein Hillebrand for all the good help. Because of the critical view and thinking out of the box, it helped me to improve the quality of the research.

In addition, I would like to thank Dr. F. Kavoura for being my daily supervisor. I could always come to her with my questions. I would like to express my appreciation for Prof.dr. M. Veljkovic for his professional guidance and critical view, helping me to improve the quality of the work. I need to thank Prof.dr. H. Jonkers, who advised, supervised and helped me with the environment part. Furthermore, I want to thank Ir. A. Christoforidou for helping with the research and answering my questions. Thank you for joining my board towards the end.

Finally, I want to thank my friends and family for their continuous support and care. My sister for reading the different sections of my report over and over, and special thanks go to my girlfriend. During my whole thesis, you've been by my side and kept me motivated until the finish line.

*Niels Buiting
Delft, February 2023*

Abstract

Rijkswaterstaat aims to build circularly from 2030 onward, with the purpose of having a fully circular economy by 2050. Therefore, the aim of this study is to design a reusable modular superstructure, with a small span, which can replace an existing so-called volstortligger superstructure. This is a structure that Dura Vermeer often uses and it regularly happens that these constructions are demolished after a lifespan of, for example, 10 years. This is a waste of materials and therefore an alternative will be investigated in this research. The following research question guides this study:

What is the optimal structure, in terms of shadow costs, mass and financial costs, for a modular superstructure?

In order to answer this question, a parametric study is performed using the software Grasshopper, using the Finite Element Model plug-in Karamba3D. In this way, quick structural analyses were performed, to explore multiple options. In total, more than 11.000 bridge design variants have been generated, divided over 12 different runs. The model allowed targeted optimization of shadow costs, weight and financial costs. Optimization is achieved by varying the following input parameters: number of steel girders, steel profile girders, outrigger deck, concrete deck thickness, concrete class, outrigger deck, FRP sandwich panel height, facing thickness, web thickness, and fibre volume.

In total, 6 different variants would be developed in this way, 3 with a concrete deck and 3 with an FRP deck. However, the optimization results in only 4 different variants, 3 with a concrete deck and just one with an FRP deck. The results show that the variant with the FRP deck is indicative for Shadow costs, Financial costs and weight.

After the four pre-designs had been developed, these variants were weighed against each other by means of a Trade-Off Matrix (TOM). Using this method, a distinction is made between the variants based on the pre-chosen performance indicators. All performance indicators have a weighting that adds up to a total of 100. The TOM results of all variants can be found in Table 1.

Table 1: Results TOM of all variants

Trade-Off Matrix						
Category	Performance indicator	Weight	V1	V2	V3	V4
Effective	Construction height	15	+	0	+	++
	Deflection	5	+	++	+	0
Shadow Costs		25	+	+	++	--
Demountability	Number of connections	15	++	++	+	--
	Complexity	10	-	-	-	+
Transportable	Weight	10	-	--	--	++
Costs		20	++	++	+	--
Total		100	73.75	68.75	68.75	35

This study concludes that it can be advantageous to replace the traditional design with a demountable design, with the assumed boundary conditions of this study. All developed variants have an advantage with regard to environmental impact and financial costs compared to the traditional design, assuming a lifespan of 100 years in which it is moved 10 times.

Contents

Preface	i
Abstract	ii
Nomenclature	vi
List of Figures	viii
List of Tables	xi
I Research framework	1
1 Introduction	2
1.1 Background & relevance	2
1.2 Research definition	2
1.2.1 Objectives	2
1.2.2 Research questions	3
1.2.3 Research Methodology	4
1.2.4 Assumptions & Limitations	5
1.3 Thesis structure	6
II Study Phase	7
2 Design space and requirements	8
2.1 Replacement task	8
2.2 Circular Design	8
2.2.1 Circularity	8
2.2.2 Definition and principles	9
2.2.3 Bridge Structure	10
2.2.4 Traditional Design	11
2.3 Design requirements	11
2.3.1 Loads	12
2.3.2 Norms and regulations	14
3 Design options	15
3.1 Typologies	15
3.1.1 Composite interaction	17
3.2 Materials	22
3.2.1 FRP Material	22
3.2.2 Steel	27
3.2.3 Concrete	27
3.3 Connections	28
3.3.1 Push-out procedure	28
3.3.2 Welded headed studs	29
3.3.3 Demountable Connections	30
4 Environmental impact	50
4.1 Shadow costs	50
4.1.1 Life Cycle Assessment	50
4.1.2 Environmental Impact Categories	52
4.1.3 Shadow costs construction materials	54

4.1.4	Boundary conditions of the expected lifespan estimation.	55
4.1.5	End-of-life materials	55
4.2	Design strategies	57
III	Circular design	58
5	Set-up of design of Bridge layout	59
5.1	Assembling process	59
5.1.1	Cost inputs	60
5.1.2	Sensitivity analysis	63
5.2	Maintenance	64
5.3	Damage during lifetime.	64
6	Structural parametric model	66
6.1	Definition of the parametric model.	66
6.1.1	Conceptual overview	67
6.1.2	FEM elements and analysis	68
6.1.3	Variant calculations	71
6.1.4	Model output	72
6.1.5	Detailed model overview	73
6.2	Model input	74
6.2.1	Steel.	74
6.2.2	Concrete	74
6.2.3	Fibre Reinforced Polymers	74
6.3	Design verification	74
7	Bridge design	75
7.1	Trade-off matrix	75
7.2	Variants	76
7.2.1	Variant 1	77
7.2.2	Variant 2	78
7.2.3	Variant 3	79
7.2.4	Variant 4	80
7.3	Life Cycle Assessment	81
7.3.1	LCA input	81
7.4	Cost analysis	82
7.5	Results	83
7.5.1	Environmental impact results	83
7.5.2	Costs results	85
7.5.3	Time to mould	89
7.6	Final design.	90
7.6.1	Result TOM	90
IV	Results and final remarks	91
8	Discussion	92
8.1	Discussion	92
8.1.1	Structural analysis	92
8.1.2	Weight.	92
8.1.3	Maintenance	93
8.1.4	ECl	93
9	Concluding remarks	94
9.1	Conclusion	94
9.1.1	Answer to the sub-questions.	94
9.1.2	Answer to the main research question	97
9.2	Recommendations for further research	98

References	102
A Hand calculations superstructure with concrete deck	103
A.1 Verification parametric model with concrete deck103
A.1.1 General data103
A.2 Analytical approach variant 2105
A.2.1 General data105
A.3 Deflection107
A.3.1 Deflection Self Weight107
A.3.2 Deflection Variable loads107
A.3.3 Total deflection109
A.4 Verification Structure109
A.4.1 Bending moment resistance109
A.4.2 Slip deformation111
A.5 Concrete Deck111
A.5.1 Concrete cover111
A.5.2 Main Reinforcement112
A.5.3 Shear reinforcement113
A.5.4 Crack width113
B FRP properties	116
B.1 Material properties116
B.1.1 Fibre properties116
B.2 Resin properties117
B.3 Core material properties117
B.3.1 UD-plyies118
B.3.2 Laminate theory119
B.4 Verification parametric model with FRP deck123
B.4.1 FRP material properties123
B.4.2 Effective bending stiffness124
B.4.3 Displacements125
C LCA	127
D Costs	131
E Trade-Off Matrix analysis	138
E.1 Structural analysis138
E.2 Trade-off matrix138
E.2.1 Explanation of scoring138

Nomenclature

Abbreviations

Abbreviation	Definition
ADP	Abiotic Depletion Potential
AP	Acidification Potential
CAD	Computer-Aided Design
CE	Circular Economy
CFCs	Chloro-Fluoro-Carbons
CO ₂	Carbon Dioxide
DDT	Dichlorodiphenyltrichloroethane
DfA	Design for Adaptability
DfD	Design for Disassembly
DfME	Design for Material Efficiency
ECI	Environmental Cost Indicator
EP	Eutrophication Potential
EPD	Environmental Product Declaration
FAETP	Freshwater Aquatic Eco-Toxicity Potential
FEA	Finite Element Analysis
FEM	Finite Element Modelling
FRP	Fibre-Reinforced Plastics
GFRP	Glass Fibre-Reinforced Plastics
GWP	Global Warming Potential
HCFCs	Hydro-Chloro-Fluoro-Carbons
HS	High Strength
HTP	Human Toxicity Potential
iSRR	injected Steel Reinforced Resin
LBDSC	Locking-Bolt Demountable Shear Connector
LCA	Life Cycle Assessment
LCI	Life Cycle Inventory
LM	Load Model
MAETP	Marine Aquatic Eco-Toxicity Potential
MCI	Material Circularity Indicator
MOE	Modulus Of Elasticity
NH ₄	Ammonium
N ₂ O	Nitrous Oxide
NO _x	Nitrogen Oxides
NMD	Nationale Milieu Database
O ₃	Ozone
ODP	Ozone Layer Depletion
P	Phosphorous
POCP	Photochemical Ozone Creation Potential
POPs	Persistent Organic Pollutants
POT	Push-Out Test
PUR	Polyurethaan
PVC	Polyvinylchloride
ROK	Richtlijnen Ontwerp Kunstwerken
SLS	Serviceability Limit State
SO ₂	Sulphur Dioxide

Abbreviation	Definition
SRR	Steel Reinforced Resin
TETP	Terrestrial Eco-Toxicity Potential
TOM	Trade-Off Matrix
TS	Tandem System
UD	Unidirectional
ULS	Ultimate Limit State
UV	Ultraviolet
VARTM	Vacuum Assisted Transfer Molding
VOCs	Volatile Organic Compounds

List of Figures

1.1	Diagram of methodology	4
1.2	Layout of the report	6
2.1	Circular Economy [40] [8]	9
2.2	Targets for a circular economy (adapted from [46])	9
2.3	Superstructure & Substructure (adapted from [24])	10
2.4	Superstructure (adapted from [76])	10
2.5	Traditional design volstortliggers	11
2.6	Load Model 1 according to NEN-EN 1991-2 [51]	12
2.7	Value of α_Q according NEN-EN 1991-2 [51]	13
2.8	Table 6.2 NEN-EN 1991-2 [51]	13
2.9	Lay-out Load Model 2 according to NEN-EN 1991-2 [51]	13
3.1	Optimal span length bridge types (adapted from [64])	15
3.2	Demountable bridges	16
3.3	Composite interaction (adapted from [44])	17
3.4	Interaction level a) Non-Composite b) Fully-Composite c) Partially-Composite [3]	18
3.5	First FRP bridge in Harlingen, the Netherlands (adapted from [72])	19
3.6	Friedberg Bridge	19
3.7	Cross sections of Friedberg bridge - design as pre-stressed concrete, steel composite and FRP superstructure (adapted from [35])	20
3.8	Types of deck	20
3.9	Processing methods	20
3.10	Illustration of effective width FRP decks (adapted from [77])	21
3.11	FRP Composite Graph (adapted from [25])	22
3.12	Lay up FRP (adapted from [56])	26
3.13	Push out test (adapted from [74])	28
3.14	Slip capacity push-out test (adapted from [53])	29
3.15	Welded stud (adapted from [53])	29
3.16	Load-slip curve - welded headed stud [19]	29
3.17	Assembling method demountable steel-concrete deck (adapted from [62])	30
3.18	Friction Grip Bolt connector (adapted from [32])	30
3.19	Load-slip curve - friction grip bolt connectors [36]	31
3.20	Load-slip curve - friction grip bolt connectors [38]	31
3.21	Without embedded nut connector (adapted from [32])	32
3.22	Load-slip curve - Without embedded nut connector [39]	32
3.23	Single embedded nut connector (adapted from [32])	33
3.24	Load-slip curve - Single embedded nut [61]	33
3.25	Double embedded nut (adapted from [32])	34
3.26	Load-slip curve - Double embedded nut [38]	34
3.27	Novel bolted connector (adapted from [32])	35
3.28	Load-slip curves Novel bolted connector [36]	35
3.29	Double-parameter fitting results of load-slip curves of each push-out test [75]	36
3.30	LBDSC Connector (adapted from [32])	37
3.31	Push-out test by Jun et al. [32]	37
3.32	Resin Injected Bolt (adapted from [69])	38
3.33	Air channel girder flange	38
3.34	Steel spheres (adapted from [54])	39
3.35	Load-slip curves [36]	39

3.36 Results of the push out tests [69]	40
3.37 Push-out tests Steel Reinforced Resin injected vs. Resin injected connection	40
3.38 Oversized holes	41
3.39 Ajax Connector (adapted from [11])	42
3.40 Load-slip curve Ajax Connector [11]	42
3.41 Installation of Ajax Connector (adapted from [11])	43
3.42 Lindapter Connector (adapted from [11])	43
3.43 Load-slip curve Lindapter Connector [11]	44
3.44 Installation of Lindapter Connector (adapted from [11])	44
3.45 Resin Injected Coupler Connector (adapted from [11])	45
3.46 Load-slip curve Resin Injected Coupler Connector [11]	45
3.47 Failure of different connectors in FRP (adapted from [11])	47
3.48 Graph Demountable FRP connectors	48
3.49 Relative stiffness decrease under cyclic loading [60]	49
4.1 The relationships between the three different levels (adapted from [12])	50
4.2 Stages in life cycle assessment according to EN15804 [49]	51
4.3 System overview reusable structure (adapted from [17])	52
4.4 Different kinds of End Of Life (adapted from [58])	55
4.5 Different alternatives for composite waste materials (adapted from [20])	56
4.6 All phases LCA (adapted from [37])	57
5.1 Connection between cross beam and girder beam	59
5.2 Construction method with threaded rods (adapted from [21])	59
5.3 Demountable iSRR Connector	60
5.4 Damage due to placing deck (adapted from [21])	64
6.1 Logo's of the used software for the design, analysis and optimization of the superstructure	66
6.2 Flowchart conceptual overview parametric model	67
6.3 FEM elements (adapted from [63])	68
6.4 Rhino spring component	69
6.5 Detail of spring element that connect steel beam to FRP deck in model	69
6.6 Top view of deck with corresponding girder beam	70
6.7 Overview Grasshopper Model	73
7.1 Variant 1	77
7.2 Variant 2	78
7.3 Overview variant 3	79
7.4 Overview variant 4	80
7.5 Shadow costs all variants over time	83
7.6 Distribution shadow costs all variants	84
7.7 Distribution costs all variants	86
7.7 Distribution costs all variants	87
7.8 Costs over lifetime all variants	88
7.9 Labour hours per design	89
9.1 Financial costs plotted over time	96
9.2 Shadow costs plotted over time	97
A.1 Rhino structure verification	103
A.2 Differential equation for composite interaction	104
A.3 Analytical deflection Concrete	105
A.4 Rhino deflection Concrete	105
A.5 Variant 2	106
A.6 Differential equation for composite interaction	108
A.7 Deflection SLS due to variable load	108
A.8 Deflection ULS	109

A.9	Moment distribution ULS	110
A.10	Normal force ULS	110
A.11	Slip deformation	111
B.1	Input online tool	120
B.2	ABD matrices tool facings	120
B.3	Input online tool	121
B.4	ABD matrices tool webs	122
B.5	FRP variant	123
B.6	Cross section of sandwich panel deck, with steel girder beam (Adapter from [70])	124
B.7	Displacement Rhino	126

List of Tables

1	Results TOM of all variants	ii
1.1	Score factors of TOM	5
2.1	Material Densities	12
3.1	Characteristic E-glass and High strength carbon material properties [2]	23
3.2	Characteristic resin material properties [2]	24
3.3	Characteristic core material properties [2]	25
3.4	Characteristic stiffness properties of UD-plyes with E-glass and polyester resin	25
3.5	Laminate properties facings	26
3.6	Laminate properties webs	26
3.7	Steel material properties [15]	27
3.8	Concrete material properties [14]	27
3.9	Initial Stiffness demountable connections	41
3.10	Results push-out tests according [11]	46
4.1	Shadow prices per environmental indicator [31]	54
4.2	Average ECI per structural material	54
5.1	Structural Material costs	60
5.2	Connector costs	61
5.3	Manufacturing costs prefab concrete deck	61
5.4	Assembling time	61
5.5	Telescopic crane costs	62
5.6	Transportation costs	62
6.1	Generate possibilities	71
6.2	Generate possibilities	72
6.3	Analytical verification FEM model	74
7.1	Weight factors of TOM	75
7.2	Criteria for TOM	76
7.3	Properties variant 1	77
7.4	Properties variant 2	78
7.5	Properties variant 3	79
7.6	Properties variant 3	80
7.7	Overview environmental costs per design	83
7.8	Overview financial costs traditional design	85
7.9	Overview costs per design	85
7.10	Overview costs Variant 2	88
7.11	Structural analysis results for variants	90
7.12	Results TOM of all variants	90
B.1	Characteristic E-glass and High strength carbon material properties [2]	117
B.2	Characteristic resin material properties [2]	117
B.3	Characteristic core material properties [2]	118
B.4	Characteristic stiffness properties of UD-plyes with E-glass and polyester resin	119
B.5	Laminate properties facings	121
B.6	Laminate properties webs	122

- C.1 Environmental impact values 128
- E.1 Structural analysis results for variants 138
- E.2 Score TOM on effective strategy: construction height 138
- E.3 Score TOM on effective strategy: deflection SLS 138
- E.4 Score TOM on shadow costs 138
- E.5 Score TOM on demountability strategy: number of connections 139
- E.6 Score TOM on demountability strategy: Complexity 139
- E.7 Score TOM on transportable strategy: weight 139
- E.8 Score TOM on costs 139



Research framework

1

Introduction

1.1. Background & relevance

Today's construction industry is the world's largest consumer of raw materials. The construction industry is still based on a linear way of consuming materials, which causes a large amount of waste, high greenhouse gas emissions and the depletion of finite resources. This has a negative impact on the environment, which has to change, and that is why the search for sustainable solutions is becoming more considerable. One good structural solution is switching to a circular economy where the entire structure can be re-used.

The Dutch government aims to have a total circular economy by 2050. All bridges must be built circular from 2030 onwards. Therefore, it is not surprising that the construction industry is one of the five industries on which the Dutch government focuses [48]. They state that circularity for construction through smart reuse not only yields cost savings, but also demands for new products and services. Hollberg & Ruth [29] say that the construction sector is responsible for 50% of all processed raw material consumption, 33% of greenhouse gas emissions and more than 40% of the world's primary energy demand, which together have a huge environmental impact.

Dura Vermeer's design department is also interested in the possibilities of reusing structures, which, together with opting for modular structures, could be a good way to achieve this. These modular constructions can be deconstructed after they have been used and rebuilt somewhere else. In this way, the entire structure is reused without wasting materials.

Composite bridges are advantageous structures when used in combination with a short span. The composite action obtained by shear connectors ensures efficient use of both materials. Composite designs generally have a rather high construction height-to-span ratio. Therefore this type of bridge can only be used up to a certain span.

1.2. Research definition

1.2.1. Objectives

During this Master's thesis, the main goal is to research how structures can be made more sustainable through a circular application. This thesis will focus on bridges with a span of around 12 meters and the width of two lanes. Dura Vermeer builds a large amount of this (relatively) simple type of bridge structure of which a certain amount is used for a temporary duration, for example, to span small canals during a temporary diversion. Normally, these structures are executed with prefab girders and partly in situ concrete, which is why they are demolished after use; a waste of materials. If the time span of the temporary bridge is very short, it is also possible to choose to rent a circular steel superstructure (Section 3.1). However, renting these bridges is very expensive and it is not feasible to use a rented bridge in the long term. Therefore, the assumption for this research is to develop a circular bridge which

will be moved once every 10 years. This type of bridge can be increasingly beneficial if it is reused somewhere else. Furthermore, Rijkswaterstaat also requires that all bridges built after 2030 must be modular so that they can be rebuilt after use. That is why this research will focus on these structures with the exception of the substructure.

Different ways of designing circular superstructures will be investigated during this research. The research will be performed on how the construction can be easily taken apart so that it can be rebuilt somewhere else. Firstly, the challenges of reusing bridge constructions must be investigated to achieve this. Furthermore, several modular variants from different materials (composite, FRP and steel) will be composed which will be parametrically optimized on shadow costs, mass and financial costs, to see whether a suitable design can be made for circular purposes. In this way, it is possible to properly investigate how a circular bridge structure design can be made.

1.2.2. Research questions

In this section, the main research question and sub-questions are defined.

1.2.2.1. Main research question

This study will answer the following main research question.

What is the optimal structure, in terms of shadow costs, mass and financial costs, for a modular superstructure?

1.2.2.2. Sub-questions

The main research question will be answered with the help of the sub-questions.

- What are the specific limitations and challenges of Steel, FRP and composite?
- What are the influential components during developing a demountable superstructure?
 - Connections
 - Weight
 - Time to mound and dismount
- What is the cost analysis per design?
- What is the environmental impact of the developed designs?
 - Which factors influence the quantification, and how can an objective comparison be obtained?
 - What is the total carbon footprint of the different designs?

1.2.3. Research Methodology

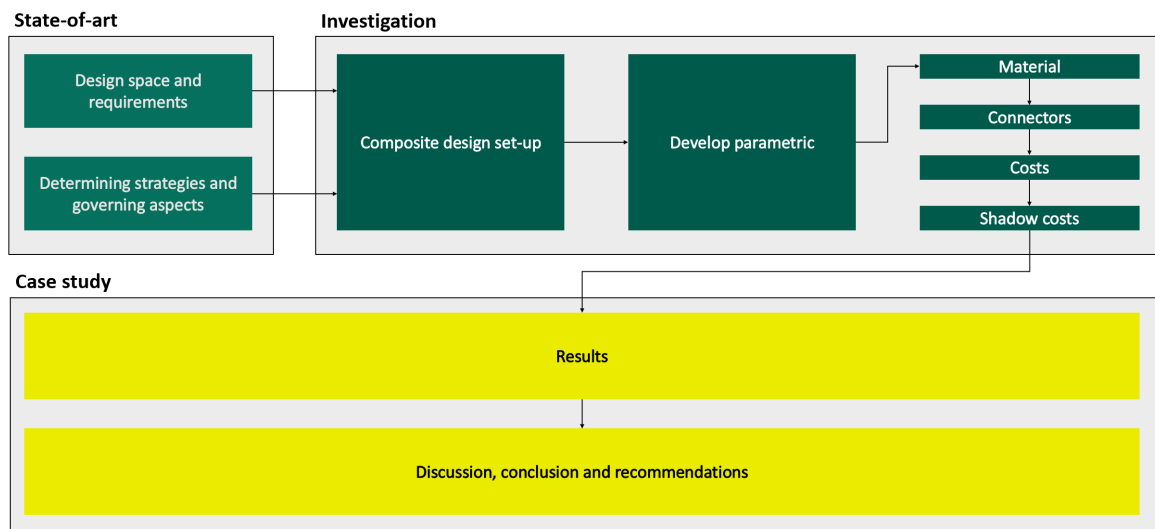


Figure 1.1: Diagram of methodology

In Figure 1.1, an overview of this research methodology is shown. As can be seen, the research is divided into three parts: study phase, circular design, and results. In the first phase, the study phase, a study is performed into the design space and the requirements that are set for the design. Furthermore, a literature research is performed into the steel-FRP & steel-concrete composite design options, de-mountable shear connectors and into the circular economy. This study phase results in the formulation of the design strategies.

In the second part, the bases for the modular system are derived, after which it is translated into a parametric model. A parametric model was chosen because it is widely applicable and increases the ease of considering the bridge in an early design stage. By using a parametric model, the geometry and choice of materials can be easily optimized. The model is developed in the Rhinoceros/Grasshopper environment, where Grasshopper provides visual programming to generate geometry and uses Rhino's viewport to display the geometry representation. Instead of programming by writing lines of text, components are connected to each other which sends data between the two. Within Grasshopper, many plug-ins exist. Karamba3D is one of these plug-ins. Karamba3D is a commercial parametric structural engineering plugin, which has a high calculation speed with accurate global results. Adding these Karamba-components for analysis to Grasshopper can perform Finite Element Modelling (FEM) analysis on models with, for example, bars, beams and shells. The obtained results of forces and deflections are verified by hand calculations.

By optimization in the parametric model, multiple variants will be developed. Optimization will happen based on the following results; costs, weight and shadow costs of the generated designs. The variants will be equipped with a concrete or FRP deck in combination with steel girder beams. When all variants are developed, the best-suited design is chosen using a trade-off matrix (TOM). This method can determine performance indicators with an associated weight for each design option. Table 1.1 presents the scores which are given to the performance indicators.

Table 1.1: Score factors of TOM

Score	Description	Value
++	Most favourable	1
+	Favourable	0.75
0	Neutral	0.5
-	Unfavourable	0.25
--	Negative	0

In the third and last part, when the final design is obtained, the parametrically generated design will be verified by hand calculations. Hereafter, the design will be compared with the traditional non-circular design obtained with Dura Vermeer's help. Furthermore, a discussion, conclusion and recommendations will also be drawn up in this part.

1.2.4. Assumptions & Limitations

Scope limitations are necessary due to the time frame of a Master's thesis. This section describes all limitations:

- Only the superstructure will be developed during this study. An assumption will be made for the entire foundation.
- Dynamic effects are out of the scope.
- The superstructure will have a free span of 12 metres and a width of 7 meters with 2 lanes.
- Life Cycle Costs (LCC) of the bridge are not included.
- Load cases for explosions, snow, thermal and wind are not taken into account.
- Fatigue load models (FLM1 to FLM 5) from NEN-EN 1991-2 [51] are not taken into account.

1.3. Thesis structure

The structure of this thesis report will be described in this section. Figure 1.2 presents the structure, and as can be seen, the report is divided into four different parts.

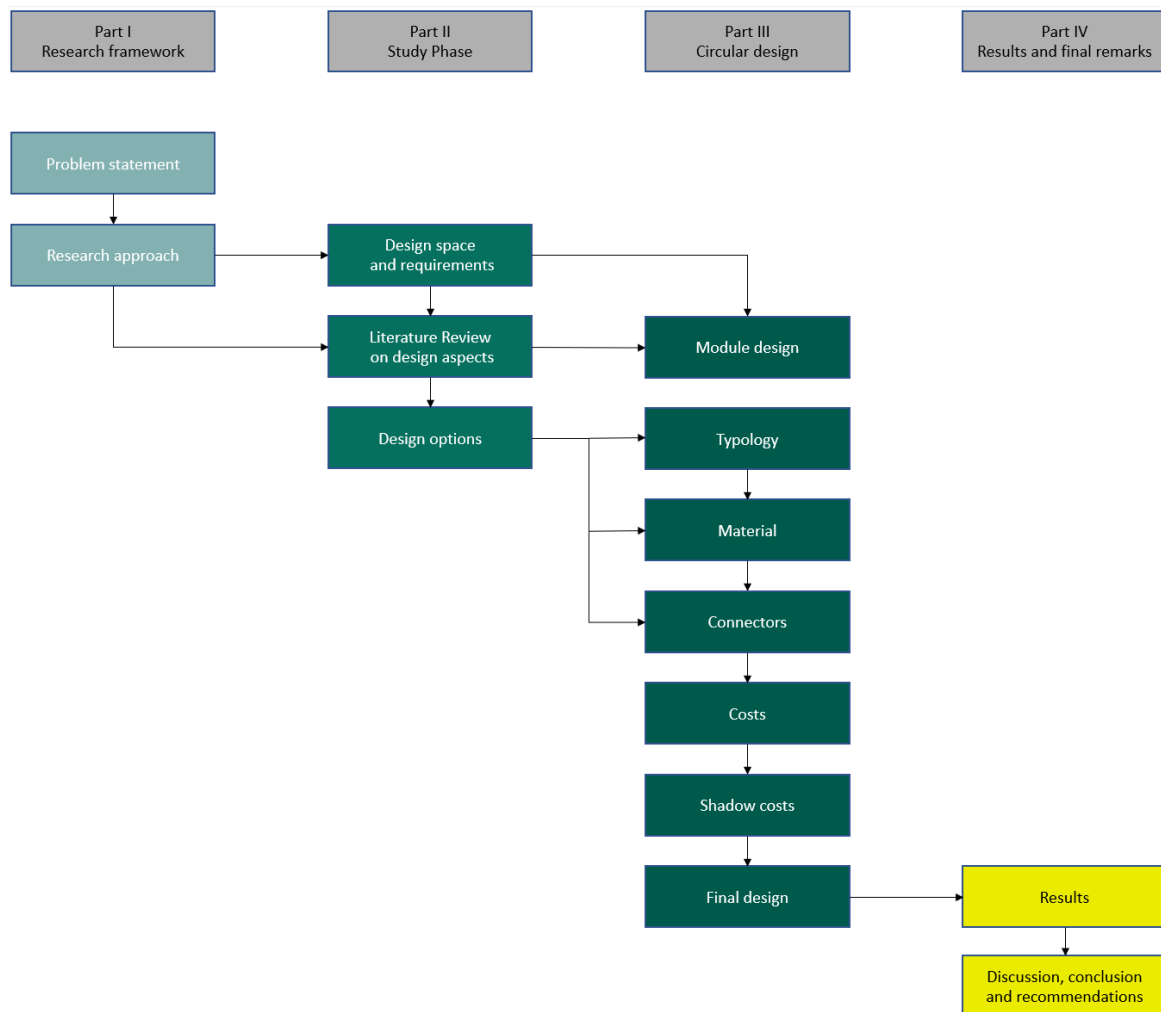


Figure 1.2: Layout of the report

In part I, the problem statement and research approach are drawn up. Following, part II studies the literature review, design aspects and options.

After all the literature has been studied and collected, part III describes the development of the circular design. First of all, a composite design is determined. After which a typology study is performed, the material and connector properties are added to the parametric model. The costs and shadow costs are connected to the variable parameters so that the design can be optimized for the final design.

Lastly, after all comparisons with the traditional design have been made, the research questions can be answered, and subsequently the discussion, conclusion, and recommendations are presented.



Study Phase

2

Design space and requirements

This chapter starts with describing the traditional design and context of the replacement task from Dura Vermeer, for which this demountable superstructure is made. Subsequently, the design requirements and boundary conditions are stated. Furthermore, an overview of the load conditions is given. Lastly, an overview of used norms and regulations is presented, which are used during this research.

2.1. Replacement task

On a yearly basis, Dura Vermeer builds a large number of bridges, most of which have a limited span (7 to 15 metres). These small spans are often carried out as cheaply as possible without any aesthetic value, and that is why Dura Vermeer regularly uses 'Volstortligger' superstructures. This traditional design will be further explained in Section 2.2.4. These types of structures partly consist of concrete poured in situ and are therefore not reusable. At the end of life, the entire construction will therefore have to be demolished without elements being able to be reused. This is a waste of materials; therefore, this study will investigate whether it is possible to apply a circular design.

When a span is required for a very limited time (1-3 years) there is the option to rent temporary steel bridge structures, see Section 3.1. These structures are completely modular and are often used by Dura Vermeer as a temporary construction. It may happen that a span of the above length is required for a life span of for example 3 to 15 years. In this case, the non-reusable structure is chosen because renting a temporary construction for a longer period is not profitable. That is why this research will focus on designing a reusable structure with a temporary lifespan of 10 years.

2.2. Circular Design

2.2.1. Circularity

Nowadays the construction industry is still dominated by linear processes economies. This causes a large amount of waste, high greenhouse gas emissions, and depletion of finite resources, which all have a negative impact on the environment [40]. Due to these adverse effects of linear processes, change in the construction sector is required. The construction sector has been focusing on recycling for several decades. However, as can be seen in figure 2.1, this reuse economy still produces a certain amount of non-recyclable waste. In a circular economy, all material will be reused and no waste will be created. The Dutch government aims to have a total circular economy by 2050. All bridges must be built circular from 2030 onwards. Therefore it is not surprising that the construction industry is one of the five industries on which the Dutch government focuses [48]. They state that circularity for construction through smart reuse not only saves costs, but also demands new products and services. Hollberg & Ruth [29] say that the construction sector is responsible for 50% of all processed raw material consumption, 33% of greenhouse gas emissions and more than 40% of the world's primary energy demand, which together have a huge environmental impact.

The main focus of a circular economy is the optimal use of energy and materials: reduce, reuse, and recycle. In this economy, products should be designed for reuse and recycling of associated material with focus on eco-effectiveness [13].

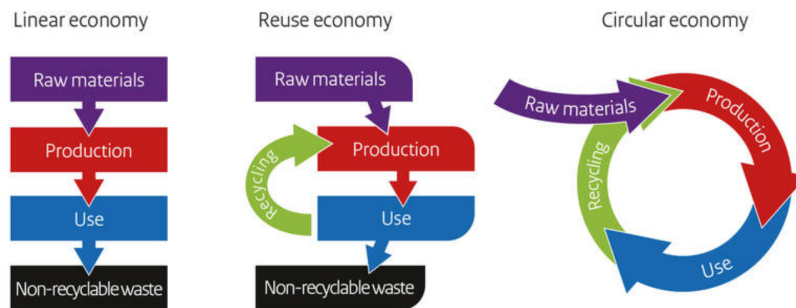


Figure 2.1: Circular Economy [40] [8])

2.2.2. Definition and principles

There are multiple conceptual frameworks that explain the circular economy (CE) with which the circular design strategy can be determined. These circular frameworks can be used as an indication for circular design strategies. One of these circular frameworks is the 10R-model [34], see figure 2.2. This 10R-model consists of 10 circular design strategies (levels) which are based on their impact on reducing the consumption of resources and the production of waste. The highest levels consume fewer resources and produce less waste leading to a lower environmental impact [65]. All strategies are presented in distinct subsections. Morseletto [46] states that because of stimulation of circularity, implementation of circularity must start as soon as possible, the strategies associated with the design of a structure are the most favourable. Because this research mainly focuses on the design phase, the focus is on strategies R1, R2 & R3: Rethink, Reduce & Reuse. Due to the bridge structure can be used for multiple purposes. The design will be done efficiently and the structure will be designed in such a way that it can be reused.

Smarter product use and manufacture	R0	Refuse	Make product redundant by abandoning its function or by offering the same function with a radically different product
	R1	Rethink	Make product use more intensive (e.g. through sharing products or by putting multi-functional products on market).
	R2	Reduce	Increase efficiency in product manufacture or use by consuming fewer natural resources
Extend lifespan of product and its parts	R3	Reuse	Re-use by another consumer of discarded product which is still in good condition and fulfils its original function
	R4	Repair	Repair and maintenance of defective product so it can be used with its original function
	R5	Refurbish	Restore an old product and bring it up to date
	R6	Remanufacture	Use parts of discarded product in a new product with the same function
	R7	Repurpose	Use discarded products or its part in a new product with a different function
Useful application of materials	R8	Recycle	Process materials to obtain the same (high grade) or lower (low grade) quality
	R9	Recovery	Incineration of material with energy recovery

Figure 2.2: Targets for a circular economy (adapted from [46])

2.2.3. Bridge Structure

During this thesis, research will only be done on the superstructure. A bridge can be divided into two different principal components: the superstructure and the substructure. As shown in Figure 2.3, the superstructure consists of the structure above the bearings, and the substructure includes all the parts below. The superstructure can be divided into the main deck and the longitudinal girder system below the deck, see Figure 2.4.

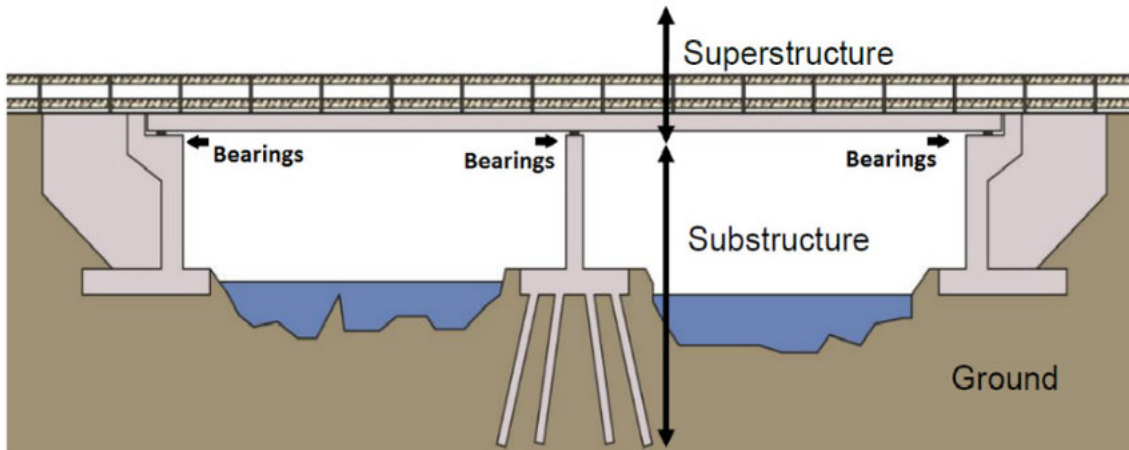


Figure 2.3: Superstructure & Substructure (adapted from [24])

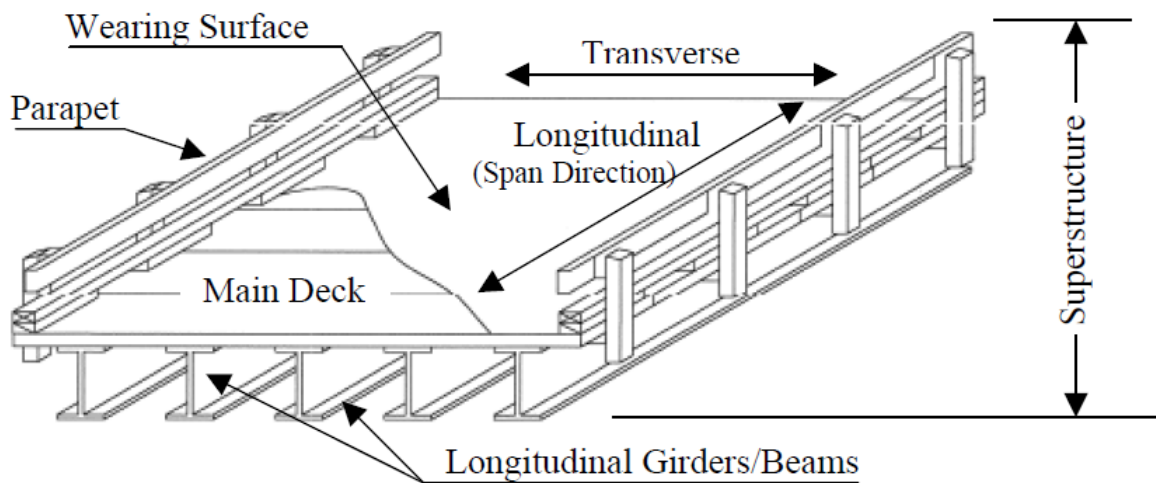


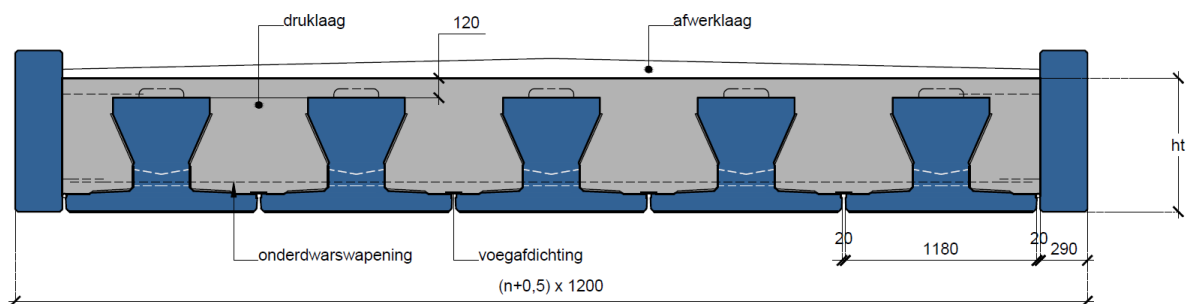
Figure 2.4: Superstructure (adapted from [76])

2.2.4. Traditional Design

Normally Dura Vermeer uses so-called 'volstortliggers' to bridge a comparable span. These volstortliggers consist in part of prefab concrete and pouring in-situ concrete resulting in the most economical solution. Furthermore, because it benefits from all advantages of precast concrete, such as casting and reinforcement, it also saves a lot of time. Therefore, it is by far the most popular beam in the Netherlands in civil-engineering projects [23]. Figure 2.5 shows how the separate volstortliggers are placed against each other, after which they are filled using in-situ concrete



(a) Picture of prefab part of volstortliggers [28]



(b) schematization volstortliggers [10]

Figure 2.5: Traditional design volstortliggers

Pre-cast girder elements are available with a length of 6 to 15 metres, in combination with a respective element height of 300 to 550 mm, to be able to apply in combination with the traffic load models according to NEN-EN 1991-2 [51] [16]. As shown in Figure 2.5b, a finishing layer of 120 mm is applied on top of the girder elements. This causes this type of superstructure to have a construction height-to-span ratio of about $\frac{1}{14}$ until $\frac{1}{22}$. When designing this superstructure a ratio of $\frac{1}{15}$ is retained as a design requirement.

2.3. Design requirements

- The free span of the bridge is 12 metres.
- The bridge is designed with a width of 7 meters with 2 lanes of 3 metres.
- To increase the number of possibilities of the bridge, it must be possible to connect the bridge to other superstructures.
- The maximum construction-height-to-span ratio is 1/15
- The design life of the superstructure is 100 years

2.3.1. Loads

The relevant loads of the bridge structure are: dead load and traffic load. Wind, temperature and collision loads are not considered in this study. The loads will be assessed on the parametric model, including the safety factors for permanent and variable loads as prescribed in the Eurocode 1990 [50].

2.3.1.1. Dead load

The self-weight of the structure is determined by the material use. Table 2.1 displays all densities of the used materials, which are obtained from Section 3.2.1.1.5, 3.2.2 & 3.2.3.

Table 2.1: Material Densities

Material	Density [kg/m ³]
Steel	7850
Concrete	2500
FRP	V40 1748
	V50 1885
	V60 2022
	V70 2159

2.3.1.2. Traffic load

2.3.1.2.1 Load Model 1 (LM1)

According to NEN-EN 1991-2 [51], the traffic Load Model (LM) 1 depends on the width of the road and the number of vehicles per year. The width of the road influences the number of lanes that should be considered. A single lane has a width of three meters, so two lanes fit on a seven-meter-wide bridge, resulting in a remaining area of 1 meter.

As shown in Figure 2.6, LM1 is divided into a so-called tandem system (TS) consisting of double-axis concentrated loads and a uniformly distributed load. Each wheel's contact surface should be considered as a rectangle of sides 0.40 m and 0.40 m.

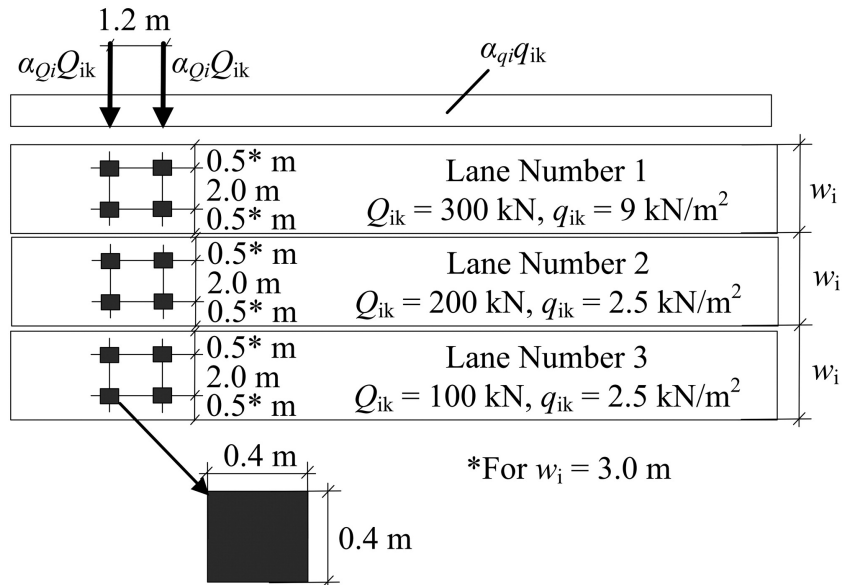


Figure 2.6: Load Model 1 according to NEN-EN 1991-2 [51]

Each load is multiplied by the adjustment factors α_Q , which depend on the number of heavy vehicles per year and the length of the superstructure. The values of α_Q according to NEN-EN 1991-2 [51] are presented in Figure 2.7. During this research, the value of $\alpha_Q = 1.0$, as the maximum amount of heavy traffic is assumed.

Tabel NB.1 — Correctiefactoren α_{Q1} , α_{q1} en α_{qr}

Aantal vrachtwagens per jaar per rijstrook voor zwaar verkeer N_{obs} ^a	α_{Q1} en α_{q1}				α_{qr}
	Lengte van de overspanning of invloedslengte (L)				
	20 m	50 m	100 m	≥ 200 m	
$\geq 2\,000\,000$	1,0	1,0	1,0	1,0	
200 000	0,97	0,97	0,95	0,95	0,90
20 000	0,95	0,94	0,89	0,88	0,80
2 000	0,91	0,91	0,82	0,81	0,70
200	0,88	0,87	0,75	0,74	0,60

^a Tussengelegen waarden mogen worden geïnterpoleerd.

Figure 2.7: Value of α_Q according NEN-EN 1991-2 [51]

Location	Tandem system <i>TS</i> Axle loads Q_{ik} (kN)	<i>UDL</i> system q_{ik} (or q_{rk}) (kN/m ²)
Lane Number 1	300	9
Lane Number 2	200	2,5
Lane Number 3	100	2,5
Other lanes	0	2,5
Remaining area (q_{rk})	0	2,5

Figure 2.8: Table 6.2 NEN-EN 1991-2 [51]

2.3.1.2.2 Load Model 2 (LM2)

The second Load model (LM2) consists of an axle load of 400 kN. LM2 can be applied at any location on the carriageway and the contact surface of each wheel consists of a rectangle of sides 0.35 m and 0.60, as pictured in Figure 2.9.

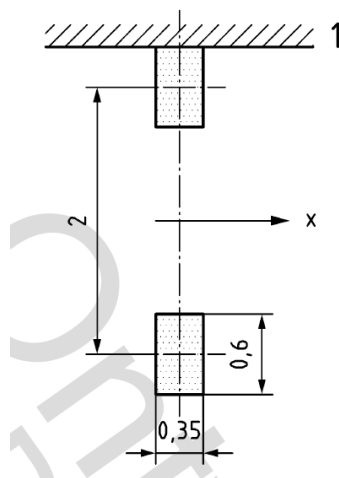


Figure 2.9: Lay-out Load Model 2 according to NEN-EN 1991-2 [51]

2.3.1.2.3 Load Model 3 (LM3)

Traffic load model 3 should be defined as the load of special vehicles and will not be taken into account in this research.

2.3.1.2.4 Load Model 4 (LM4)

Load model 4 simulates a crowd loading during, for example, evacuation or busy events such as a marathon. In this load case a uniformly distributed load of 5 kN/m^2 is applied over the entire bridge deck.

2.3.2. Norms and regulations

Existing standards and regulations must be used to verify the structural requirements of a demountable bridge. In Europe, these regulations come from the Eurocode. However, the Dutch recommendation CUR is also used. Because FRP is a relatively new material in civil engineering, no Eurocode exists yet. Furthermore, there are, other than the Eurocode and the CUR, additions or alterations to the Eurocode. The Netherlands uses the national annex to the Eurocode (NEN-NB) and the (Richtlijnen Ontwerp Kunstwerken) ROK (design guidelines for civil engineering works). The Dutch government published the ROK; the leading document for civil engineering works in the Netherlands.

The following rules and regulations are used to conduct thorough research and to achieve a demountable design:

- EN1990 → Basis of structural design
- EN1991 → Actions on structures
 - Part 1-1 → General actions
 - Part 1-5 → Thermal actions
 - Part 2 → Traffic loads on bridges
- EN1992 → Design of Concrete structures
 - Part 1 → Concrete buildings
 - Part 2 → Concrete bridges
- EN1993 → Design of steel structures
 - Part 2 → Steel bridges
- EN1994 → Design of composite steel and concrete structures
 - Part 2 → Composite steel and concrete bridges
- CUR 96 (Dutch) → FRP in structural and civil engineering structures
- ROK (Dutch) → Design guidelines for civil engineering works

3

Design options

This chapter describes the design options for the superstructure that will be developed in this study. First, the type of superstructure has been explained, and existing structures are described. Secondly, the materials used in this study are explained with all properties. Lastly, research has been done into the demountable connectors that are suitable for use in this study.

3.1. Typologies

Figure 3.1 presents the bridge typologies including their optimal span lengths. As can be seen, simple concrete girder or slab spans are the most optimal types for a span of 12 meters. However, as mentioned before, concrete bridges are difficult to design demountable, and therefore less suitable as an opportunity to replace traditional design.

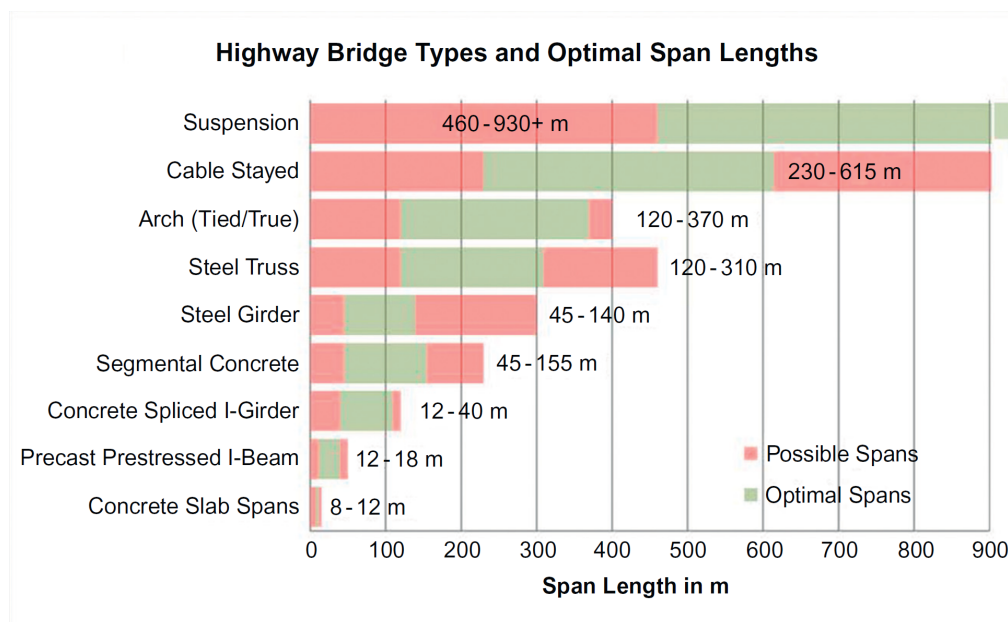


Figure 3.1: Optimal span length bridge types (adapted from [64])

As can be seen in Figure 3.1, the most optimal span for steel girder bridges is between 45 and 145 meter, this is due to steel structures being lighter than concrete structures and therefore more suitable for larger spans. However, steel structures have a higher financial cost than concrete structures, so

concrete spans are more suitable within their span limit [64].

When Dura Vermeer needs temporary superstructures, there are possibilities to rent them for a period. Two examples of demountable bridges are Janson Bridging (Figure 3.2a) or Retro Bridge (Figure 3.2b). These bridges consist entirely of steel elements and are based on standard dimensions of the elements [30]. For example, the superstructures can easily be adjusted in length and width. With these two examples, a free span of more than 30 meters can be achieved, making it an extremely suitable option for temporary construction. However, renting these bridges is very expensive. Especially because at Dura Vermeer it happens that a bridge only needed is for a period of 10 years and for cases like this, despite the wasting of material, it is more economically beneficial to opt for a non-circular bridge consisting of concrete girders.



(a) Example Janson Bridging (adapted from [30])



(b) Example Retro Bridge (adapted from [67])

Figure 3.2: Demountable bridges

Since demountable steel bridges already exist and demountable concrete bridges are difficult to design in situ, it will be investigated during this study whether it is possible to come up with a replacement pre-design that will consist of a composite bridge.

3.1.1. Composite interaction

Composite structures are composed of several parts connected to each other to exhibit a composite effect. The composite elements in this research consist of a concrete or FRP deck with steel beams underneath. In this combination, the concrete slab is activated by compression and the steel beam in tension stress, which are the most favourable properties of the materials. Therefore, the structures can be reduced to relatively slender, resulting in a material and weight reduction. Traditionally, the composite action is created with shear connectors welded onto the steel beam's top flange. In this way, the two different components work together as one structure in which the shear connectors transfer all transverse forces.

Since this thesis focuses on a demountable design, the applied shear connections cannot be welded on the upper flange of the steel beam and have to be connected by a demountable connection. Therefore, in Section 3.3.3, alternatives are described, which ensure that the entire design can be taken apart.

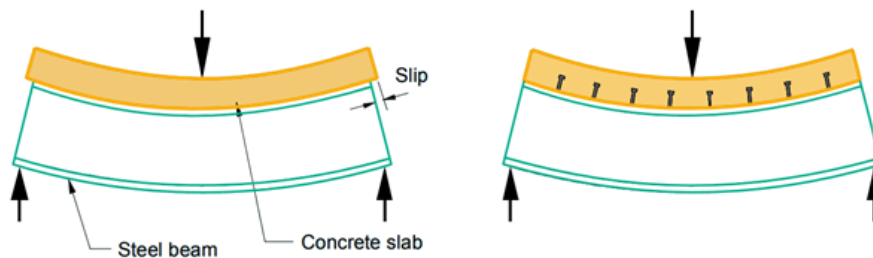


Figure 3.3: Composite interaction (adapted from [44])

3.1.1.1. Theoretical background shear interaction

Composite bridges can have three different interaction stages: Fully-composite, Partially-composite and Non-composite (See Figure 3.4). These terminologies are used to indicate the extent to which the steel girders interact with the deck above.

3.1.1.1.1 Non-Composite behaviour

A girder is defined to be non-composite when both the steel girder and deck bend separately. No shear force is transferred from the deck to the steel girder, which is why the slip displacement between the steel and the deck will be relatively large. In reality, a non-composite interaction is almost impossible because some shear force is always transferred due to friction.

3.1.1.1.2 Fully-Composite behaviour

As can be seen in Figure 3.4, a girder is in fully-composite behaviour when the full plastic flexural capacity of the composite section is developed. Sufficient shear connectors must be present to achieve this, resulting in a small deformation and negligible amount of slip under service loads.

3.1.1.1.3 Partially-Composite behaviour

In Partially-Composite behaviour, the flexural strength of the girder is governed by the strength of the shear connectors. An important difference between partially and fully shear interaction is the slip. In partial interacting girders, the slip is significant under service loads. Therefore, the slip needs to be considered in the design and certainly in a demountable design since the slip must be prevented from entering the plastic region and causing permanent deformations. For partially-Composite girders, the composite ratio is defined by $\frac{N}{N_f}$, where N is the number of used shear connectors and N_f is the number

of shear connectors required for full shear interaction. A value of 1 means that the girder behaves fully composite.

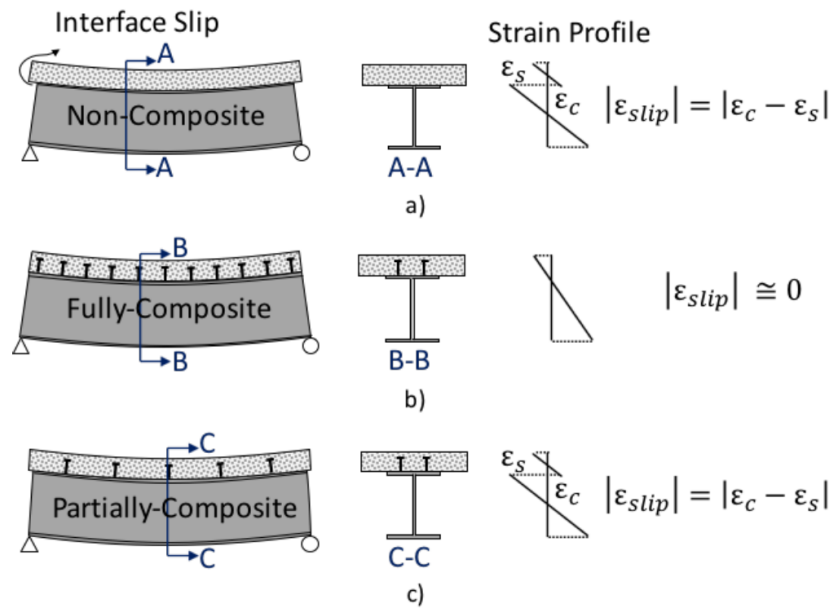


Figure 3.4: Interaction level a) Non-Composite b) Fully-Composite c) Partially-Composite [3]

The formulas below (Equations 3.1 to 3.6) clearly describe the advantages of fully interactive behaviour over non-interactive behaviour. Assuming the deck and the steel girder are two rectangular blocks with the same dimensions and material. When it comes to stiffness, a beam with full shear interaction results in 2 times higher resistance compared to a beam (with the same height) with non-composite behaviour:

$$W_{\text{non-interaction}} = 2 \cdot \left(\frac{1}{6}bh^2 \right) = \frac{1}{3}bh^2 \quad (3.1)$$

$$W_{\text{fully-interaction}} = \frac{1}{6} \cdot b(2h)^2 = \frac{2}{3}bh^2 \quad (3.2)$$

$$\frac{W_{\text{fully-interaction}}}{W_{\text{non-interaction}}} = 2 \quad (3.3)$$

When it comes to stiffness, a beam with fully shear interaction has 4 times higher stiffness:

$$I_{\text{non-interaction}} = 2 \cdot \left(\frac{1}{12}bh^3 \right) = \frac{1}{6}bh^3 \quad (3.4)$$

$$I_{\text{fully-interaction}} = \frac{1}{12} \cdot b(2h)^3 = \frac{2}{3}bh^3 \quad (3.5)$$

$$\frac{I_{\text{fully-interaction}}}{I_{\text{non-interaction}}} = 4 \quad (3.6)$$

Between these two theoretical situations lies the partial shear connection, which reflects the actual behaviour of composite beams.

3.1.1.1.4 FRP deck

Worldwide the number of FRP composites in bridge design has been increasing since the first FRP footbridge was built in 1995 in the Netherlands, see Figure 3.5 [72]. After expanding pedestrian bridges to bicycle bridges, FRP became a worthwhile competitor to traditional materials, even for road traffic bridges. Figure 3.6 shows a Steel-FRP composite road traffic bridge with a free span of 21.5 meters [35].

Due to the high strength-to-weight ratio, FRP decks are excellent to use during the construction of new bridges and the renovation of existing bridges. They result in lightweight FRP decks which can be rapidly installed [18]. This saves costs and improves work-zone safety. Furthermore, an FRP deck protects the steel girder/beam system below the deck against environmental effects such as rain and frost [7]. FRP has a high environmental resistance and low future maintenance requirements, this reduces inspection and repair costs [66].



Figure 3.5: First FRP bridge in Harlingen, the Netherlands (adapted from [72])



(a) Cross section Friedberg bridge (adapted from [35])



(b) Picture of friedberg bridge (photo made by Jan Knippers)

Figure 3.6: Friedberg Bridge

Figure 3.7 compares three superstructures suitable to the same span and loading conditions. As can be seen, the structure height between all variants is similar. The pre-stressed concrete bridge has a dead load of approximately 84 kN/m, for the steel-concrete composite superstructure this is 62 kN/m. On the other hand, the Steel-FRP variant has a dead load of 14 kN/m which is considerably less than the other designs [35]. This makes it very interesting to research the possibilities of an FRP deck during this master thesis. Because the entire bridge has to be transportable, it is an enormous advantage that an FRP deck drastically reduces the dead loads.

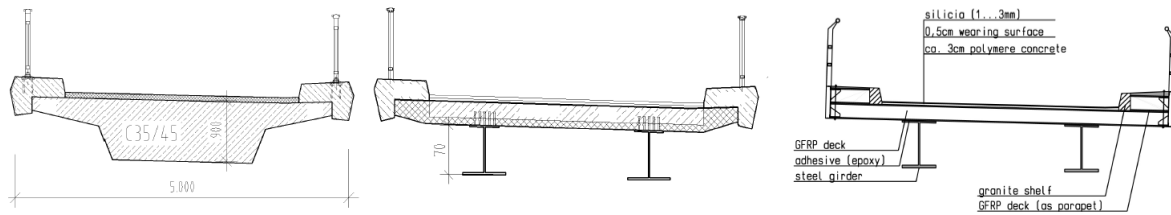
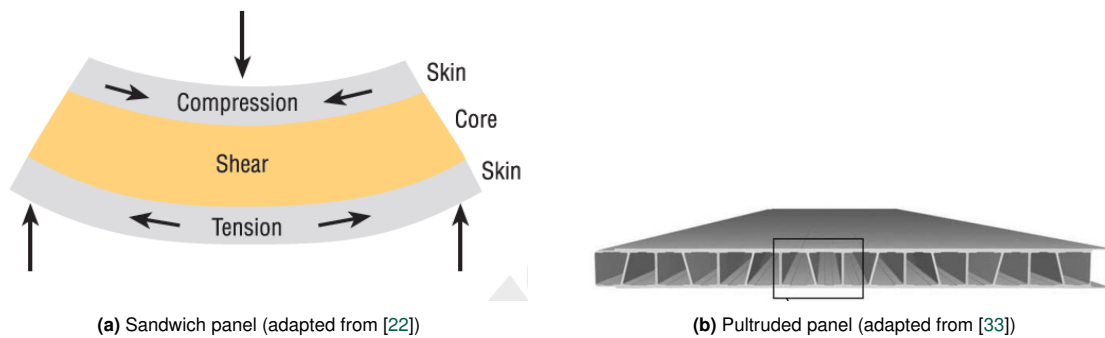


Figure 3.7: Cross sections of Friedberg bridge - design as pre-stressed concrete, steel composite and FRP superstructure (adapted from [35])

FRP Panels

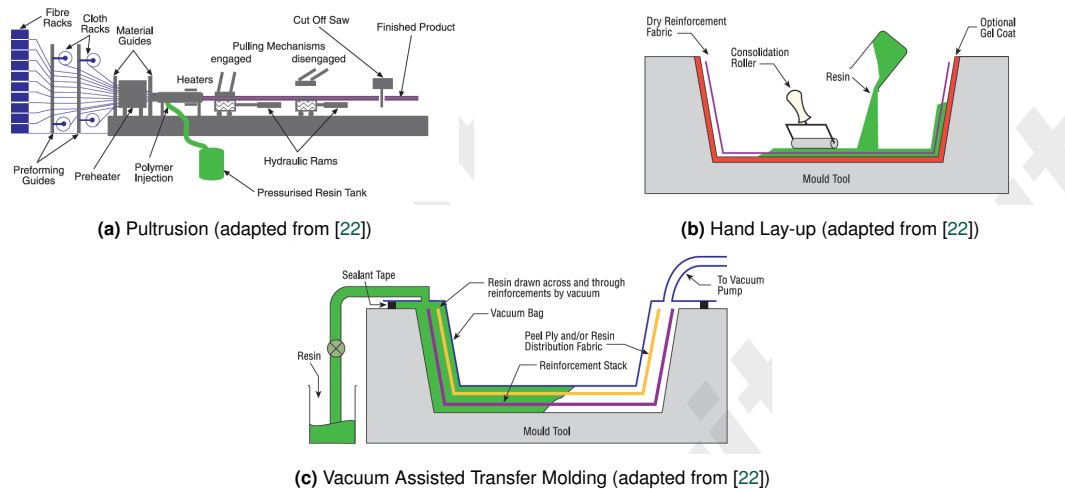
When choosing an FRP deck, there are multiple types of panels. Some commonly used decks are made of sandwich panels (Figure 3.8a) and pultruded panels (Figure 3.8b). Pultruded panels are created through pultrusion (Figure 3.9a), in which the reinforcement materials are impregnated by the resin and are pulled through a heated mould with the shape of the profile cross-section. In this way, an infinitely long profile can be created. Sandwich panels are usually made by Vacuum Assisted Transfer Molding (VARTM) (Figure 3.9c) or the manual hand lay-up method (Figure 3.9b). This last method is very labour-intensive and is only used in small production amounts. When using the VARTM method, the fibres and resin flow through an airtight mould. It is a relatively simple process, moreover the quality of products is good and large products can be made in large quantities. Furthermore, sandwich panels have greater flexibility in cross-section than pultruded decks and can be formed in large deck sections.



(a) Sandwich panel (adapted from [22])

(b) Pultruded panel (adapted from [33])

Figure 3.8: Types of deck



(a) Pultrusion (adapted from [22])

(b) Hand Lay-up (adapted from [22])

(c) Vacuum Assisted Transfer Molding (adapted from [22])

Figure 3.9: Processing methods

3.1.1.1.5 Effective width

The in-plane shear strain in the deck of a composite section under bending results in longitudinal displacements in the slab remote from the steel web to lag behind near the web [41]. The effect that occurs here is the so-called shear lag effect and is referred in design guidelines as the effective width. As can be seen in figure 3.10, the distribution of elastic bending stresses peaks at the location of connection between the deck and the steel girder beam. The elastic bending stresses decrease with distance from the connection.

Moses et al. [47] states that the effective width of GFRP decks are approximately 75-80% of that of a comparable concrete deck, depending on the capacity of the shear connection. This is because FRP has a lower stiffness in longitudinal direction compared to concrete.

The mathematical expression of the effective width has been established using the following definition:

$$b_e = \frac{1}{\sigma_{max}} \cdot \int_{-b/2}^{b/2} \sigma_x dy$$

Where:

σ_{max} is the highest longitudinal normal stress at the girder-deck function

σ_x is the longitudinal stress distribution along the width (b) of the corresponding deck panel (See Figure 3.10).

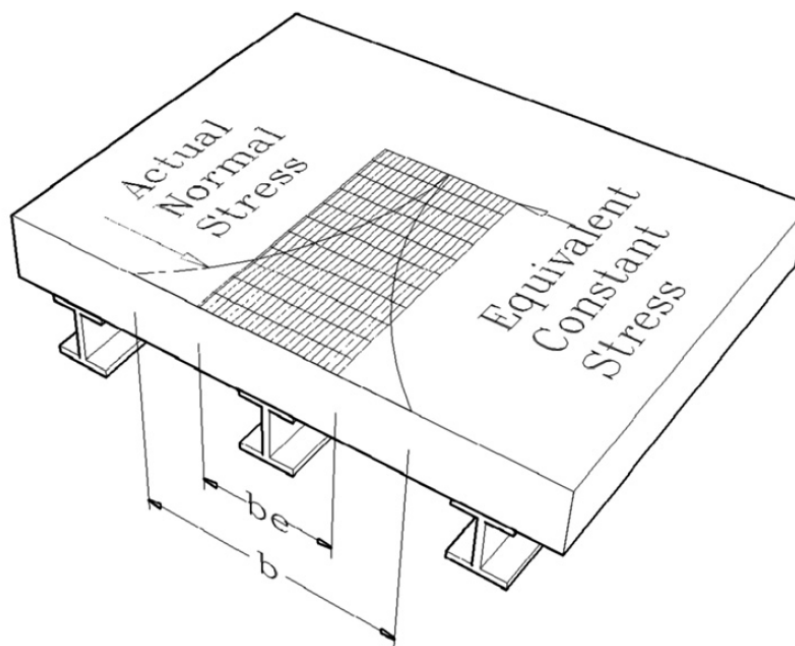


Figure 3.10: Illustration of effective width FRP decks (adapted from [77])

3.2. Materials

In this section all material properties of the materials used in this study are described.

3.2.1. FRP Material

As described in Section 3.1.1, composite structures are composed of several parts connected to each other to exhibit a composite effect. This section describes all properties of the FRP material that the sandwich panel consists of.

3.2.1.1. Material properties

Fibre reinforced polymer composite consists of two main components: resin and fibres. Due to these two components, numerous FRP variations can be composed with all different properties. These variations differ in the ratio of fibres to resin, geometry, and adhesion between the two constituents of the orientation of the fibres [56].

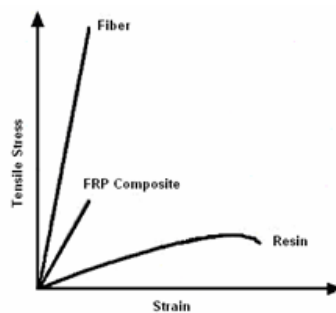


Figure 3.11: FRP Composite Graph (adapted from [25])

As shown in Figure 3.11, both components have different stress properties and differ significantly in strength. The fibres have high tensile strength and the resin has a high strain. By combining these different properties, a strong material can be created. Because the high strength of the fibres is only in the longitudinal direction and the strength in the transverse direction is much lower, the strength and stiffness of the FRP material depends on how the fibres are oriented. As a result, FRP elements can be made up of laminates, consisting of multiple layers with fibres in different directions. With this lay-up, a quasi-isotropic material can be created in which the laminates are often designed in a symmetrical order, see Figure 3.12. In this way, torsion due to in-plane stresses is prevented, and the lay-up ensures that normal forces occur solely due to strains and moments forces occur solely due to curvature (See appendix B). The resin in the material acts as a matrix between the fibres. It transfers the loads and determines the geometry of the structure. The resin also prevents buckling of the fibres as it gives a specific resistance against compression to the FRP.

3.2.1.1.1 Fibre properties

The most commonly used fibres in FRP structures are carbon and glass fibres. Carbon fibres generally have better properties (see Table 3.1), higher ultimate tensile strength and stiffness, and better fatigue resistance. However, carbon fibres are 4 [56] times more expensive than glass fibres, explaining why glass fibres are often chosen over carbon fibres in the construction sector. Carbon fibre materials are preferred in the aerospace or nautical engineering industry where weight is of significant influence.

In the construction world, E-glass and R-glass fibres are used. The most common type of glass fibre are the E-glass fibres, which is why only these characteristics are displayed in table 3.1 [2]. The table also shows the characteristics of High Strength (HS) carbon fibre to demonstrate the properties of glass and carbon fibres. However, as mentioned before, carbon fibres are hardly used in Building engineering.

Table 3.1: Characteristic E-glass and High strength carbon material properties [2]

Characteristic material properties fibres					
	Material Characteristic	Symbol	E-glass	Carbon (HS)	Unit
Tension in fibre direction	Poisson ratio	ν_f	0.24	0.3	-
	Young's Modulus	E_{f1}	73100	238000	N/mm ²
	Strain limit	ϵ_{f1}	3.8	1.5	%
	Strength	f_{f1}	2750	3600	N/mm ²
Tension perpendicular fibre direction	Poisson's ratio	ν_f	0.24	0.02	-
	Young's modulus	E_{f2}	73100	15000	N/mm ²
	Strain limit	ϵ_{f2}	2.4	0.9	N/mm ²
	Strength	σ_{12}	1750	2140	N/mm ²
Compression in fibre direction	Strain limit	ϵ_1	2.4	0.9	%
	Strength	σ_{11}	1750	135	N/mm ²
Shear	Modulus	G_f	30000	50000	N/mm ²
	Strain limit	γ_{12}	5.6	2.4	%
	Strength	τ_{12}	1700	1200	N/mm ²
Density		ρ	2570	1790	kg/m ³
Thermal expansion		α	5.0	-0.4	10 ⁻⁶ /°C]

3.2.1.1.2 Resin properties

The most common resins are polyester, vinyl ester and epoxy [2]. Epoxy shrinks less than resins and polyester but is the most expensive (see Table 3.2).

Table 3.2: Characteristic resin material properties [2]

Charasteristic material properties resin					
	Symbol	Polyester	Vinyl ester	Epoxy	Unit
Density	ρ_r	1200	1100	1250	kg/m ³
Poisson's ratio	ν_r	0.38	0.26	0.39	-
Glass transition temperature	T_g	approx. 60	approx. 100	approx. 80-150	°C
Tensile or compression strength	f_r	55	75	75	N/mm ²
Young's modulus in tension	E_r	3550	3350	3100	N/mm ²
Strain limit in tension or compression	ε_r	1.8	2.2	2.5	%
In-plane shear modulus	G_r	1350	1400	1500	N/mm ²
Shear strength	τ_r	approx. 50	approx. 65	approx. 80	N/mm ²
Shear strain limit	γ_r	3.8	3.7	5	%
Thermal expansion coefficient	α_r	50-120	50-75	45-65	10 ⁻⁶ /°C

3.2.1.1.3 Core material properties

As mentioned before, the bridge deck can be constructed with or without a foam core. Generally speaking, three types of cores form the central part of sandwich panels: solid cores, foam cores, and honeycomb cores. Manufacturing of the foam cores exceed that of the other structural sandwiches due to their favourable strength and stiffness-to-weight ratios together with their relatively low price. Typically the rigid, closed-cell foam core materials are used for structural applications, with a core density of 32 to 300 kg/m³ [22]. A trade-off should select good core material between mechanical properties, weight and price.

Table 3.3 describes the properties of the most used core materials; Polyvinylchloride (PVC), Polyurethaan (PUR), and PMI.

Table 3.3: Characteristic core material properties [2]

Charasteristic material properties core									
	Symbol	PUR	PVC	PMI	Unit				
Density	ρ_r	50	100	40	80	80	30	70	kg/m ³
Compression strength	f_r	0.3 - 0.5	0.6 - 1.0	0.5 - 0.8	1.2 - 2.0	approx. 0.9	approx. 0.5	approx. 1.5	N/mm ²
Elasticity modulus	E_r	6 - 10	approx. 30	20 - 30	60 - 90	approx. 50	approx. 30	approx. 90	N/mm ²
In-plane shear modulus	G_r	4 - 5	approx. 10	approx. 10	20 - 30	20	approx. 15	approx. 30	N/mm ²
Shear strength	τ_r	approx. 0.2	0.3 - 0.5	0.3 - 0.4	0.7 - 1.0	0.5 - 1.0	approx. 0.3	approx. 1.0	N/mm ²

3.2.1.1.4 UD-plies

Unidirectional (UD) plies are the most used plies in bridge structures due to the advantage that design strength properties can be determined per direction (Figure 3.12). The properties of the UD plies depend on the direction, fibres, and resin that are used. The calculation of the UD-ply properties can be found in Appendix B, and are calculated according to JRC 2017 [2].

The characteristic stiffness properties of UD-plies with E-glass and polyester resin, which will be used in the bridge design, are shown in Table 3.4.

Table 3.4: Characteristic stiffness properties of UD-plies with E-glass and polyester resin

Charasteristic stiffness properties of UD-plies				
V_f	E_1 [kN/mm ²]	E_2 [kN/mm ²]	G_{12} [kN/cm ²]	ν_{xy}
40%	30.4	8.9	2.7	0.30
50%	37.2	11.4	3.4	0.29
60%	43.9	14.6	4.3	0.27
70%	50.7	19.4	5.8	0.26

3.2.1.1.5 Laminate theory

After the characteristic stiffness properties are known, the material properties can be calculated. The FRP material is built up of several layers, whereby it is possible to determine all different directions (Figure 3.12, to achieve the most optimal material. The facings that will be used will be made from a different laminate composition than the webs. This is due to the facings being mainly loaded in the longitudinal direction and the webs mainly with shear forces. The full calculations can be found in Appendix B.

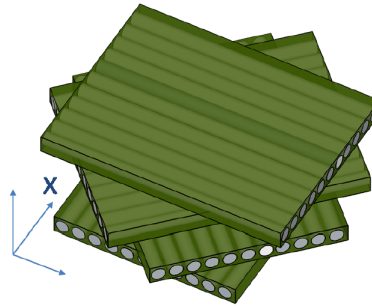


Figure 3.12: Lay up FRP (adapted from [56])

Facings

In sandwich panels, the common anisotropic Glass Fibre-Reinforced Plastics (GFRP) laminate proportion for the facings is [55%/15%/15%/15%] in orientations [0°/+45°/90°/-45°]. The laminate properties for the facings are given in Table 3.5.

Table 3.5: Laminate properties facings

Laminate properties facings											
V_f	E_x	E_y	G_{xy}	ν_{xy}	σ_1	σ_2	τ_{xy}	α_x	α_y	ρ	
	[kN/mm ²]	[kN/mm ²]	[kN/cm ²]		[N/mm ²]	[N/mm ²]	[N/mm ²]	[·10 ⁻⁶ K ⁻¹]	[·10 ⁻⁶ K ⁻¹]	[kg/m ³]	
40%	21.3	13.0	4.5	0.33	256	157	72	15.4	25.2	1748	
50%	26.3	16.3	5.6	0.32	315	196	89.6	12.7	20.5	1885	
60%	31.3	20.0	6.9	0.31	376	240	110.4	10.9	17.0	2022	
70%	37.1	25.0	8.7	0.30	445	300	139.2	9.3	13.9	2159	

Webs

For the webs a quasi-isotropic laminate proportions [25%/25%/25%/25%] in orientations [0°/+45°/90°/-45°] is applied. In this way the material is equal in strength in both directions. The laminate properties for the webs are given in Table 3.6.

Table 3.6: Laminate properties webs

Laminate properties webs											
V_f	E_x	E_y	G_{xy}	ν_{xy}	σ_1	σ_2	τ_{xy}	α_x	α_y	ρ	
	[kN/mm ²]	[kN/mm ²]	[kN/cm ²]		[N/mm ²]	[N/mm ²]	[N/mm ²]	[·10 ⁻⁶ K ⁻¹]	[·10 ⁻⁶ K ⁻¹]	[kg/m ³]	
40%	15.2	15.2	5.7	0.33	183	183	91.2	21.5	21.5	1748	
50%	18.9	18.9	7.1	0.33	227	227	113.6	17.7	17.7	1885	
60%	22.9	22.9	8.7	0.33	275	275	138.4	14.8	14.8	2022	
70%	28.0	28.0	10.6	0.32	336	336	169.6	12.4	12.4	2159	

3.2.2. Steel

The steel material properties, which are used in this research are shown in Table 3.7. This material will be used for the girder beams and cross beams.

Table 3.7: Steel material properties [15]

Material properties steel				
Material Characteristics	Symbol	S235	S355	Unit
Yield strength	f_y	235	355	N/mm ²
Ultimate strength	F_u	360	460	N/mm ²
Modulus of elasticity	E	210000	210000	N/mm ²
Shear modulus	G	81000	81000	N/mm ²
Density	ρ	7850	7850	kg/m ³

3.2.3. Concrete

For the concrete deck, Table 3.8 shows the material properties which are used in this research.

Table 3.8: Concrete material properties [14]

Material properties concrete						
Material Characteristics	Symbol	C20/25	C25/30	C30/37	C35/45	Unit
Characteristic cylinder compressive strength	f_{ck}	20	25	30	35	N/mm ²
Mean tensile strength	f_{ctm}	2.21	2.56	2.90	3.21	N/mm ²
Modulus of elasticity	E_{cm}	29962	31476	32837	34077	N/mm ²
Shear modulus	G	12484	13115	13682	14199	N/mm ²
Density	ρ	2500	2500	2500	2500	kg/m ³

3.3. Connections

Traditional steel-concrete composite bridges are equipped with welded shear stud connectors. In comparison with these conventional welded stud connectors, bridges with demountable shear connectors have the benefit that they consist of prefabricated concrete slabs, this could shorten the construction period and reduce the construction cost. Furthermore, bridges with demountable connectors have the advantage that they are easier to take apart. This makes the entire bridge demountable and allows rapid replacement of deteriorated concrete slabs.

Results of push tests show that even with the smallest loads, slip is never zero. This means, that despite the full composite interaction (assuming slip was zero everywhere), it is necessary to discover how the presence of slip modifies the behaviour of the beam.

3.3.1. Push-out procedure

Because forces have to be transferred between the different materials, shear connectors are used. The transferable forces depend on the strength and stiffness of various components of the composite beam and the shear connectors. Therefore, determining the design parameters, such as shear strength and stiffness of the stud, is necessary and can be done by conducting experiments. The ultimate slip and strength of stud shear connectors can be determined using static push-out testing.

A detailed procedure is provided in Eurocode 4 Annex B [53] to examine the shear capacity of welded studs in solid slabs made of concrete. As can be seen in Figure 3.13, the test setup consists of two reinforced concrete slabs and a steel beam section connected with shear connectors. The specimen is loaded in increments with up to 40% of the expected failure load and then cycled 25 times between 5% and 40% of the predicted failure load.

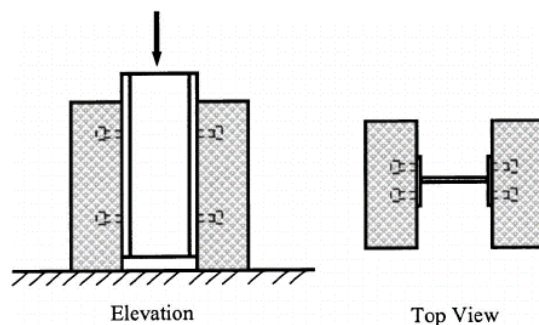


Figure 3.13: Push out test (adapted from [74])

After testing, the characteristic resistance P_{Rk} is taken as the minimum failure load per shear connector with a reduction of 10%. Furthermore, the ductility of the shear connector can be derived and depends on the slip capacity of the steel section-concrete slab interface. Figure 3.14 shows the maximum slip capacity that corresponds to the characteristic resistance. This characteristic slip capacity is equal to the maximum slip reduced by 10%. A shear connector can be considered ductile when the slip at failure is larger than 6 mm. However, if the slip at failure is smaller than 6 mm, the shear connector is considered brittle [53].

The design resistance P_{Rd} should be calculated from:

$$P_{Rd} = \frac{f_u}{f_{ut}} \frac{P_{Rk}}{\gamma_V} \leq \frac{P_{Rk}}{\gamma_V}$$

Where:

F_u is the minimum specified ultimate strength of the connector material;

f_{ut} is the actual ultimate strength of the connector material in the test specimen;

γ_V is the partial safety factor for shear connection (the recommended value is 1.25).

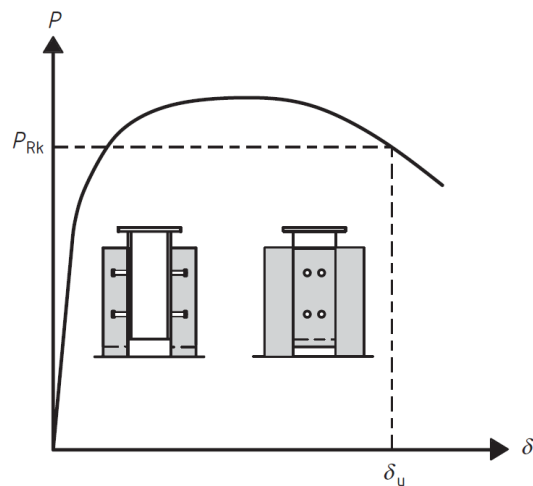


Figure 3.14: Slip capacity push-out test (adapted from [53])

3.3.2. Welded headed studs

In the construction industry, welded headed studs are the most used shear connectors. These studs are welded on the top flange of the steel beam before casting the concrete slabs to provide a shear connection in terms of strength and fatigue. In this way, a strong connection is created causing composite interaction between the concrete slab and the steel beams. However, because this connection type is welded to the top flange, it cannot be disassembled. Therefore, in Section 3.3.3, different types of connections will be described as suitable in a demountable design.

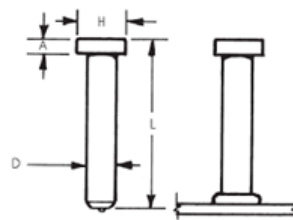


Figure 3.15: Welded stud (adapted from [53])

Figure 3.16 presents the load-slip curve of a headed welded stud. As can be seen is the maximum shear force resistance of this specimen 108 kN.

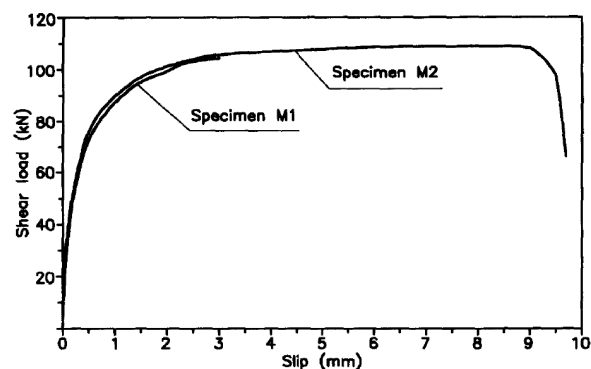


Figure 3.16: Load-slip curve - welded headed stud [19]

3.3.3. Demountable Connections

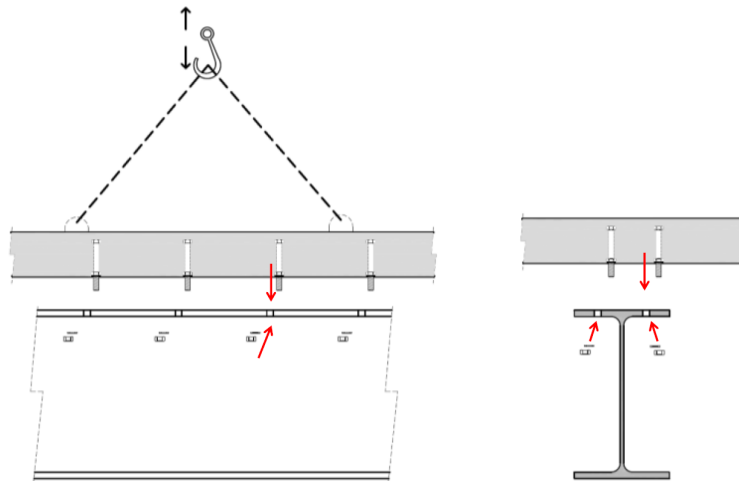


Figure 3.17: Assembling method demountable steel-concrete deck (adapted from [62])

3.3.3.1. Steel-Concrete Connections

3.3.3.1.1 Friction Grip bolt

The friction grip bolt is a demountable connection wherein the bolt is passed through the concrete deck and the upper flange of the steel girder and becomes preloaded. Due to preloading, the friction grip bolts transfer interface shear forces between the concrete slab and the flange of the steel profile through friction. However, this preloading creates high local compressing stress in the concrete slab. Therefore, unfavourable loss of preloading force due to creep can occur [62].

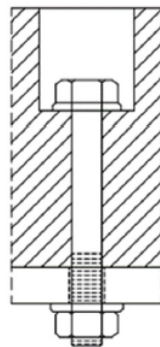


Figure 3.18: Friction Grip Bolt connector (adapted from [32])

As can be seen in Figures 3.19 and 3.20, friction grip bolts usually have zero slip at the serviceability stage due to friction by preloading. After the force exceeds this friction, large slip is clearly seen until the bolt starts bearing on the hole in the walls. The hole tolerance causes this large slip that occurs. In the third and final stage, the connector bears on the steel and concrete deck up until failure.

Kozma et al., [36] conducted a series of push-out tests with friction grip bolt connectors in solid concrete slabs 3.19. Test results showed initial stiffness in the early load stage of 250 kN/mm, which subsequently decreased significantly to 15 kN/mm. The average shear failure of the bolts occurred at a load of 141 kN shear connector.

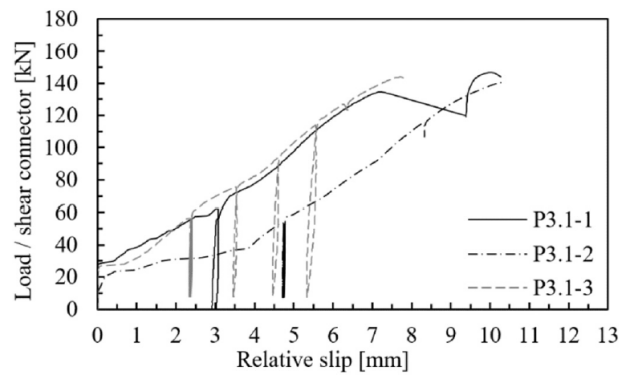


Figure 3.19: Load-slip curve - friction grip bolt connectors [36]

Marshall [43] conducted static push-out tests and composite beam experiments using friction grip bolts with a diameter of 16 mm to investigate the behaviour of various concrete strengths. He executed 11 tests with concrete cube strength varied from 36 to 50 MPa. All bolts were preloaded to achieve a friction coefficient of 0.45. The area of the base of the connector was tested after the concrete was crushed in all specimens. The ultimate load per shear connector results varied between 100 to 122 kN, with an average of 114 kN. The connection behaviour is very ductile with a slip that varies from 41 to 63 mm according to Eurocode 4 [53].

Kwon et al., [38] examined friction grip bolts by performing so-called direct shear tests on specimens with a bolt diameter of 22 mm. The friction grip bolt was tested under static and fatigue loading. In total, three specimens were tested, two for static loads and one for fatigue loading with 5 million cycles. The force-slip curves are shown in Figure 3.20.

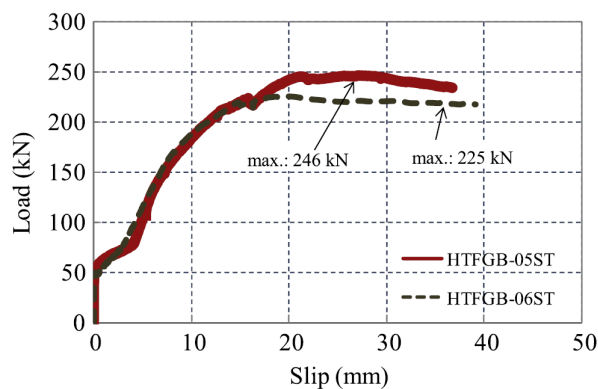


Figure 3.20: Load-slip curve - friction grip bolt connectors [38]

3.3.3.1.2 Without embedded nut

Another demountable connector is the embedded bolted shear connectors. These connectors will transfer the shear force by bearing on the concrete and the hole in the steel flange. There are also variants of this type of connection with one or two embedded nuts. These will be explained in the sections below.

Hawkins [26] executed multiple single bolt shear tests on stud bolts without embedded nuts and used the bolt diameter, height and concrete strength as experimental parameters. The results were that the shear strength of these connection is low, at 80% of the shear strength of welded studs, furthermore the shear stiffness due to the slip around the hole was only 15%.

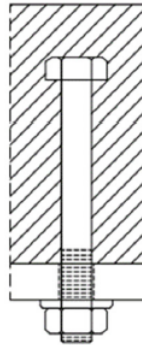


Figure 3.21: Without embedded nut connector (adapted from [32])

Push-out tests have been carried out by Lam et al., [39] on solid slabs with a thickness of 300 mm. In total, eight push-out tests were performed using studs of 19 mm and various concrete strengths. Figure 3.22 displays that connectorip, the shear resistance of demountable shear connectors is 16% lower than welded headed studs. Moreover, the connectors without embedded nuts are more ductile but have lower stiffness.

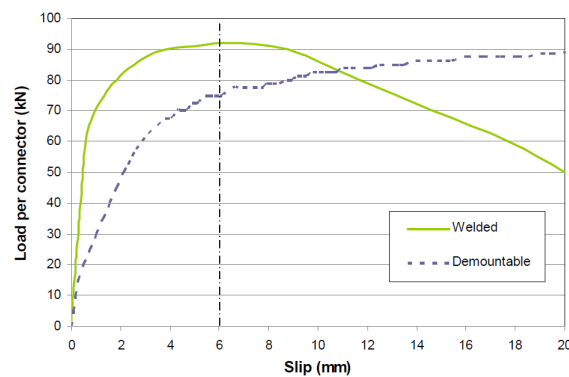


Figure 3.22: Load-slip curve - Without embedded nut connector [39]

3.3.3.1.3 Single embedded nut

The single embedded nut is a type of connection that can be executed with one or two nuts. As can be seen in Figure 3.23, this type of shear connector has one nut. Due to these nuts, the bolt can be exposed to preloading that does not create stress in the concrete, as was the case with the friction grip bolt in Section 3.3.3.1.1 [62]. In this connection, the shear forces are transferred by the shear in the bolt's thread and bearing in the hole. The stiffness compared to the use of bolts without an embedded nut is higher.

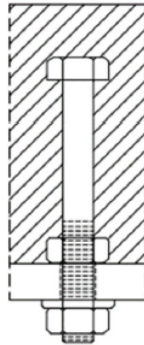


Figure 3.23: Single embedded nut connector (adapted from [32])

Pavlovic [62] executed standard push-out tests for M16, grade 8.8 bolted shear connectors with single embedded nuts (see Figure 3.24). It has been concluded that the shear connector achieved 95% of the shear resistance of welded headed studs under static loading. However, single-bolted M16 connectors gained only 50% of the stiffness of traditional welded studs.

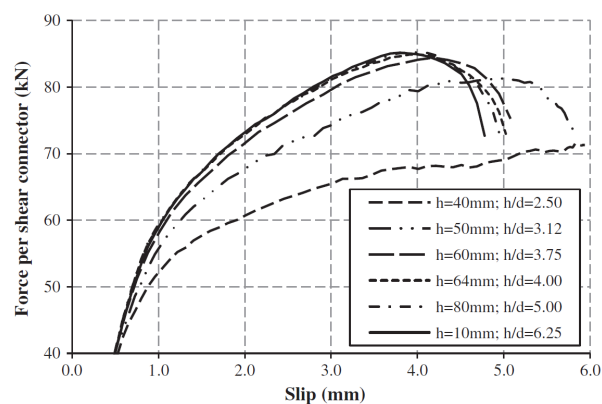


Figure 3.24: Load-slip curve - Single embedded nut [61]

3.3.3.1.4 Double embedded nuts

The connector with double embedded nuts works the same as the single embedded nut connector described above in Section 3.3.3.1.3. However, instead of one, this version has two embedded nuts.

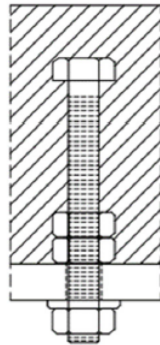


Figure 3.25: Double embedded nut (adapted from [32])

Figure 3.26 displays the load-slip curve of a double embedded nut connector, which comes from a series of direct shear tests by Kwon et al. [38]. The study concludes that the average strength of the 22 mm bolt, was 183 kN and the average slip at failure was 8.7 mm.

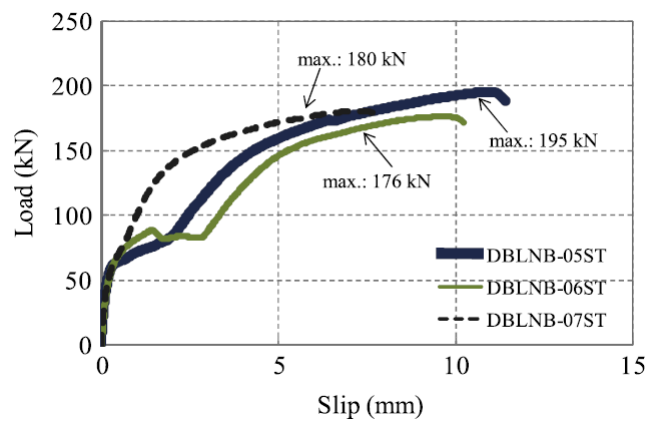


Figure 3.26: Load-slip curve - Double embedded nut [38]

3.3.3.1.5 Novel bolted connector

The bolted shear connector with a coupler system is a novel demountable shear connector. A novel bolted connector consists mainly of a short bolt, a long bolt and a coupler. An advantage of this connector type is that the dismantling process is facilitated and simplified by unscrewing the external bolt. This can all be done from underneath the bridge deck.

In this connection, the coupler is designed with a higher steel grade (10.9) compared to the bolts (8.8). This is done because only the external bolt is damaged and the deck can still be reused in case of overloading.

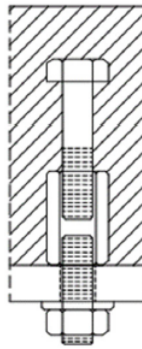


Figure 3.27: Novel bolted connector (adapted from [32])

Figure 3.28 presents the results of the tests with the coupler connector performed by Kozma et al. [36]. The load-slip curves show that the initial stiffness was 70 kN/mm and the first slip occurred at 50 kN per shear connector. The stiffness was reduced to 30 kN/mm at a 2 mm slip, causing all tests to fail due to brittle shear failure with an average load level of 142 kN per shear connector.

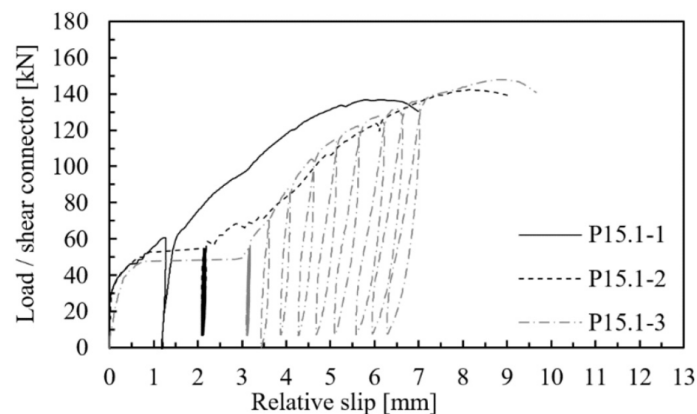


Figure 3.28: Load-slip curves Novel bolted connector [36]

Yang et al. [75] performed static push-out experiments on four groups of bolted connector specimens and one group of welded stud specimens to examine the influence of bolt strength, diameter, and flange hole tolerance of Novel bolted connectors to conventional welded stud connectors. All load-slip curve test results are shown in Figure 3.29. Yang et al. concluded that the shear bearing capacity of M22 grade 8.8 bolted connector is almost equal to 22 mm welded stud connector and that M27 grade 8.8 bolted connectors are nearly 1.6 times that of 22 mm welded studs connectors. According to Yang, the shear bearing capacity of each bolted connector can be predicted as 0.8 times the bolt's characteristic tensile strength.

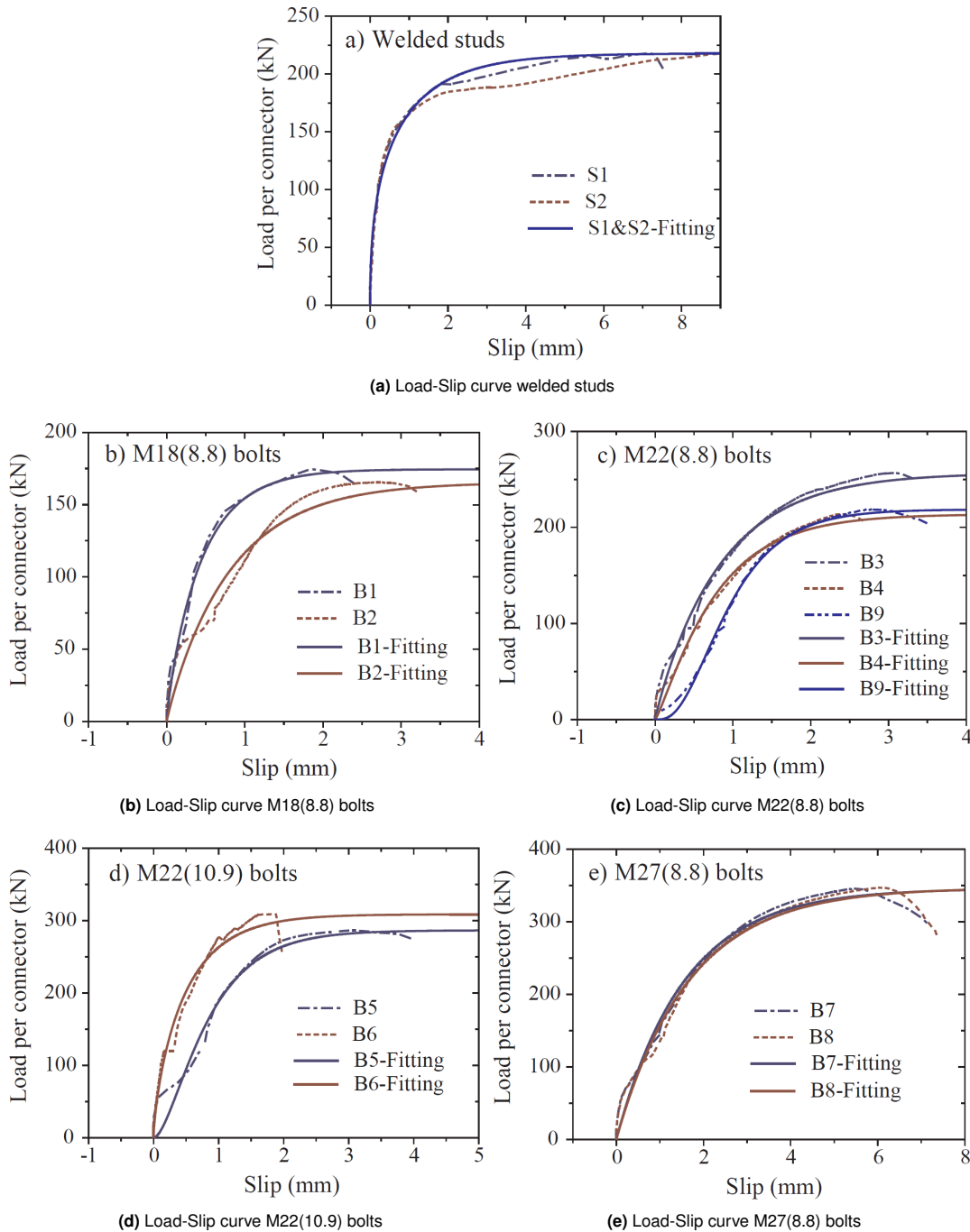


Figure 3.29: Double-parameter fitting results of load-slip curves of each push-out test [75]

3.3.3.1.6 LBDSC

The locking-bolt demountable shear connector (LBDSC) is a structure that 'locks' the bolt in predrilled holes and eliminates initial slip and construction tolerance issues.

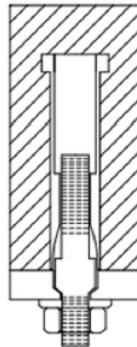


Figure 3.30: LBDSC Connector (adapted from [32])

Jun et al. [27] evaluated the structural behaviour through nine push-out tests. These push-out tests assess the effect of the tube thickness, strength of the solid concrete slab, and strength of infilled grout on the shear resistance, initial stiffness, and ductility of the LBDSC. Based on the experimental and numerical investigation, the most favourable connector exhibited 202 kN of shear resistance and 27 mm of slip capacity (see Figure 3.31b). According to these results, the shear resistance and slip capacity are larger than those of the welded headed studs. Furthermore, the LBDSC has a similar stiffness to that of a traditional welded stud.

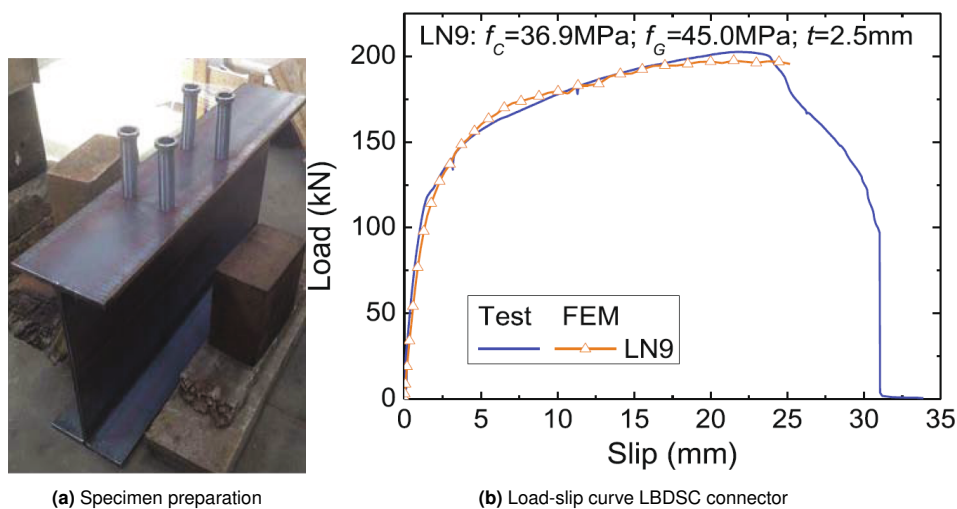


Figure 3.31: Push-out test by Jun et al. [32]

3.3.3.1.7 Resin Injected Bolts

As an improvement of the novel bolted connector, the technical university (TU) Delft has done extensive research into resin injected bolts [55] [36][69]. As mentioned in Section 3.3.3.1.5, the holes in the upper flange are oversized to form a cavity. In this variant, the clearance between the bolt and the hole is filled with resin. In this way, the connection is more slip-resistant.

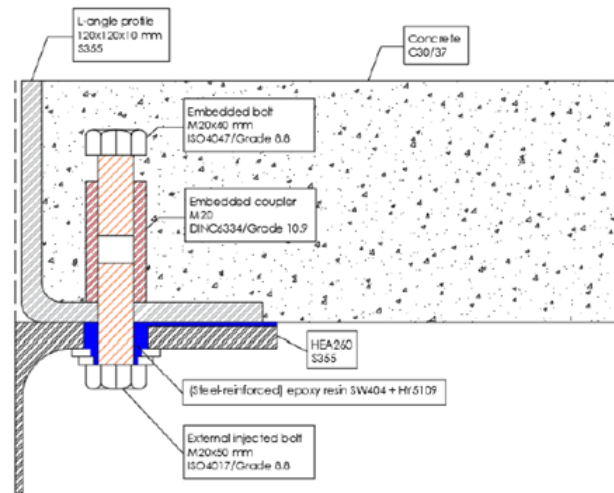
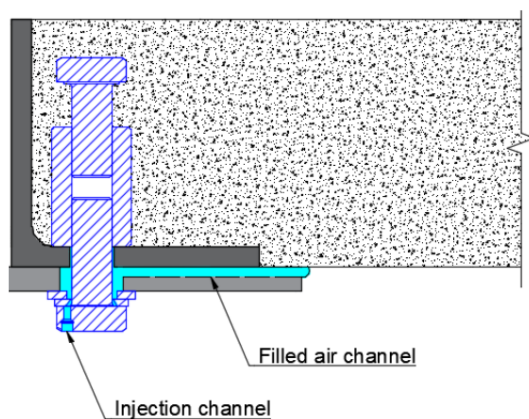


Figure 3.32: Resin Injected Bolt (adapted from [69])

As can be seen in Figure 3.33, the clearance in the connection is injected with the resin through a small hole in the bolt's head by using a caulking gun. To ensure that the resin will completely fill the void between the hole in the wall and the bolt shank, there is an air channel in the upper flange of the girder beam (see Figure 3.33b). Due to this, the trapped air can escape from the cavity and when the resin comes out of the air channel, one knows that the entire clearance is filled with the resin.



(a) figure air channel (adapted from [21])



(b) Picture of air channel (adapted from [21])

Figure 3.33: Air channel girder flange

It is also possible to add small steel spheres in the resin to create a Steel Reinforced Resin (SRR). This increases stiffness by 1.5-2 times and reduces creep by about 40% compared to pure polymer resin [54].

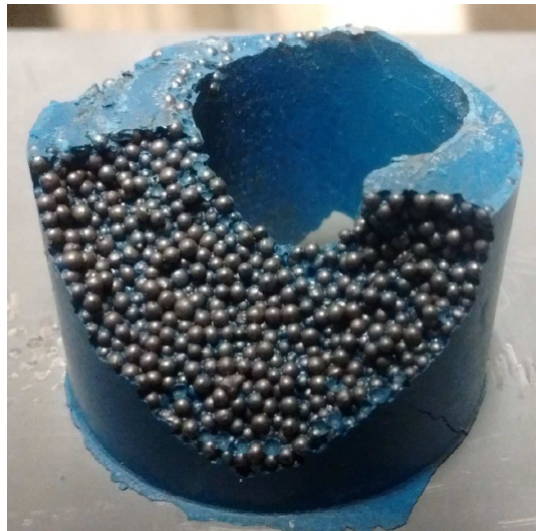


Figure 3.34: Steel spheres (adapted from [54])

Push-out tests have been carried out by [36] on solid slabs with a thickness of 150 mm. The bolts fail at an average load level of 131 kN per connector, as can be seen in Figure 3.35; the initial stiffness decreased from 100 kN/mm at load level of 50 kN to 30 kN/mm.

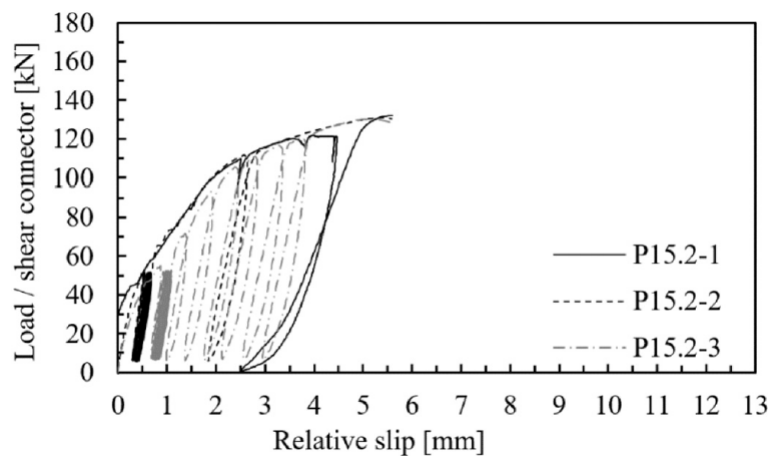


Figure 3.35: Load-slip curves [36]

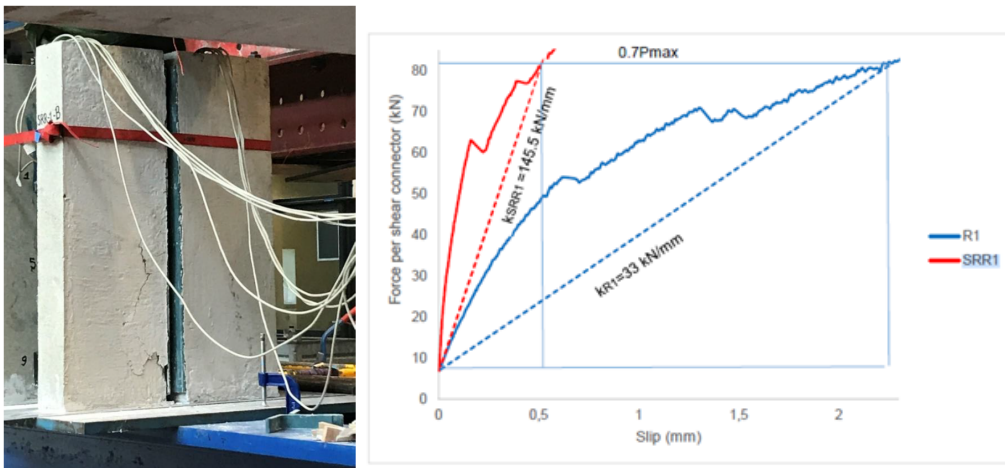
Sarri [69] executed, during his Master Thesis, six push-out tests in two different test configurations. M20 bolts were used for both experiments, one test configuration was performed with resin injected bolts and the other with reinforced resin injected bolts. In both variants, three specimens were tested which were identical to each other. As can be seen in Figure 3.37a, each specimen consisted of four solid concrete decks connected with eight shear connectors to the steel girder beam.

Figure 3.37 displays all push-out test results. The figure shows that the average maximum force per shear connector derived from tests R1, R2, R3 and SRR1 and SSR2 is 116.9 kN. SRR3 is not included due to the fact that this test result is not reliable because damage to the concrete has been detected beforehand. It can be noted that due to concrete failure in tests R1 and SRR1, the shear connectors behaved in a very ductile manner. Other tests failed due to shear failure of the bolts; the slip was very close to the limit for ductile behaviour according to NEN-EN 1994-1-1 [53].

Test	Max force per shear connector (kN)	Slip at 90% of the max force (mm)	Failure mode
R1	117,2	20,6	concrete failure
R2	115,5	5,9	shear failure of the bolts
R3	110,2	7,3	shear failure of the bolts
SRR1	118,2	14,7	concrete failure
SRR2	123,6	5,6	shear failure of the bolts
SRR3	111,0	23,1	shear failure of the bolts

Figure 3.36: Results of the push out tests [69]

Figure 3.37b shows the Force-Slip curve for the shear connector second stiffness.



(a) Test setup of Sarri [69]

(b) Load-Slip curve Steel Reinforced Resin injected vs. Resin injected connection [69]

Figure 3.37: Push-out tests Steel Reinforced Resin injected vs. Resin injected connection

3.3.3.1.8 Initial stiffness Steel-Concrete connections

Using the results of the push-out tests performed, the initial stiffness of the connection type can be calculated according to NEN-EN 1994-1-1 [53]:

$$k_{sc} = \frac{0.7 * F_R}{s} \quad (3.7)$$

F_R is the maximum shear resistance of the connector and s is the slip displacement at $0.7F_R$. The initial stiffness of a connection is an important property, because a stiffer connection limits the amount of slip. The initial stiffness value of all connectors are displayed in Table 3.9. As can be seen, the coupler connector M27 executed by Yang et al. [75] has the highest shear resistance of all demountable connectors. However, the connection behaves more brittle than the SRR injected connection.

Table 3.9: Initial Stiffness demountable connections

Overview Steel-Concrete Connectors					
Type of connection	Diameter Bolt [mm]	F_R [kN]	$S_{0.7F_R}$ [mm]	k_{sc} [kN/mm]	Source
Friction Grip Bolt	22	246	10	17.22	Kwon [38]
Without embedded nut	19	90	3.1	20.3	Lam et al. [39]
Single embedded nut	16	80	1.1	50.9	Pavlovic [61]
Double embedded nut	22	195	3.9	35	Kwon [38]
Coupler Connector M27	27	245	2	85.75	Yang et al. [75]
LBDSC	-	202	3.7	38.2	Jun et al. [32]
Coupler Connector Resin injected	20	116.9	2.48	33	Sarri [69]
Coupler Connector Steel Reinforced Resin injected	20	116.9	0.56	145.5	Sarri [69]

3.3.3.1.9 Oversized holes

To make it possible to assemble, disassemble and reassemble bolted connections, there is a need for oversized holes in the upper steel flange. However, increasing this hole clearance has the disadvantage that the bolt has more space to slip and this results in a less stiff connection. In addition to the advantage that the connection with an oversized hole is easier to assemble, it also determines the maximum amount of slip allowed in the structure, which is established at 0.50 mm. Due to the clearance, bearing of the bolt on the hole walls is prevented and thereby also permanent deformations.

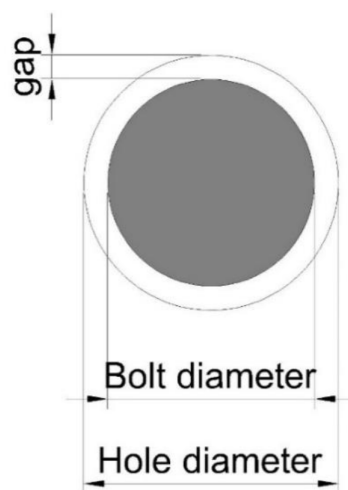


Figure 3.38: Oversized holes

3.3.3.2. Steel-FRP connections

Csillag [11] selected three different types of shear connector systems and evaluated the structural performance of the shear connectors in combination with FRP panels based on push-out tests. Two blind bolted shear connectors and a novel, hybrid SRR-joining technology were analyzed. The blind bolted shear connectors consist of the Ajax connector (Figure 3.39) and the Lindapter connector (Figure 3.42). The section below will elaborate the different connection types and will show the results of the push-out tests obtained by Csillag.

3.3.3.2.1 Ajax Connector

The Ajax connector is a blind bolt connection type and has the advantage that it requires only one face access, moreover, they can be installed from underneath the bridge. The Ajax system will be installed with the special installation tool, Figure 3.41 shows the installation process and how Csillag [11] executed it.

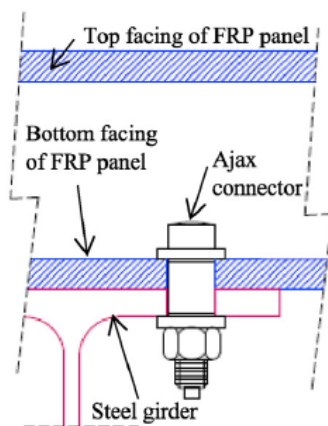


Figure 3.39: Ajax Connector (adapted from [11])

In total, push-out tests were executed by Csillag [11] to investigate the shear behaviour. Csillag performed multiple push-out tests which table 3.10 shows the results.

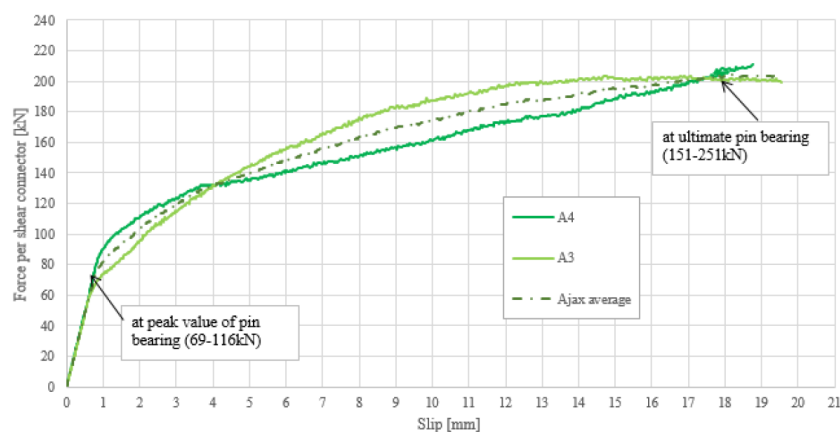


Figure 3.40: Load-slip curve Ajax Connector [11]

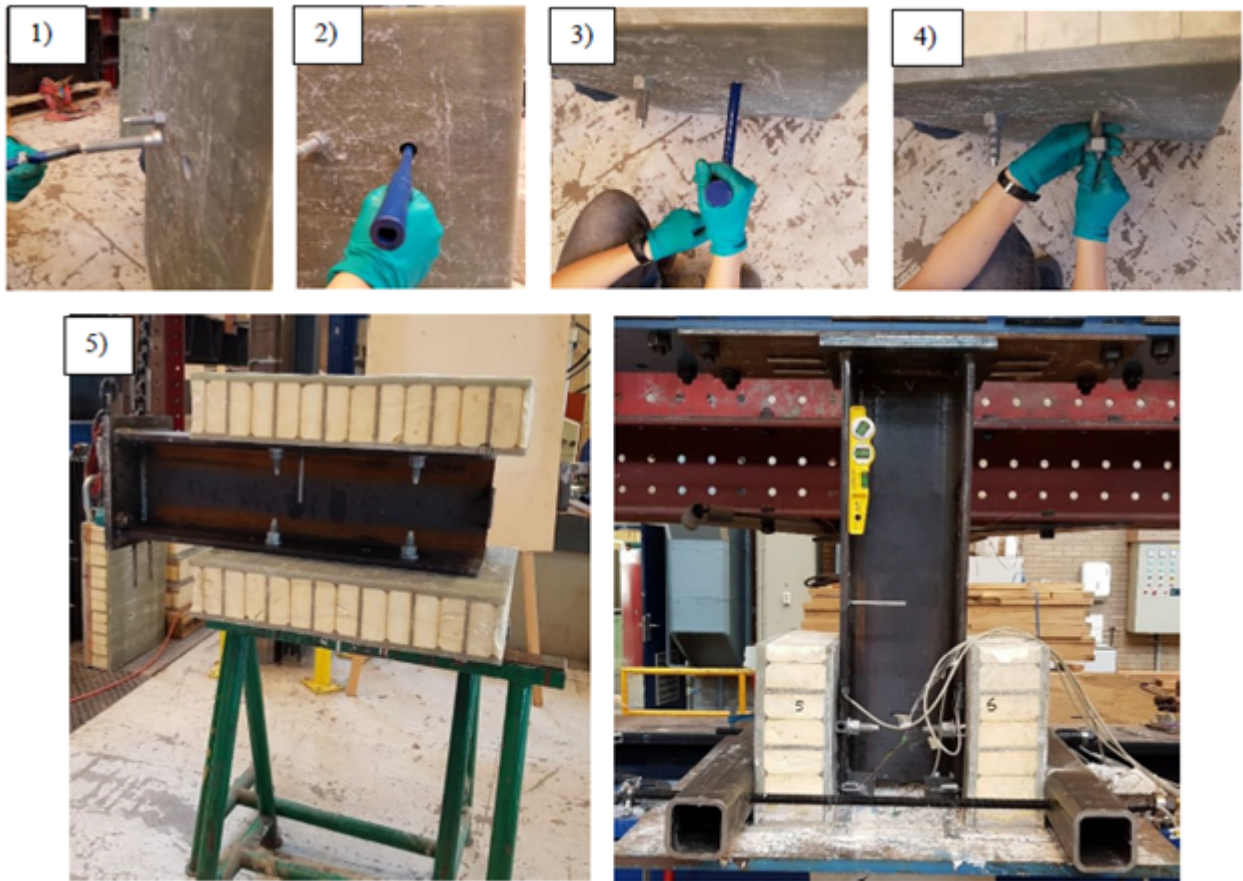


Figure 3.41: Installation of Ajax Connector (adapted from [11])

3.3.3.2 Lindapter Connector

Similarly to the Ajax connector, the Lindapter connector is also a blind bolt connector. Csillag [11] concluded that installation of this type of connection is considerably more complicated and takes a lot more time compared to the Ajax connector. Furthermore, the criteria for demountability is a problem. After installing it is difficult to disassemble the connection and after reusing the connection loses a high amount of stiffness.

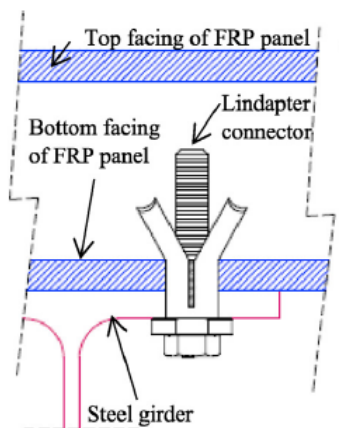


Figure 3.42: Lindapter Connector (adapted from [11])

According to executed push-out tests, the Lindapter has an average shear resistance of 164.3 kN per shear connector. Figure 3.43 displays the force-slip curve, and as can be seen, the shear connection exhibited large deformation prior failure. Csillag [11] states that this may be because a plastic hinge develops leading to a resistance plateau.

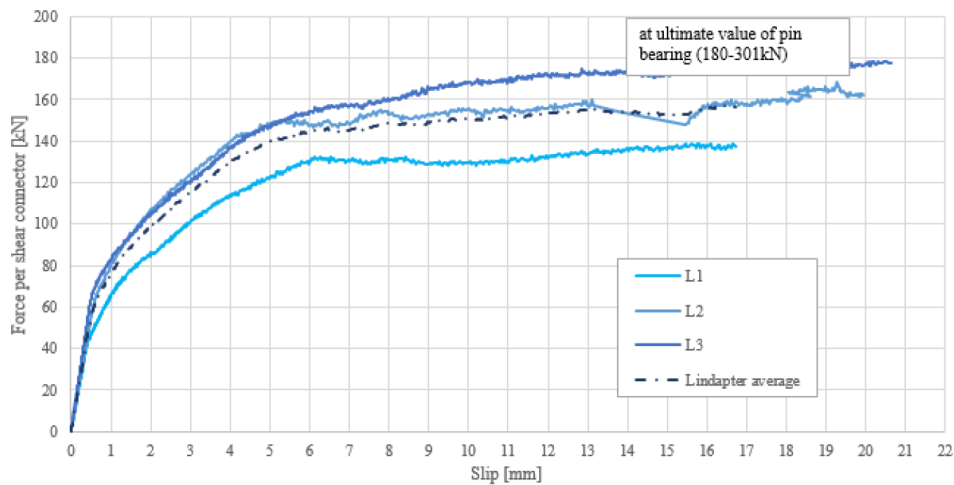


Figure 3.43: Load-slip curve Lindapter Connector [11]

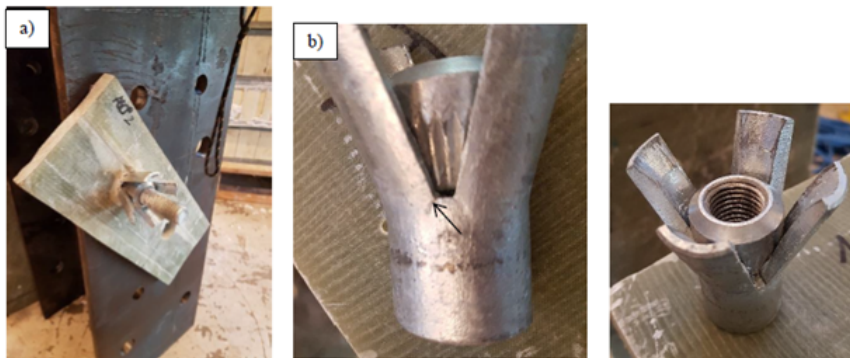


Figure 3.44: Installation of Lindapter Connector (adapted from [11])

3.3.3.2.3 Resin Injected Coupler Connector

The third connector tested by Csillag [11] is the injected shear connector. This connector is installed by first drilling an oversized hole in the sandwich panel. Then, the coupler and embedded bolt are placed on the top flange of the steel profile and are secured with the outer bolt. Afterwards, the sandwich panel is placed on top of the steel beam after which the steel shot particles and resin are injected through the 5 mm hole of the top facing.

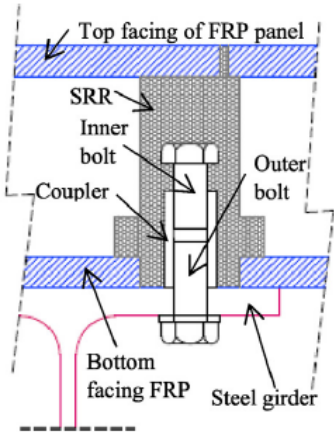


Figure 3.45: Resin Injected Coupler Connector (adapted from [11])

The connector has another static performance compared to the Ajax and Lindapter connector. The push-out test showed significantly less slip displacement in the initial stage for the injected Steel Reinforced Resin (iSRR) connections. Therefore, iSRR connectors have great potential for applications where high fatigue endurance is required. As can be seen in Figure 3.46, the average shear resistance is 120 kN. This is excluding I1 due to different failure modes.

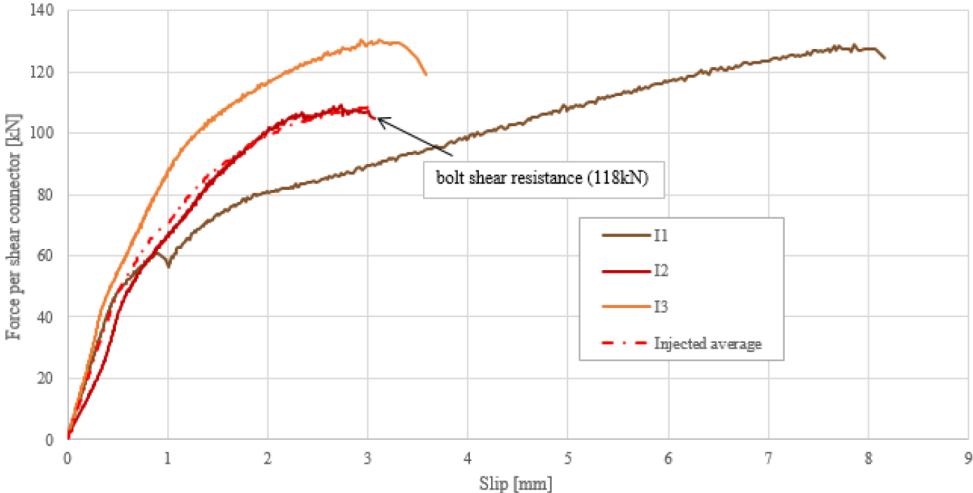


Figure 3.46: Load-slip curve Resin Injected Coupler Connector [11]

3.3.3.2.4 Overview

For the demountable Steel-FRP connectors the same Equation 3.7 is used to calculate the initial stiffness. The results per demountable connector is shown in Table 3.10.

Table 3.10: Results push-out tests according [11]

Overview Steel-FRP Connectors				
Type of connection	F_R [kN]	$S_{0.7F_R}$ [mm]	k_{sc} [kN/mm]	Source
Ajax	207.4	5.5	26.4	Csillag [11]
Lindapter	164.3	2.8	41.1	Csillag [11]
Injected	120.0	1.15	73.0	Csillag [11]

3.3.3.3. Conclusion

Csillag [11] concluded from the outcomes of the push-out tests that the shear connector stiffness of all three connectors (around 100 kN/mm) is comparable to bolted connections in steel-concrete composite structures. Furthermore, both blind bolted shear connectors (Ajax and Lindapter) failed due to local crushing of the bottom FRP facing in combination with the yielding of the bolts. With up to 20 mm ultimate slip, the connections exhibit many ductile behaviours according to Eurocode 4 [53]. On the other hand, bolt shear failure resulted in no damage of the FRP panel on all injected specimens, meaning that the reuse of the panel in a second life cycle is possible, see Figure 3.47c.



(a) Failure Ajax Connector



(b) Failure Lindapter Connector



(c) Failure SRR Connector

Figure 3.47: Failure of different connectors in FRP (adapted from [11])

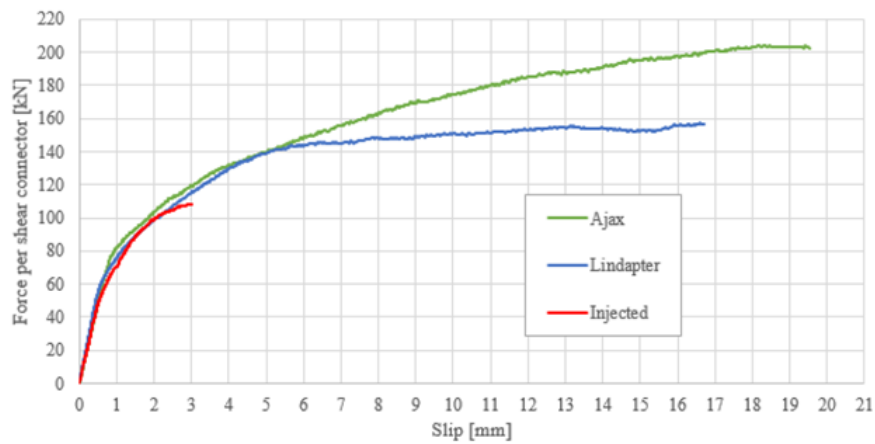


Figure 3.48: Graph Demountable FRP connectors

3.3.3.4. Fatigue

3.3.3.4.1 Steel-Concrete Connections

The behaviour of welded shear studs under fatigue loading is investigated by Slutter and Fisher [71]. In their research, they examined the effects of stress range, minimum stress, and load reversal on fatigue life. They concluded that stress range is the most important variable when it comes to fatigue life.

In addition to investigating the behaviour of post-installed shear connectors under static loading, Kwon et al. [38] also investigated fatigue loading. For this fatigue test, it was examined at which number of cycles of loading, under a specified stress range, the connector failed.

Fatigue tests of the friction grip bolt (Figure 3.18), did not fail after 5 million cycles with a shear stress range of 241 MPa. From this it can be concluded that the connector has good performance.

Fatigue tests for double embedded nuts (Figure 3.25) are also performed by Kwon et al. [38]. One of the four specimens was tested for fatigue loading with 5 million cycles. The connector showed good performance, with a shear stress range of 310 MPa, because it did not fail.

3.3.3.4.2 Steel-FRP Connections

Olivier and Csillag [60] performed fatigue experiments for the following demountable shear connectors in combination with FRP sandwich panels; iSRR connection, Lindapter and regular injected injection bolts.

During their investigation of the fatigue performance of these connections, a ± 40 kN cyclic loading was applied until a total displacement of 0.3 mm was achieved. The experimental results can be seen in Figure 3.49, where the F-series are the experiments under cycling loading. Olivier and Csillag [60] conclude that the stiffness of the iSRR connection decreased by 45% due to cyclic loading. Moreover, it was suggested that the fatigue performance of the iSRR connector compared to the Lindapter and regular injection bolts was by far superior.

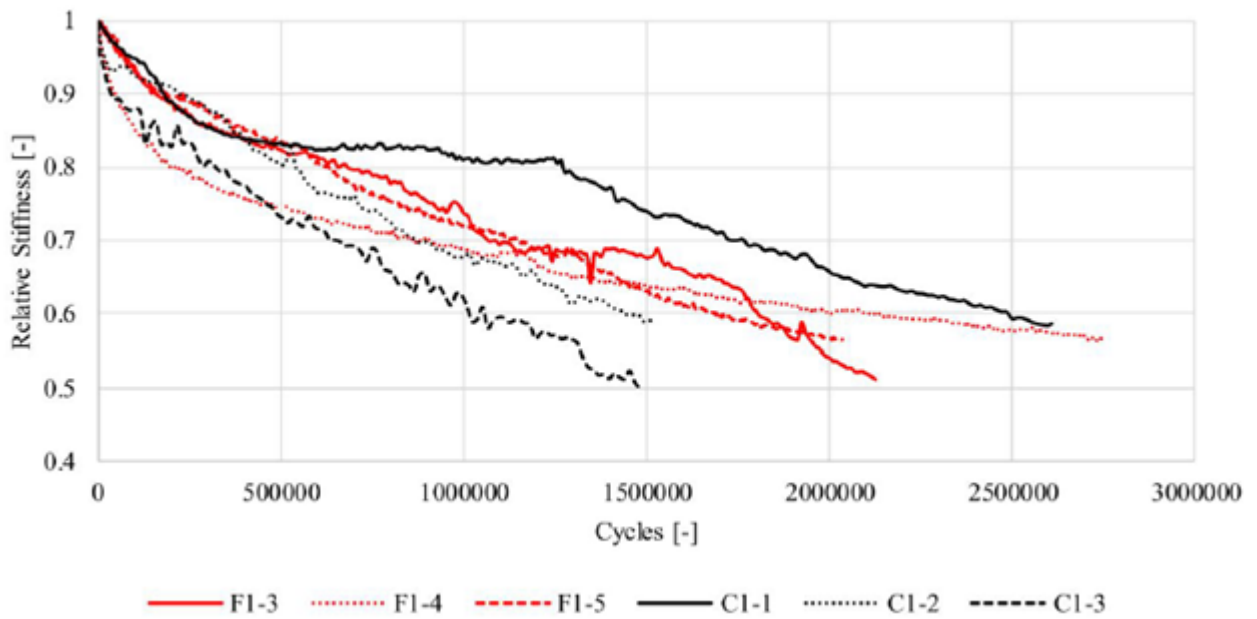


Figure 3.49: Relative stiffness decrease under cyclic loading [60]

4

Environmental impact

4.1. Shadow costs

As can be seen in figure 4.1 the shadow costs can be presented at three different levels; on pollutant level, at midpoint level and at endpoint level [12]. The shadow costs at pollutant level have a value for emissions of environmentally hazardous substances. At midpoint level, shadow costs are valued on environmental themes and on endpoint-level valued on the impacts of environmental pollution on human health or ecosystems.

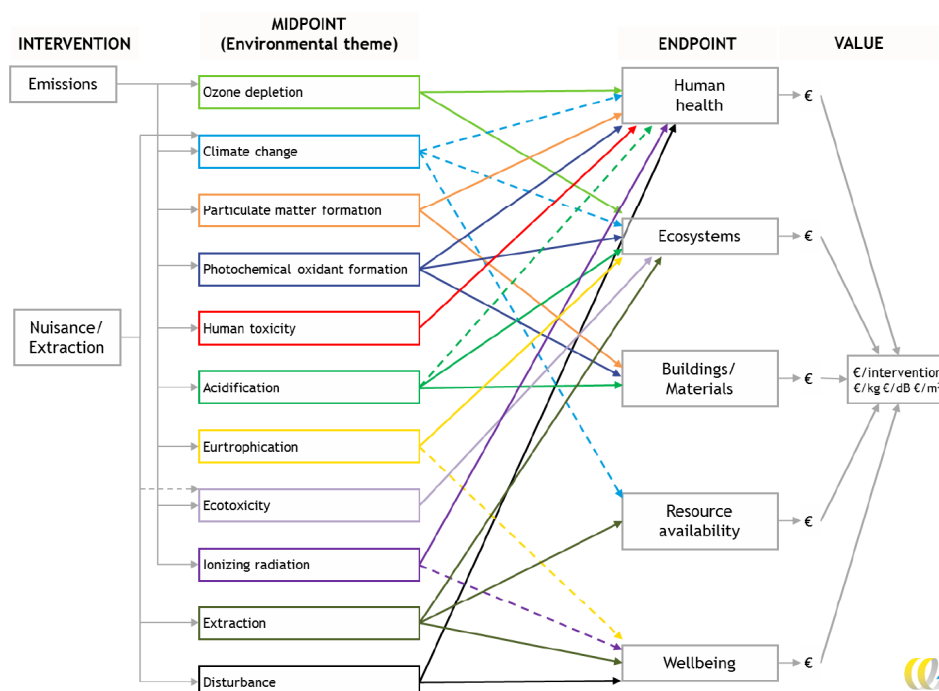


Figure 4.1: The relationships between the three different levels (adapted from [12])

4.1.1. Life Cycle Assessment

The objective of this research is to develop a demountable superstructure of a bridge with reduced environmental impact. There are multiple methods to quantify this environmental impact performance. The Life Cycle Assessment (LCA) is a widely used method worldwide that can be used to compute the environmental 'performance' of 'impact' related to all life cycle stages of buildings [31]. Utilizing the tool helps with comparing different designs and/or to optimize designs for the contributions with the greatest environmental impact. Calculating an LCA requires extensive knowledge on the production process,

energy use, origin of materials, and emissions during all stages (Figure 4.2). However, data from Environmental Product Declarations (EPDs) will be used during this research. These EPDs presents an LCA for standard units of a specific product from manufacturers.

As can be seen in Figure 4.2, the life cycle consist of four stages which are construction stage (A), the use stage (B), the end of life stage (C) and the beyond end of life stage (D). Each phase consist of multiple sub-phases.

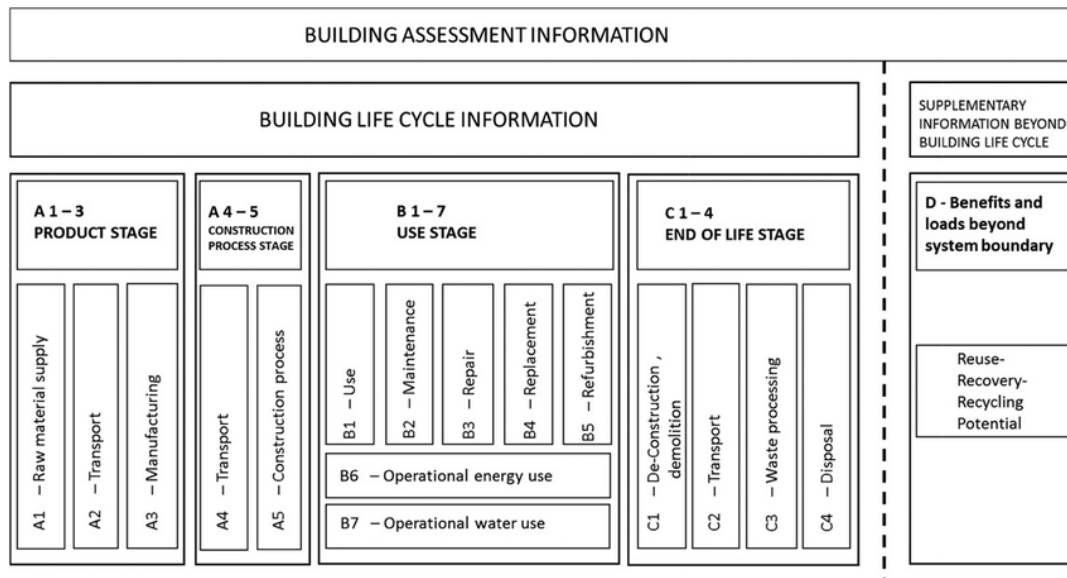


Figure 4.2: Stages in life cycle assessment according to EN15804 [49]

4.1.1.1. System boundaries

The LCA aims to ensure comparing the designs is possible using different materials. Therefore, it is only important to consider the stages and processes that differ between the different designs. The main differences between the designs with an FRP deck and a concrete deck can be summarized as follows:

- Production stage (A1-A3): differences in material and quantities per design
- Construction process (A4 + A5): especially the difference in weight and number of elements of the designs.
- Use stage (B1-B7): some materials require more maintenance than others.
- End of life (C1-C4 and D): The different materials lead to differences in waste processing, reuse and recycling potential.

To conduct an accurate comparable LCA, all these differences must be considered. The use stage is of all stages the most unpredictable stage, because it is very difficult to attach a reliable and realistic value to this.

Since this structure is designed as a reusable structure, the progress of the different stages as shown in Figure 4.3 is different from a non-reusable structure. With a non-reusable structure, the progression is linear from the production to the end-of-life stage. With a reusable structure, the construction stage will have to be taken into account again and again when the end-of-life stage is reached (except for the deconstruction stage, C1). The elements have already been produced and only need to be transported after which they can be assembled again.

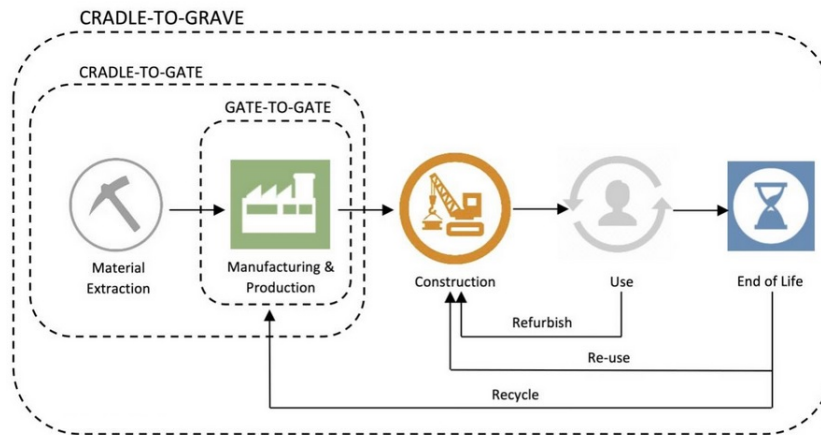


Figure 4.3: System overview reusable structure (adapted from [17])

For the case study superstructure, it is assumed that there are a total of 10 life cycles in total during the reference period of 100 years. The design will be disassembled and reused a total of 10 times, the construction (A4+5) and use stage (B1-7) will be included in the calculations a total of 10 times, and the production (A1-3) and end-of-life stages (C1-4 and D) only have to be included once.

4.1.2. Environmental Impact Categories

As mentioned in Section 4.1.1, the LCA components are based on environmental impact categories. In this study, the EPDs will be expressed in environmental impact categories according to the Nationale Milieudatabase (NMD), which is a widely used recognized determination method. In the text below, the different impact categories will be described according to Materials and Ecological Engineering [31].

4.1.2.1. Abiotic Depletion Potential (ADP-non fuel, ADP fuel)

Due to the fact that there is no endless supply of abiotic resources, the consumptions should be limited. Abiotic resources include not only fossil fuels, but also certain minerals and metals. Using ADP the scarcity of abiotic finite resources can be expressed. Within ADP, a distinction can be made between abiotic depletion potential of fossil fuels (ADP-fuel) and abiotic depletion of non-fossil fuel compounds (ADP-non-fuel).

4.1.2.2. Global Warming Potential (GWP)

Global warming potential is a measure to express the human induced effect on the heat radiation absorbing capacity of the lower atmosphere. Human activities release so-called greenhouse gasses, such as carbon dioxide (CO₂), methane (CH₄), and nitrous oxide (N₂O) and these gasses absorb infrared radiation, causing in additional warming of the Earth's surface. The most worrisome problem caused by global warming is the melting of glaciers and ice caps in the polar regions. This has already led to a rise in sea level of 19 cm since the beginning of the 20th century.

4.1.2.3. Ozone Layer Depletion Potential (ODP)

The powerful greenhouse gas (in the lower atmosphere) ozone (O₃) is naturally produced in the higher atmosphere (stratosphere) and protects the life on Earth against damaging ultraviolet (UV) radiation. UV light can be dangerous because it increases the risk of skin cancer as it causes mutations in DNA. Decomposition of O₃ happens when halogenated compounds reach the stratosphere. UV radiation decomposes the halogenated compounds creating chlorine and bromines which act as chemical catalysts in the decomposition of ozone. Some examples of ozone depleting compounds are chloro-fluoro-carbons (CFCs), hydro-chloro-fluoro-carbons (HCFCs) and bromo-chloro-fluoro-carbons (halons) which are widely used in refrigerators, air-conditioners and electronic equipment.

4.1.2.4. Human Toxicity Potential (HTP)

Human toxicity potential is a measure to express which compounds are harmful to human health. These compounds can be found in many different compartments, such as air, water and soil. The harm of a specific compound differs between which compartment they are found in and in what concentrations they are present.

4.1.2.5. Fresh Water Aquatic Eco-Toxicity Potential (FAETP)

The fresh water environment can become polluted due to wastewater dumps, heavy metals, and compounds released in association with mining, oil and gas extractions. With regard to civil engineering activities, this pollution is mainly emitted during the production of building materials, such as steel and cement.

4.1.2.6. Marine Aquatic Eco-Toxicity Potential (MAETP)

The Fresh Water Aquatic Eco-Toxicity Potential also exists for marine life. Many toxic compounds end up in the marine environment due to air and freshwater flows. An example of a compound that causes problems are persistent organic pollutants (POPs). These compounds accumulate in the marine environment food chain as that they do not or only very slowly degrade.

4.1.2.7. Terrestrial Eco-Toxicity Potential (TETP)

Besides the pollution of the freshwater and marine environment, these problems also occur on land. In the agricultural sector, crops are sprayed with pesticides and insecticides to protect them. These pesticides and insecticides can accumulate in the food chain and become toxic at a certain level. An example of a common insecticide is Dichlorodiphenyltrichloroethane (DDT).

4.1.2.8. Photochemical Ozone Creation Potential (POCP)

Sunlight reacts with emitted airborne pollutants, and forms specific chemically reactive compounds which can be damaging for both human health and the environment. An example of a reactive photochemical oxidant is ozone which occurs in the lower atmosphere (troposphere) due to the photochemical oxidation of volatile organic compounds (VOCs) and carbon monoxide (CO) in the presence of nitrogen oxides (NO_x). These compounds are produced during the combustion of fossil fuels.

4.1.2.9. Acidification Potential (AP)

Acids can be emitted as compounds or are produced when reacting with water. Sulphur dioxide (SO₂), NO_x and ammonium (NH₄) are some examples of common acids. Acids can have effects on the natural environment (detrimental effects on soil, groundwater and ecosystems) and also on the built environment (by damaging structures due to their corrosive properties).

4.1.2.10. Eutrophication Potential (EP)

Eutrophication is the process of excess nutrient loading in the environment. The agricultural sector is a major contributor as they apply nutrients to soils to increase the production yield of crops. Nitrogen (N) and phosphorous (P) are the two most common compounds in fertilizers and despite the fact that these fertilizers increase the growth yields of plants, it is not good for the environment. As a consequence of these growths, one type of plant starts to overgrow others, causing low biodiversity. This also occurs in surface water; because of rain or irrigation, the applied nutrients can end up in the groundwater or in surface waters. Specific algae will grow in excessive amounts, smothering other types of life. This leads to oxygen deprivation at night, causing animals to die, resulting in 'black' dead and smelly waters [31].

The corresponding shadow prices:

Table 4.1: Shadow prices per environmental indicator [31]

Shadow prices per environmental indicator		
Environmental indicator	Equivalent unit	Weighted factor [€/kg eq.]
Global warming (GWP)	kg CO2 eq.	0.05
Ozone layer depletion (ODP)	kg CFC-11 eq.	30.00
Human toxicity (HTP)	kg 1,4 DB eq.	0.09
Aquatic tox. fresh water (sweet) (FAETP)	kg 1,4 DB eq.	0.03
Aquatic tox. fresh water (salt) (MAETP)	kg 1,4 DB eq.	0.0001
Terrestrial toxicity (TETP)	kg 1,4 DB eq.	0.06
Photochemical oxidation (POCP)	kg C2H4 eq.	2.00
Acidification (AP)	kg SO2 eq.	4.00
Eutrophication (EP)	kg PO43 eq.	9.00
Abiotic resources depletion (ADP non fuel)	kg Sb eq.	0.16
Fossil energy carriers depletion (ADP fuel)	kg Sb eq.	0.16

4.1.3. Shadow costs construction materials

The shadow costs of the construction materials for this research need to be determined to provide as input for the parametric model. In this section, these costs will be described. The data that is used comes from the course "Material and Ecological Engineering" and which this data the quantitative value of each design can be determined. This value represents the cost necessary to reverse the damage caused by the structure. Table 4.2 displays for materials the environmental impact value. Because connections are only a small part of the total weight of the structure, connections are not taken into account. The full calculation to achieve these values can be found in Appendix C.

Table 4.2: Average ECI per structural material

Overview ECI per material			
Material		Average ECI [€]	Unit
Steel		0.25	kg
Concrete	C20/25	0.0073	kg
	C30/37	0.0074	kg
	C35/45	0.0075	kg
	C45/55	0.0082	kg
	C55/67	0.0090	kg
Reinforcement		0.66	kg
FRP	epoxy	1.14	kg
	polyester	1.18	kg
	vinylester	0.79	kg
	PVC Core	0.19	kg
ECI Transport			
Lorry >26 tons		0.014	ton/km

4.1.4. Boundary conditions of the expected lifespan estimation

When the expected lifetime increases, the environmental impact costs, expressed per year, decrease. However, the expected lifespan cannot simply be extended without clear substantiation, because this has no value in improving the environmental impact performance. In this section, the boundary conditions and expected lifespan estimation is described.

As can be seen in Figure 4.4, the technical lifespan is larger than the economical lifespan of structure components. Most structures are designed based on the technical lifespan, and it is over when a structure no longer fulfils the performance it needs to. To make this happen, the economical end of life is often exceeded first. This occurs when another element can fulfil the same function, or even better, but with a lower cost. The end of life that probably occurs first is the functional end of life. This occurs when the element no longer fulfils the function for which it was designed. All these three different kinds of end-of-life together determine the moment when a component needs to be replaced [58].

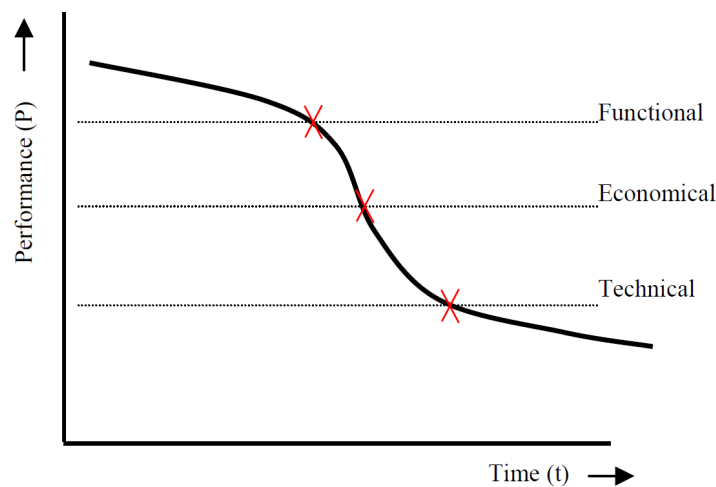


Figure 4.4: Different kinds of End Of Life (adapted from [58])

4.1.5. End-of-life materials

Module D, of an LCA, is often calculated separately, and it is often the most difficult part. In this module, the value recovery of the following strategies is considered [42]:

- Waste prevention
- Re-use
- Material recycling
- Energy recovery
- Landfill/disposal

Of these strategies, waste prevalence/reduction and re-use of materials are the most preferred options. Research shows that common steel profiles can easily be reused in constructions with different purposes. Nowadays, 49% of all beam steel is reused and 51% is recycled. Steel is 100% recyclable and today 45% of steel worldwide is made from recycled steel [6]. Not all steel is made from recycled steel because the demand for steel is higher than what is released.

When it comes to concrete elements, they are a lot more difficult to reuse than steel profiles because concrete elements are often specially made to measure. This ensures that the purpose of the elements is very limited, the advantage is that it is aimed at waste prevention. However, 50% of the total construction waste consists of concrete waste [73]. This amount can be reduced by recycling the waste. This can happen because after separating the reinforcement, the concrete is crushed into aggregates,

which can be used as raw material to make new concrete, but this is a cost-intensive process.

FRP decks are always prefabricated using different manufacturing processes, which are usually very efficient and reduce the amount of waste. However, reusing FRP elements at the end of life is very limited because the elements are very specifically produced and are difficult to use for other purposes [42]. Recycling of materials is essential for a sustainable future. Unfortunately, today GFRP production still uses 100% glass fibres and polymers. The reason for this is not that FRP composites cannot be recycled, but that recycled FRP material is not appropriate for use in structural elements. Recycling of FRP materials can take place in different ways. As shown in Figure 4.5, the first option is mechanical recycling, where the material is crushed and granulated, which can be used as filler or reinforcing material in new composite material. The second method is called thermal recycling, whereby the resin and the fibres are dissolved, allowing the former components to be reused in other composite products. The same functions are performed with the third and final thermal recycling method.

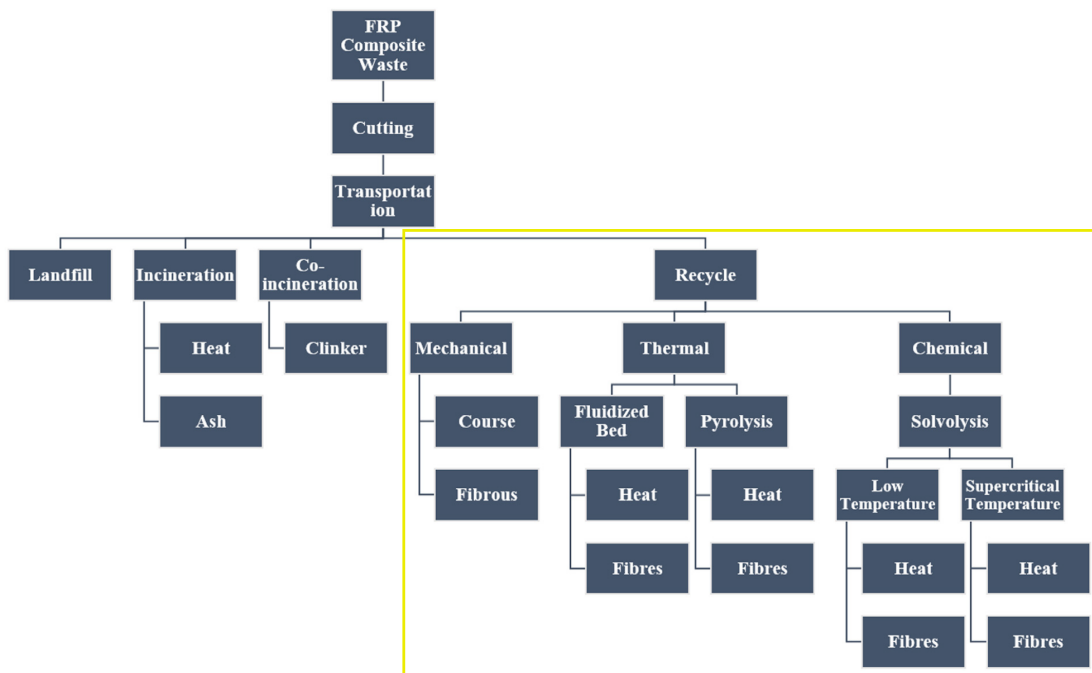


Figure 4.5: Different alternatives for composite waste materials (adapted from [20])

4.2. Design strategies

This section will explain the design strategies that lead to a circular design. The most important thing in a CE is to focus on creating an economy that reduces resource dependence and increases a regenerative system at different levels. The development of a circular construction project can be stimulated by three circular design strategies: 1) Design for Adaptability (DfA); 2) Design for Disassembly (DfD); 3) Design for Material Efficiency (DfME).

As can be seen in Figure 4.6, the circular strategies influence all distinct phases of the LCA modules. The DfME relates to stages A1-A3: production. DfA relates to B1-B5: operation and DfD relate to C1-C4: End of life. The impact of these strategies on the environmental impact of bridge structures will be studied [37].

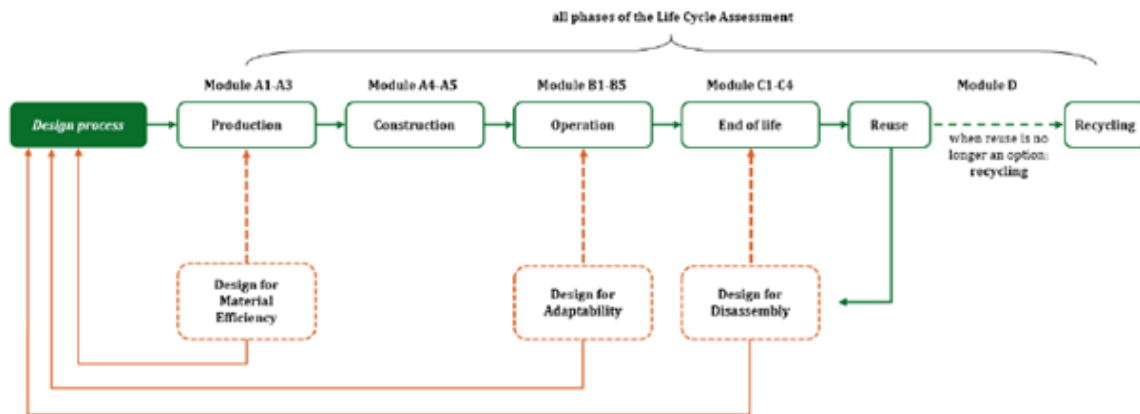


Figure 4.6: All phases LCA (adapted from [37])

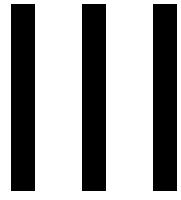
According to Abuzied et al. [1], DfD can best be achieved by involving:

- "Simplifying the de-manufacturing process"
- "Reducing needed time and cost for disassembly"
- "Allowing recovery of components and materials."

Considering these strategies, it is best to come up with a demountable design. This is fulfilled by using temporary connectors between different components of the design.

Design strategy DfME, is the strategy which focuses on the efficiency of the used materials. Within this research, efficiency is measured by the following properties: mass, construction height of the structure, and costs.

The calculations show that an FRP bridge has a higher amount of shadow costs during the production phase compared to other conventional materials such as concrete or steel. However, this study does not research the emission savings during the construction, maintenance or disposal stages of an FRP bridge compared to steel or concrete bridges (only transport is considered). [57] investigated the Life Cycle Cost (LCC) of an existing FRP bridge and concluded that during the construction stage, the shadow costs from FRP bridge decreased by about 70 % than that from a comparable pre-stressed concrete bridge.



Circular design

5

Set-up of design of Bridge layout

5.1. Assembling process

This section will describe the assembling process of the design. After the longitudinal girder beams have been placed in the desired position, the cross beams are placed in between. These cross beams are connected to the girder beam by the use of a fin plate connection, see Figure 5.1.

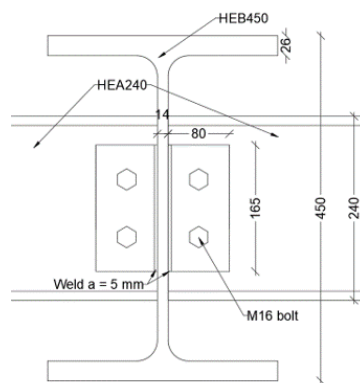


Figure 5.1: Connection between cross beam and girder beam

after the entire steel structure has been assembled, the pre-cast concrete deck is placed on top of the steel girder beams. During the thesis research of Gîrbacea [21], he developed a construction method using threaded rods that are placed into the couplers at the corners and at midspan of the deck during the installation of the concrete deck (see Figure 5.2). In this way it is ensured that the deck is placed exactly so that later the injection bolts can be placed in the couplers via the bottom of the flange.

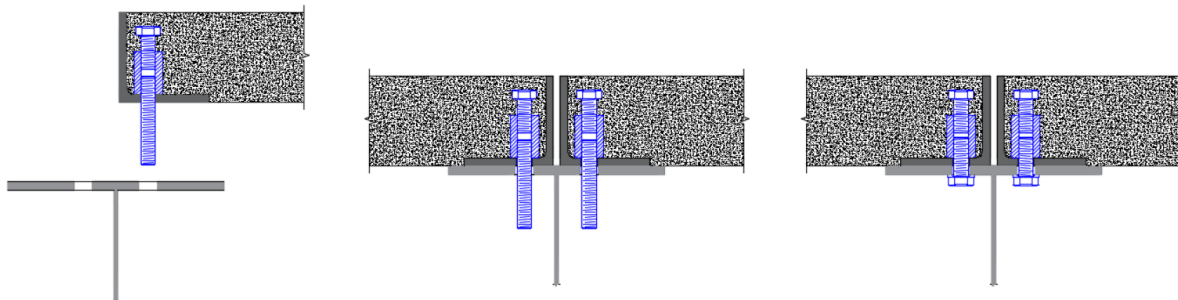


Figure 5.2: Construction method with threaded rods (adapted from [21])

After the deck is in the right place, the injection bolts can be mounted. Gîrbacea has also written an extensive injection procedure for this. Which describes that it is possible to inject 20 bolts with one batch of resin mix. This process takes 10 minutes, which equates to 30 seconds per bolt. At the same time, a second employee can prepare the next batch of resin and this also takes 10 minutes. During my research, I maintain a total assembly time of 12 minutes per bolt. This is an assumption of ASK Romein Hillebrand that is used in practice. This choice is further explained in Section 5.1.2. Figure 5.3 pictures a iSRR connector which is fully assembled.

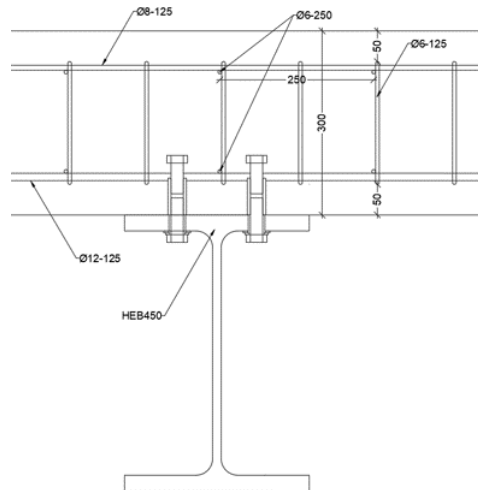


Figure 5.3: Demountable iSRR Connector

5.1.1. Cost inputs

The tables below show the different cost inputs of the following categories: material costs, connector costs, labour costs, and transport costs.

5.1.1.1. Material costs

This section lists the prices of all materials used. Because material prices are currently highly fluctuating, indications have been adopted for some prices.

Table 5.1: Structural Material costs

Structural material costs				
Materials		per Unit	€	Source
Steel	S235	kg	1.25	Hillebrand
	S355	kg	1.50	Hillebrand
Concrete	C20/25	m ³	90.70	Dura Vermeer
	C25/30	m ³	90.75	Dura Vermeer
	C30/37	m ³	90.80	Dura Vermeer
	C35/45	m ³	98.90	Dura Vermeer
	C45/55	m ³	110	Dura Vermeer
Reinforcement	B500	kg	1.50	Dura Vermeer
Fibres	Glass	kg	3.00	Literature [45]
Resin	Polyester	kg	3.70	Literature [45]
Foam Core	PVC	kg	11.40	Literature [45]

The costs for FRP with different fibre volume have been determined using this table. For example, the material costs per kilogram for FRP with a fibre volume of 40% is:

$$V_{40} = \frac{0.4 \cdot 2570 \cdot 3.00 + 0.6 \cdot 1200 \cdot 3.70}{0.4 \cdot 2570 + 0.6 \cdot 1200} = \text{€}3.29$$

Table 5.2: Connector costs

Connector costs			
Connector	Parts	€ per unit	Source
Non Injected connector	Coupler 10.8	3.00	Hillebrand
	M20 bolt 8.8	1.00	Hillebrand
	Washer	0.25	Hillebrand
	Total	5.25	Hillebrand
Injected connector	M20 Injection bolt 8.8	3.00	Hillebrand
	Steel reinforced resin	1.00	Hillebrand
	Total	8.25	Hillebrand
Welded stud	Total	0.50	Hillebrand

5.1.1.2. Manufacturing costs

Table 5.3 below shows all costs for the prefab plate which is mounted on top of the steel girder beams. Because the total deck is divided into 4 pieces, the cost is calculated for 1 piece with the dimension of 3 x 7 meter. So the production cost for the entire deck is 4 times the cost below.

Table 5.3: Manufacturing costs prefab concrete deck

Manufacturing costs prefab concrete deck					
Manufacturing		unit		price per unit	Source
Formwork	Depreciation	1.25	/unit	7.00	Dura Vermeer
	Manufacturing	1.50	hr/unit	45	Dura Vermeer
	Crane	0.2	hr/unit	60	Dura Vermeer
Concrete	Manufacturing	1.50	hr/unit	45	Dura Vermeer
	Pump	0.5	hr/unit	90	Dura Vermeer
Reinforcement	Manufacturing	80	kg/hr	40	Dura Vermeer
	Crane	1000	kg/hr	60	Dura Vermeer

5.1.1.3. In-situ costs

Table 5.4: Assembling time

Assembling time					
Assembling		Time		Price per unit	Source
Installing Girder beam	Installing per Girder	3	hr/unit	55	Hillebrand
	Installing Cross beam	1.5	hr/unit	55	Hillebrand
Concrete Deck	Placing entire slab	12	hr/unit	55	Dura Vermeer
Bolts	Resin injected bolt	0.20	hr/unit	55	Hillebrand

It is assumed that the crane has to move the heaviest parts (concrete deck) 12 meters. According to Sarens' crane tables, [68], an 80-tonne crane is sufficient for a concrete slab thickness of 25 cm. To a slab thickness of 30 cm, a 100-tonne crane is sufficient and after which a 120-tonne crane can place the concrete decks with other thicknesses. The prices for the aforementioned types of cranes are shown in Table 5.5 below. These prices include crane operator.

Table 5.5: Telescopic crane costs

Telescopic crane costs				
Connector	Parts	Unit	Price per unit	Source
Telescopic Crane	60 tons	Cr. hr.	92.50	Dura Vermeer
	70 tons	Cr. hr.	110	Dura Vermeer
	80 tons	Cr. hr.	120	Dura Vermeer
	100 tons	Cr. hr.	135	Dura Vermeer
	120 tons	Cr. hr.	150	Dura Vermeer

In addition to the above costs, there are also transport costs. One of the requirements of this research is that the bridge design must be easy to transport on the road. The maximum width is therefore limited to 3 meters, with a mass of 50 tons. The costs for this transport are shown in Table 5.6.

Table 5.6: Transportation costs

Transport costs			
Transport			Source
Transport	/unit	400€	Dura Vermeer

The results will be displayed later (Section 7.5.2) in the report. The full calculations of the costs per variant can be found in Appendix D.

5.1.2. Sensitivity analysis

During my research at Dura Vermeer, several experts helped me design the structure and made certain assumptions. The experts at Dura Vermeer mainly helped me with the practical parts of the design, such as assembling this kind of construction, with assumptions about how and how much time it takes to assemble certain elements, and providing material cost information. Since Dura Vermeer itself has too little knowledge when it comes to designing steel structures, they put me in touch with experts from ASK Romein Hillebrand. With more than 600 employees, this company is very experienced in the production of steel structures and produces 60,000 tons of steel structures on an annual basis.

This section will discuss the assumptions made in this chapter and will focus on assembling time and financial costs. It can be stated that these assumptions should not be seen as exact values, but rather as indicative values. The sensitivity analysis shows that the data on assembling time and material costs may deviate from literature or experiments performed at TU Delft.

Assembling time

Table 5.4 shows the assembling time per element used during this research. These assumptions have been provided by experts from Dura Vermeer and ASK Romein Hillebrand. For injection bolts of the size used during this research (20mm), ASK Romein Hillebrand maintains a total assembly time of 12 minutes. This duration applies to the entire assembly, from fixing the bolt, tightening the bolt to tension, preparing the two-component resin and injecting the bolts. Literature shows that an injection time of 1-2 minutes should be maintained [4]. Furthermore, there is done a lot of research at TU Delft about iSRR connectors [21] [55] [36][69]. Gîrbacea [21] states that experiments under laboratory conditions show that for roughly 20 holes, 500g of resin mix is required and that this can be injected in a time of roughly 20 minutes. This requires two workers, with one of the workers preparing the batches of resin mix, while the other injects the injection bolts with the resin. Although this 12 minutes for the entire assembling process differs with only the injection time of 1 minute, these are major differences. However, ASK Romein Hillebrand is a very experienced company and I will use their assumption during this research.

In addition to the assembling time for the connectors, assumptions are also made for the assembling of the girder beams and cross beams. During my visit, I received a lot of information about this during my tour of the factory hall. However, these times remain assumptions and may deviate from reality.

Financial Costs

To be able to properly compare the different designs, a global cost analysis is made during this research, see Section 7.4. The input costs are shown in section 5.1.1. Also for these assumptions, the steel-related assumptions come from ASK Romein Hillebrand. An assumption that is as realistic as possible has been made for these materials. However, due to the contemporary war, the material prices for steel fluctuate very much. Ukraine was an important steel producer for Europe.

All concrete-related costs come from the experts of Dura Vermeer, just like the general costs for cranes and transport. The costs for the FRP material come from Molenaar's thesis research at FiberCore [45]. Molenaar States that the costs are given by a combination of material and labour costs and that due to the price values are property from FiberCore, indicative values are shown instead of the real values. Because all material costs mentioned before do not come from the same sources, this can also result in a difference between the assumptions.

5.2. Maintenance

Compared to a concrete deck, the construction costs of an FRP deck are significantly higher. From the results of Section 7.5.2 turns out that a bridge with FRP deck is more expensive than a comparable concrete deck. However, in addition to these high construction costs, an FRP deck has the advantage of lower maintenance costs. Nystrom et al. [59], investigated the financial viability of FRP bridges. This study compared the manufacturing, transport, installation and life cycle costs of a comparable FRP and reinforced-concrete bridge. The results of the study show that the maintenance costs of FRP bridges are 44 % lower than for a comparable reinforced concrete bridge.

5.3. Damage during lifetime

It can prevent the bridge structure from being damaged during its lifetime. This can occur due to; imperfections, carelessness of workers, vandalism, use damage and even more options. During this study, these causes will not be further investigated. There will only be described which elements of the structure are assumed to be the most vulnerable and which, from the experience of ASK Romein Hillebrand and Dura Vermeer, will require the most maintenance or will have to be replaced.

Nijgh's [54] research shows that resin injected bolted connections are no less suitable with regard to reusability than bolted connections. All elements remain undamaged because all deformation is taken up by the injection resin material and all forces are equally distributed to the connected element. In addition to damage caused by assembling or disassembling, it could happen that the bolts get damaged during assembling or disassembling. overloading the connections can cause permanent deformations. However, the chance of damage is reduced by using oversized holes, which prevents the bolt from bearing against the flange hole, but that the force is distributed over the entire hole surface via the resin and steel spheres. If damage does occur, and it's just the bolts, they are easy to replace. In the case of the coupler system, this is more difficult. In this case, the entire deck section should be replaced to ensure that enough shear force can be transferred between the deck and the girder beam.

As mentioned before, several experiments have been carried out in the laboratory of TU Delft in which use has been made of iSRR coupler connectors. Section 5.1 clearly described how the assembling process must take place according to Gîrbacea [21] thesis research. This research also states the risk of damaging the decks during placement. One of the possibilities is that due to the high self-weight of the concrete deck, the rods lead to punching of the connector through the concrete, see Figure 5.4. This can occur after the deck is supported with the threaded rods on the upper flange instead of being placed through the holes in the top flange. The cause of this may be due to the inaccuracy of the workers or due to large imperfections so that the rods do not fit into the flange holes. It should be mentioned that these experiments were carried out with a deck thickness of 120 mm without any shear force reinforcement. Calculations in this study showed that a deck thickness of up to 300 mm in combination with shear force reinforcement is required. This reduces the chance punching shear failure.



Figure 5.4: Damage due to placing deck (adapted from [21])

it is possible that during the hoisting of the bridge or deck part something is hit that can cause

damage. Therefore, in the experiments carried out at TU Delft, the concrete decks are fitted with a steel L strip as protection against collision of the deck during lifting, see Figure 3.32.

Due to the fact that during this study it is assumed that the construction will be disassembled after approximately every 10 years to be moved, this is an excellent time to thoroughly inspect the entire construction for damage. Furthermore, this moment facilitates the implementation of maintenance or replacement of the elements. From research, it can be concluded that steel construction elements require more maintenance than concrete or FRP parts. Besides consideration, this will not be further included in this study.

6

Structural parametric model

The goal of the parametric model is to develop a demountable short bridge, by creating multiple variants. The variants are Weighted by means of a trade-off matrix, whose weight factors are described in section 7.1. Due to the fact that these variants can not be modelled by hand, a parametric model is developed to achieve the most optimal design.

This Chapter describes a Grasshopper parametric model for creating the different variants. The definition of the parametric model is described in Section 6.1. The model input is described in Section 6.2 and the design verification in Section 6.3. The results of the parametric model, all created variants are presented in Section 7.2.

6.1. Definition of the parametric model

To achieve the goal of this study, as described in Section 1.2.1, the parametric model has been designed to arrive at the most optimal design in terms of shadow costs, mass and financial costs. These properties to be optimized have a lot of overlap with each other. as can be seen in Section 3.2.1 & 5.1.1.1, the FRP deck has higher costs and shadow costs and a lower mass than the steel beams. This will result in the fact that for all optimizations the FRP deck will be designed as limited as possible.

With the results of the previous chapters, Chapter 2, 3, 4 and 5, it is known how to design the bridge. The parametric environment 'Grasshopper', a visual programming language that runs within the Rhinoceros 3D computer-aided design (CAD) application. The following components are present in the parametric model:

- Set up the geometry of the superstructure, based on assumption 1.2.4;
- Definition of all structural materials, as defined in Section 3.2;
- Definition of all design loads, as defined in section 2.3.1;
- Definition of the properties and behaviour of the demountable shear connectors, as defined in Section 3.3.3;
- Automatic generation and calculations of the most optimal variants, outputted in an excel data file.



Figure 6.1: Logo's of the used software for the design, analysis and optimization of the superstructure

6.1.1. Conceptual overview

Figure 6.2 displays the conceptual overview of the Grasshopper model. The figure illustrates the general set-up of the parametric model in a schematic way. As can be seen, the overview consists of three main parts; the input, Karamba FEM model and Optimization.

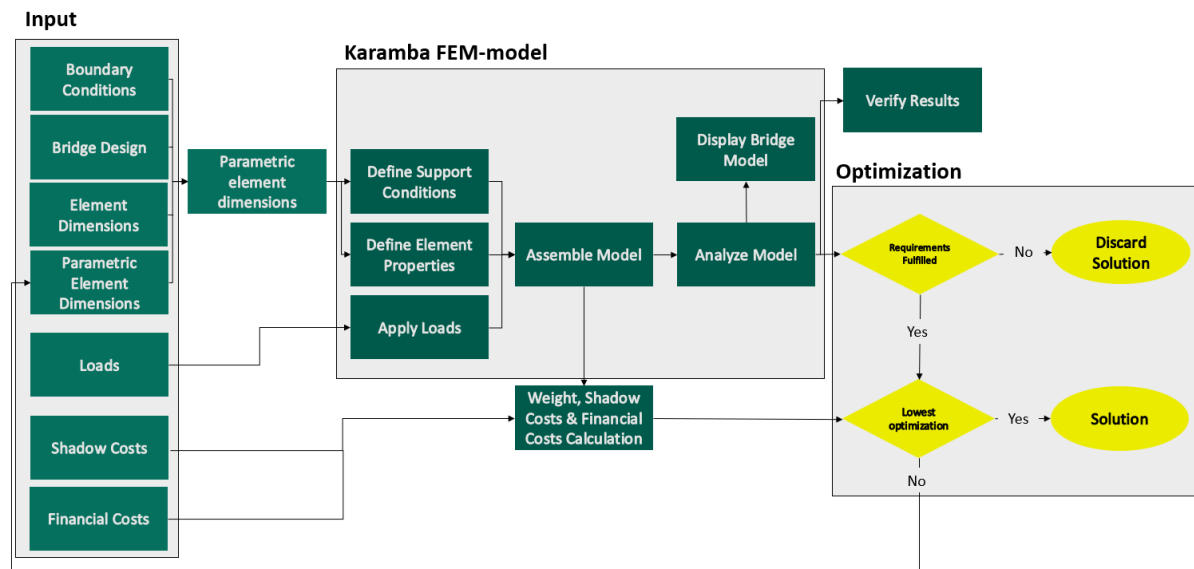


Figure 6.2: Flowchart conceptual overview parametric model

6.1.1.1. Model generation

The following properties are varied and studied during the analysis:

- General
 - Bridge length
 - Bridge Width
 - Outrigger Deck
- Demountable shear connector
- Concrete Deck
 - Concrete class
 - Thickness concrete
- FRP Deck
 - Fibre Volume
 - Height sandwich panel
 - Thickness Facings
 - Thickness Webs
 - Web spacing
- Steel
 - Steel Class
 - Longitudinal Girders
 - Cross beams

6.1.2. FEM elements and analysis

6.1.2.1. Finite element types

When performing Finite Element Analyses the element types can consist of 3 different types of elements; 1D, 2D and 3D [63]. As can be seen in Figure 6.3, 1D elements are the simplest elements. In addition to the dimension difference, the element's order may differ. An element can consist of a straight (linear) or curved (2nd order or higher) line. The advantage of using 1D elements is that the calculation time is often shorter. This makes it highly suitable for designing global load models in combination with the use of steel profiles.

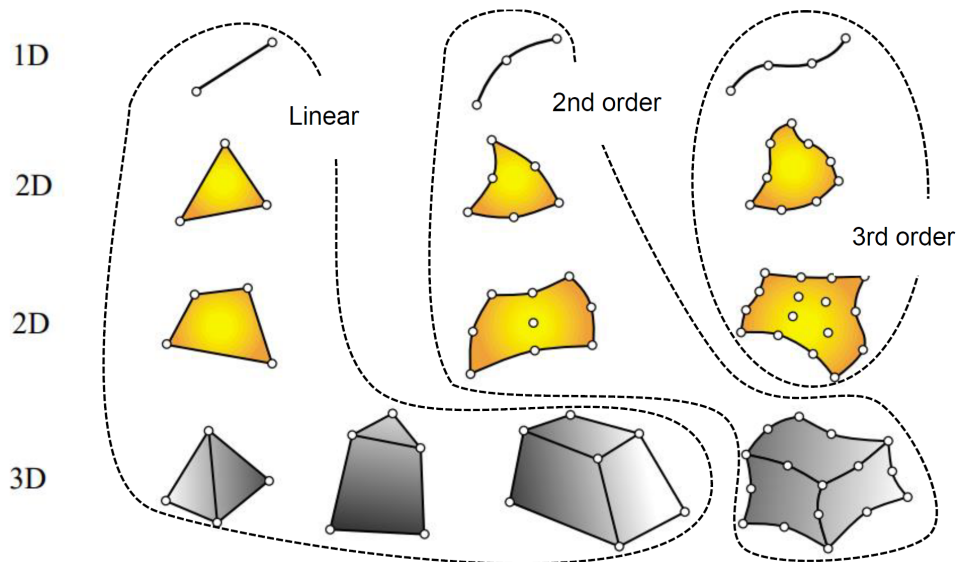


Figure 6.3: FEM elements (adapted from [63])

When a model becomes more extensive and detailed, 2D elements or so-called plate elements are used. The most commonly used is the 4-node quadrilateral shell element which can have a thickness and through linear interpolation, stresses and strains can be calculated at the bottom and top of the element [5]. For higher accuracy, the 2nd order 2D element, also known as the Lagrange quadrilateral can be used.

To model local failures it is necessary to use 3D elements. For example, for FRP material, each separate ply within the laminate can be modelled, and interface conditions can be added to define the failure characteristics of the resin in this way. These so-called volume elements can consist of linear (8 nodes) or quadratic (20) nodes.

It is important to carefully consider which elements will be used in your model. Depending on your goal you can use using higher order or higher dimension elements resulting in more realistic output. However, the calculation time increases significantly. For instance, the difference between a slab with 4-node quadrilateral elements or 8-node volume elements is a doubling of the calculation time. The calculation time becomes even higher when using 2nd-order elements instead of 1st-order elements. During my research, 1D elements are used when using the steel profiles and 2D elements to simulate the deck. The Lagrange quadrilateral elements will not be used, because the calculation time becomes higher and a 4-node quadrilateral is accurate enough.

6.1.2.2. Demountable connectors

As mentioned before, the steel girder beams are modelled as 1D elements and the deck as 2D plate element/ shell element. Between the girder beams and deck, demountable shear connectors (Section 3.3.3) are placed which transfer the forces between the elements. Since these shear connectors have a certain initial elastic behaviour, the connectors are modelled as spring elements with zero length and are generated by connecting two nodes. In this way, the elements can be equipped with an initial stiffness property, and horizontal displacement (slip) can occur (see Figure 6.4). The spring element simulates 2 shear connectors next to each other, which is why the initial stiffness property in Rhino has two times the individual initial stiffness value (2x 145.5 kN/mm, iSRR Connector, see Table 3.9). Figure 6.5 displays a detailed drawing of a spring element connected between the shell element and the beam element.

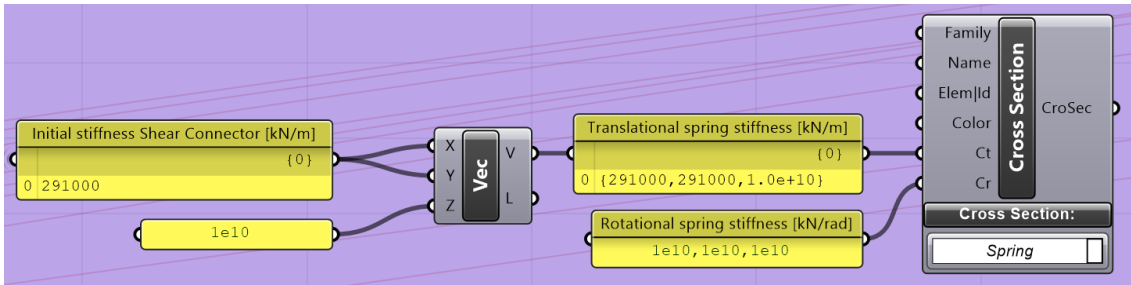


Figure 6.4: Rhino spring component

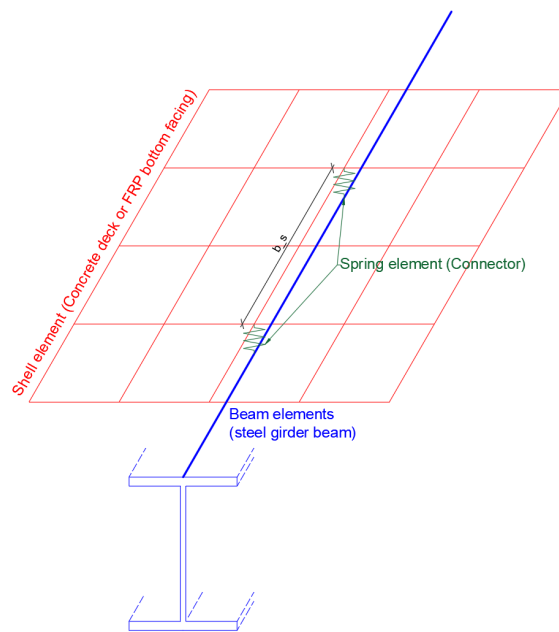


Figure 6.5: Detail of spring element that connect steel beam to FRP deck in model

To ensure that there are 2 nodes at the position of each connector, the beam element is divided into pieces with a length of the centre-to-centre distance between the connectors. Extra nodes have been added to the shell element to ensure that there are 2 nodes at the locations of the connection, see Figure 6.6.

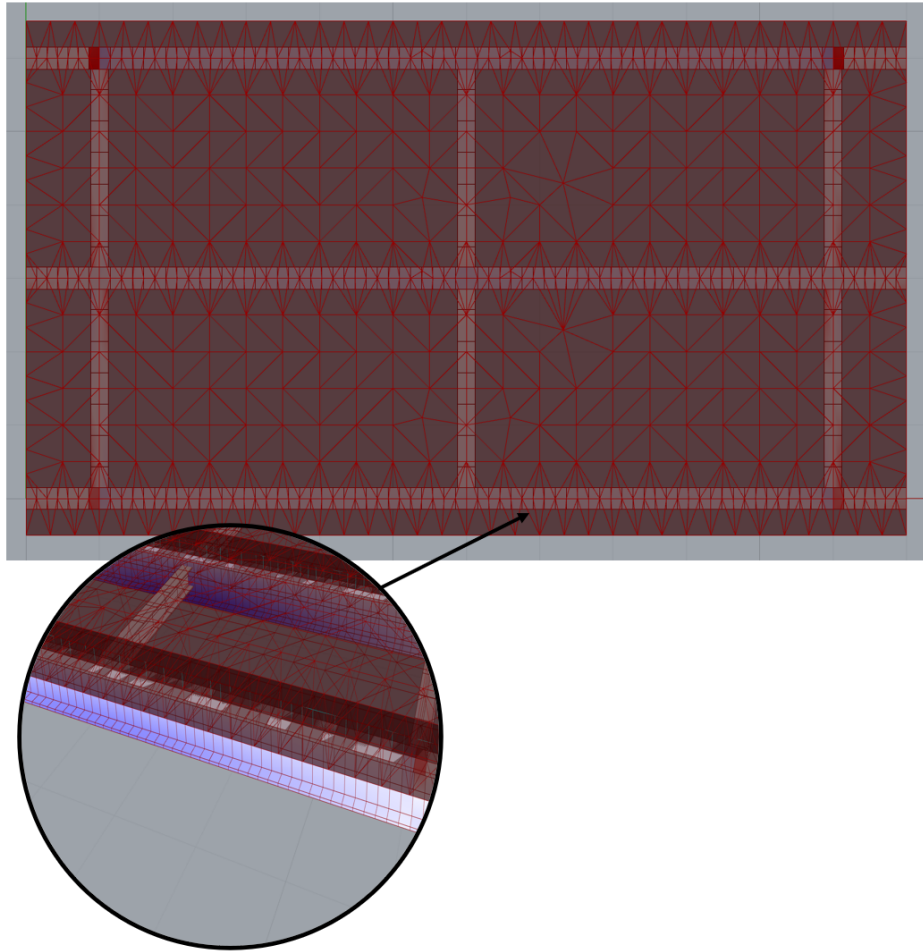


Figure 6.6: Top view of deck with corresponding girder beam

6.1.2.3. Mesh sensitivity

Besides the order of the various elements, the accuracy of the model also depends on the size of the mesh. Generally, a finer mesh results in more accurate results [5]. On the other hand, a finer mesh results in a higher calculation time.

To ensure that mesh independency is achieved it is important to perform mesh sensitivity studies. This was done for both the steel-FRP superstructure and the steel-concrete superstructure.

6.1.3. Variant calculations

First, after the scope limitations of the bridge have been determined in consultation with Dura Vermeer, all input values were gathered. All materials, loads and load combinations are determined. Together with the generated geometry of the design, these data are used for the main calculations.

The basis of the parametric model is the part where the structural calculations take place. These computations are done using the Karamba3D finite element plugin. Using this tool the geometry and loads are efficiently converted into a parametric finite element model. For this study, it is essential that both structural systems based on ULS and SLS are investigated in order to determine which design criteria are leading. Since more than 11.000 bridge design variants have to be generated, the optimization is divided into several runs because otherwise a single optimization run would take too long.

The optimisation is performed with the Galapagos component optimiser in Grasshopper. With this component, all selected inputs are combined to measure the fitness of the solution. In advance, in Galapagos must be indicated which variable should be minimized or maximized. When running the Galapagos component, initially it tries a number of random values for supplied parameters. In the following iteration, it 'cherry picks' sets of parameters that perform well according to the variable to be optimized. This is done iteratively until all possibilities have been checked or the solver times out.

As can be seen in Table 6.2, a total of 12 generate runs are executed.

Table 6.1: Generate possibilities

Material Deck	Shadow Costs	Weight	Financial Costs
Concrete	ULS	ULS	ULS
	SLS	SLS	SLS
FRP	ULS	ULS	ULS
	SLS	SLS	SLS

6.1.4. Model output

As explained before, the parametric model is able to calculate large numbers of bridge variants. The optimized output data obtained by the Galapagos component is automatically stored in a CSV data file after the run. Table 6.2 shows the input and output parameters which are stored after optimization.

Optimization on the properties of mass and shadow costs only depends on the quantities of materials and this calculation speaks for itself. Financial costs, on the other hand, are more complex and, in addition to the material costs, it also depend on the weight of the elements and the number of connections of the structure. All these different parts have been added to the parametric model to simulate a situation that is as realistic as possible.

When optimizing the concrete deck, the amount of reinforcement is also taken into account. This mainly depends on the thickness of the deck and the number of girder beams (lateral distribution). A deck with more thickness results in less need for shear force reinforcement and also a larger number of girder beams reduces the amount of reinforcement required. These quantities have been calculated analytically and added to the parametric model. However, it may be true that these amounts do not correspond exactly to reality because the amount of reinforcement has not been calculated for all assemblies.

Table 6.2: Generate possibilities

Varying input parameter	Output parameter result
Concrete Deck	
Number of Girder beams	Optimized variable (shadow costs, weight or costs)
Steel Class Girder beams	Steel Class
Concrete slab thickness	Maximum deformation
Concrete class	Deformation unity check
	Cross sections
	Thickness Concrete slab
	Concrete Class
	Verification of cross-sections
FRP Deck	
Fibre Volume	Optimized variable (shadow costs, weight or costs)
Height sandwich panel	Steel Class
Thickness Facings	Maximum deformation
Thickness Webs	Deformation unity check
Web spacing	Cross section
	All dimensions FRP sandwich panel
	Verification of cross-sections

The model has been varied with hand calculations which can be found for the steel-concrete model in Appendix A and for the steel-frp model in Appendix B.

6.1.5. Detailed model overview

An overview of the full Grasshopper model is pictured in Figure 6.7 below. To make the model clear and more understandable, all components with a common function are grouped and labelled. In the section below the figure, all labels are briefly described.

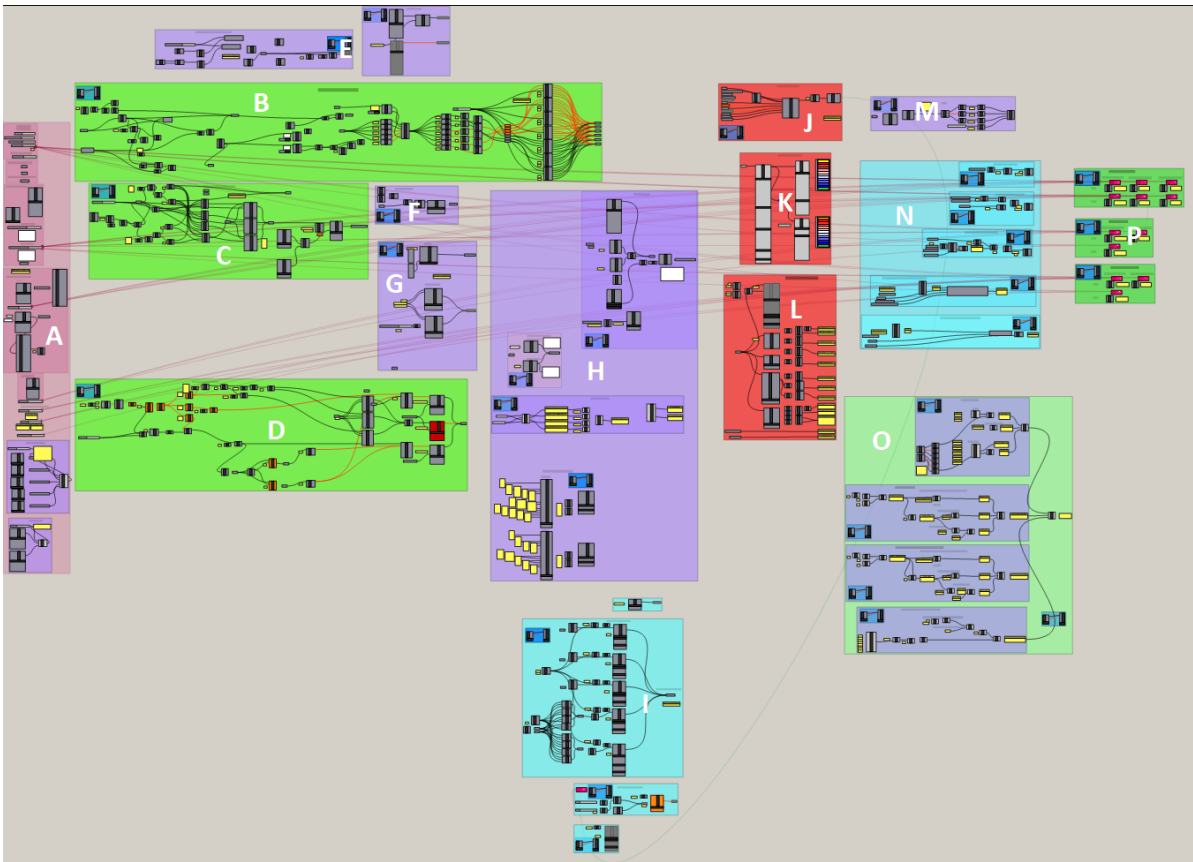


Figure 6.7: Overview Grasshopper Model

The following components correspond to the labels, which are pictured in Figure 6.7.

- A. Define input parameters
- B. Define steel geometry
- C. Define concrete deck geometry
- D. Define FRP deck geometry
- E. Define the stiffness and c.t.c. distance of demountable shear connectors
- F. Define Supports
- G. Define Connections
- H. Connecting materials to geometry
- I. Define and determine the design loads (SLS and ULS)
- J. Model calculations
- K. Model Visualization
- L. Numeric Results
- M. Calculation shadow costs
- N. Boundaries (Stress, max deflection, ratio span/construction height)
- O. Material Costs
- P. Galapagos optimization

6.2. Model input

6.2.1. Steel

6.2.1.1. Material properties

The steel material properties which are used in the parametric model are shown in Table 3.7.

6.2.2. Concrete

The concrete material properties which are used in the parametric model are shown in Table 3.8.

6.2.3. Fbre Reinforced Polymers

The FRP material properties which are used in the parametric model are shown in Table 3.2.1.1.5.

6.3. Design verification

Before optimizing, the model must first be verified to ensure that the model produces reliable results. This is done by applying a simple uniform distributed load of 10 kN/m^2 on the deck and comparing the outcomes with hand calculations. This method is carried out in combination with a concrete deck and with an FRP deck. Table 6.3 shows the results for deflection of the FEM model and the hand calculations. Full hand calculations for verification of the concrete deck can be found in Appendix A.1, and for the FRP deck in Appendix B.4.

Table 6.3: Analytical verification FEM model

Deflection at midspan			
	Rhino [mm]	Analytical [mm]	Difference [%]
Concrete	5.86	5.83	5.1
FRP	15.3	13.6	12.5

7

Bridge design

In this section, the method of the structural analyses is described.

7.1. Trade-off matrix

This section will explain how the Trade-Off Matrix (TOM) is built up and explain the performance indicator with the associated weight.

To come to the best design for a demountable short bridge, the five options are weighed against each other with this TOM. Several performance indicators are set, after which a corresponding factor is added. Table 7.1 provides an overview of all performance indicators, including the weight factors. Five categories are made, based on which features are most important. The different categories consist of a total of 9 performance indicators, where the sum of the weight of these performance indicators is set to 100.

Table 7.1: Weight factors of TOM

Weight factors TOM		
Strategy	Performance indicator	Weight
Effective	Construction height	15
	Deflection	5
Shadow Costs		25
Demountability	Reaching connections	15
	Complexity	10
Transportable Costs	Weight	10
		20
Total		100

The following Table 7.2 describes the performance criteria.

Table 7.2: Criteria for TOM

Criteria for TOM		
Strategy	Performance indicator	Criteria
Effective	Construction height	What is the required construction height conform SLS and ULS requirements
	Deflection	
Shadow Costs		What are the shadow costs per design?
Demountability	Reaching connections	Are the connections easy to reach? Do the bolts have to be fixed under the bridge?
	Complexity	Are the connections easy to take apart?
Transportable Costs	Weight	What is the total weight of the design
	Production	What are the production costs
	Displacement	What costs have to be incurred to move a bridge (including disassembly and assembly)

7.2. Variants

Parametric models, with concrete deck and FRP deck, are both optimized to create a bridge with the lowest Shadow Costs, Weight and Financial Costs whilst still fulfilling all Eurocode norms (Section 2.3.2).

This section describes the six variants which are developed. The first four are developed with a concrete deck, and the last one with an FRP deck. All variants have HEB profiles as girder beams, except for variant 2 which has HEM profiles as girder beams. All variants are developed by selecting the best design from the various optimization categories.

Optimizing the FRP deck on Shadow Costs, Mass and Financial Costs has led to the same model for all optimizations. Therefore of the following number of variants, only 1 variant with an FRP deck instead of a concrete deck.

7.2.1. Variant 1

Table 7.3: Properties variant 1

Variant 1		
Girders	Number of Girder beams	4
	Girder Profile	HEB500
Deck	Concrete Class	C45/55
	Height Deck	250 mm
Shear Connector	SRR connector	
	Initial Stiffness	145.5 kN/mm
	ctc distance	375 mm

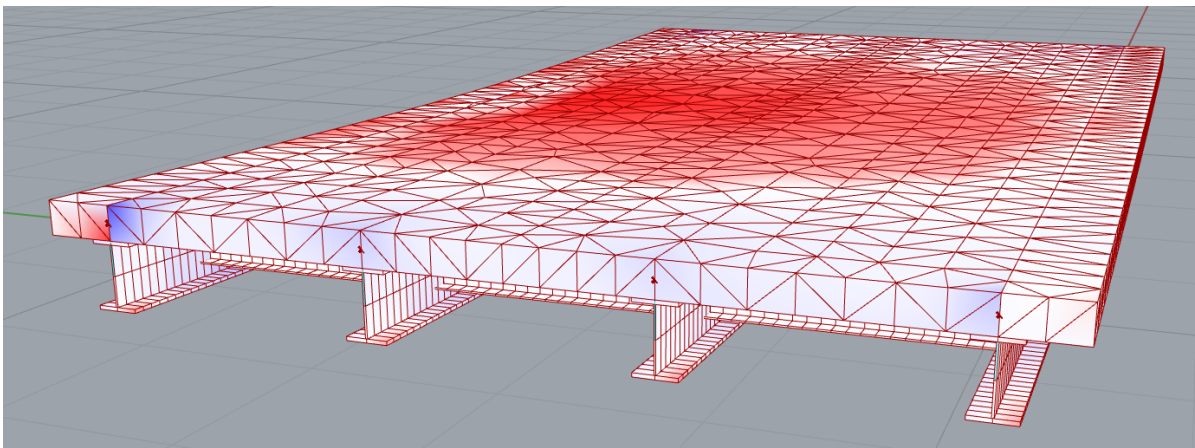


Figure 7.1: Variant 1

7.2.2. Variant 2

Table 7.4: Properties variant 2

Variant 2		
Girders	Number of Girder beams	4
	Girder Profile	HEB500
Deck	Concrete Class	C30/37
	Height Deck	300 mm
Shear Connector	SRR connector	
	Initial Stiffness	145.5 kN/mm
	ctc distance	375 mm

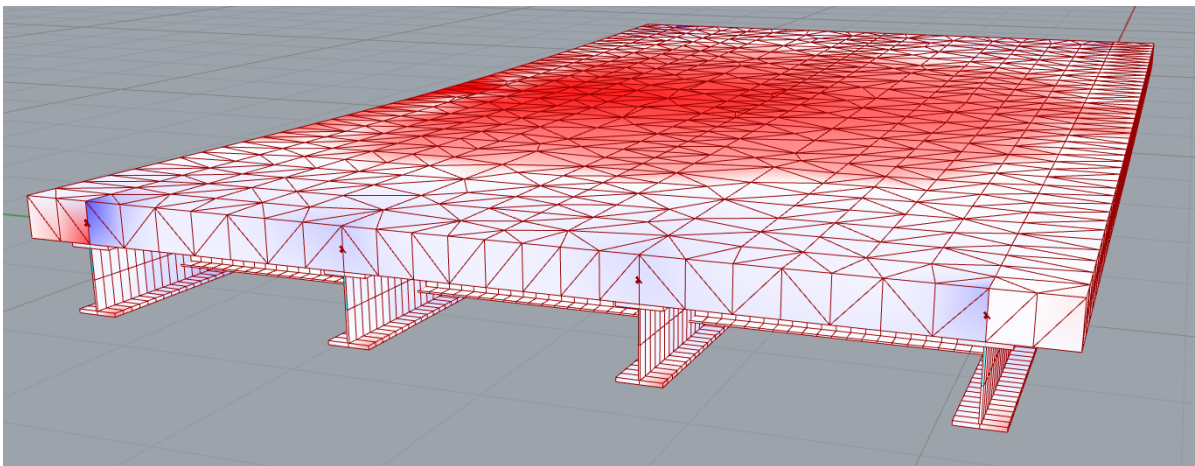


Figure 7.2: Variant 2

7.2.3. Variant 3

Table 7.5: Properties variant 3

Variant 3		
Girders	Number of Girder beams	7
	Girder Profile	HEB450
Deck	Concrete Class	C30/37
	Height Deck	300 mm
Shear Connectors	SRR connector	
	Initial Stiffness	145.5 kN/mm
	ctc distance	350 mm

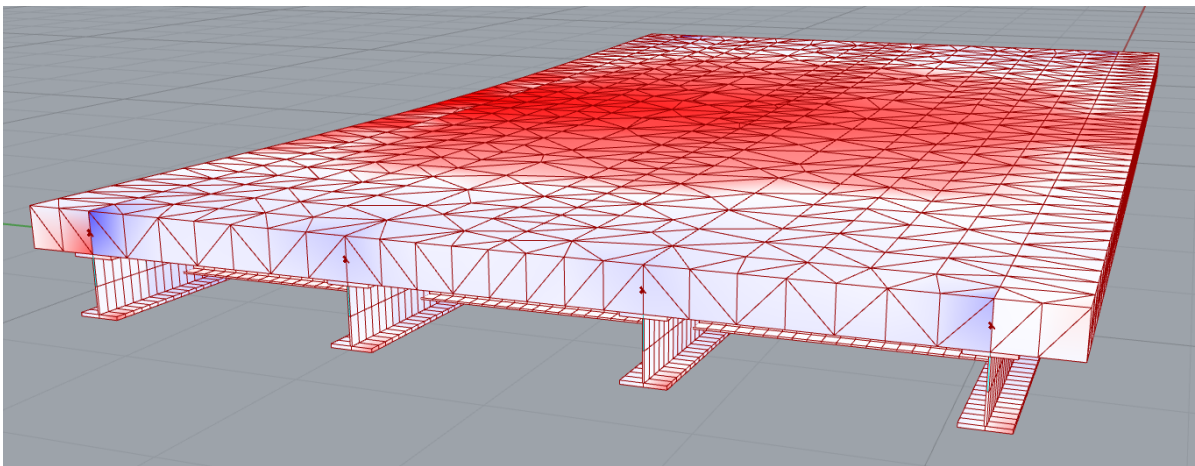


Figure 7.3: Overview variant 3

7.2.4. Variant 4

Table 7.6: Properties variant 3

Variant 4		
Girders	Number of Girder beams	5
	Girder Profile	HEB550
Deck	Fibre Volume	50 %
	Height Sandwich panel	185 mm
	Thickness Facings	25 mm
	Thickness Webs	10 mm
	ctc distance webs	100 mm
Shear Connector	SRR connector	
	Initial Stiffness	73 kN/mm
	ctc distance	160 mm

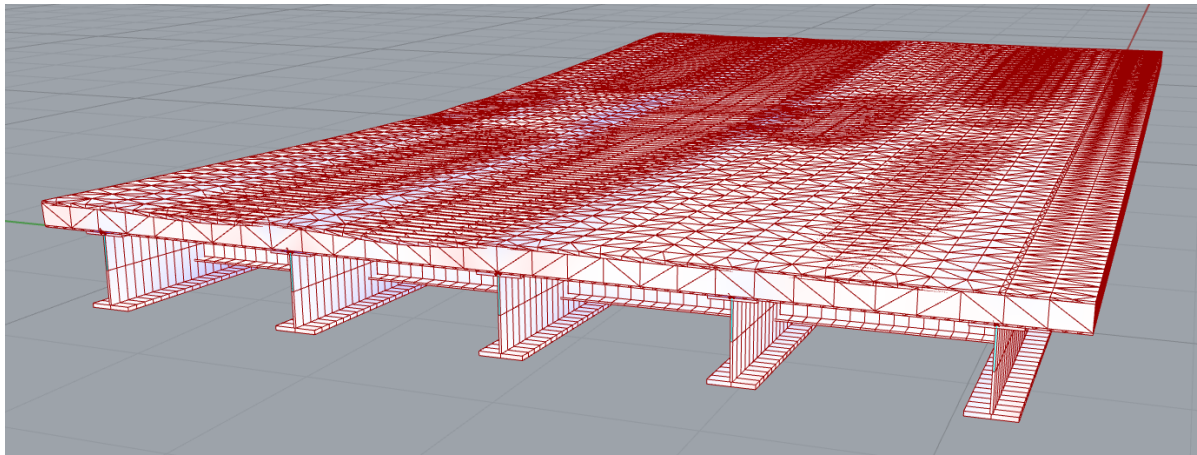


Figure 7.4: Overview variant 4

7.3. Life Cycle Assessment

This section describes the methodology in environmental impact quantification. As discussed in Chapter 4, environmental impact is an important part of this research. The environmental impact is calculated conducting an LCA. The goal of this LCA is to compare the environmental impact of the different variants and to determine to what extent the development of a circular bridge is environmentally beneficial compared to the traditional non-circular bridge. Therefore, only the stages and processes that differ between the variants and the traditional design will be taken into account.

All LCA stages are shown earlier in this report in Section 4.1.1, Figure 4.2. The stages that differ between the circular variants and the traditional design are:

- Production stage (A1-A3): because different materials are used;
- Transport to construction site (A4): the different materials entail differences in weight and size;
- Construction on-site (A5): the traditional design partly consists of in-situ concrete & heavier variants require larger cranes;
- End-of-life (C1-C4 and D): non-circular designs differ in terms of waste and reuse.

7.3.1. LCA input

The environmental impact value of all used materials can be found in Section 4.1.3, Table 4.2. The full calculations of the LCA described in Appendix C.

7.4. Cost analysis

During this research, circular alternatives are compared to the traditional solution. Therefore, it is important to take the costs into account during designing. The costs for the steel part were determined with help of the company Hillebrand. Hillebrand is one of the largest steel construction companies in the Netherlands and helped me a lot with determining the costs. The calculation department of Dura Vermeer helped me with the costs for the concrete part, labor costs and transport costs. The costs for the FRP part and the demountable connections are obtained from literature research. After the costs of all different materials, labour and parts were known, they were included in the parametric model.

7.5. Results

In this section, the results of the different analyses are described.

7.5.1. Environmental impact results

This section displays the results of the LCA, which can be found in Appendix C. As can be seen in Table 7.7, the environmental impact of the circular designs can be up to 60 % higher than the traditional non-circular design. However, after its full lifespan, the traditional design has over 400 % higher environmental impact since this design cannot be reused.

Table 7.7: Overview environmental costs per design

Shadow costs per design			
Design	Material Costs [€]	Transport Costs [€]	Total Costs (100 year) [€]
Traditional Design	3.050	369	34.191
Variant 1	5.043	198	7.022
Variant 2	4.634	227	6.906
Variant 3	4.430	225	6.678
Variant 4	15.793	73	16.524

Figure 7.5 displays the shadow costs over the lifetime of all variants and of the traditional design. The traditional design is non-circular, and that is why this graph clearly shows how much environmental impact can be saved with a circular design.

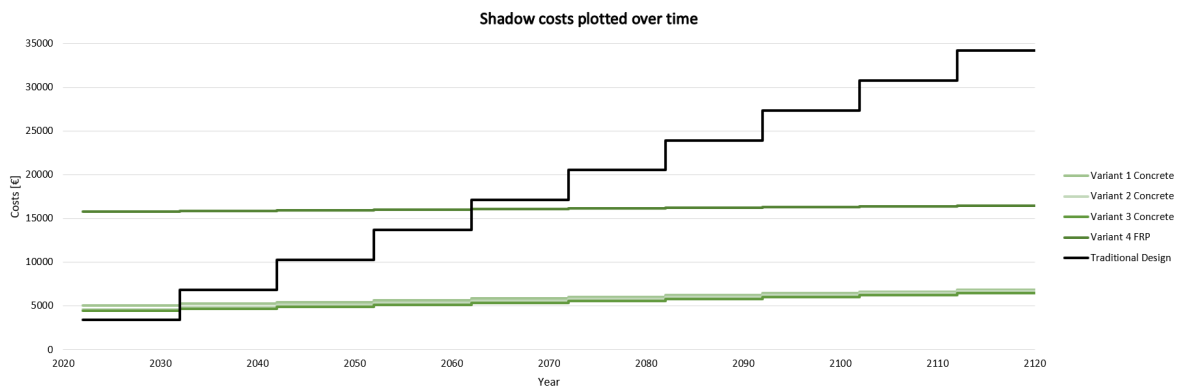


Figure 7.5: Shadow costs all variants over time

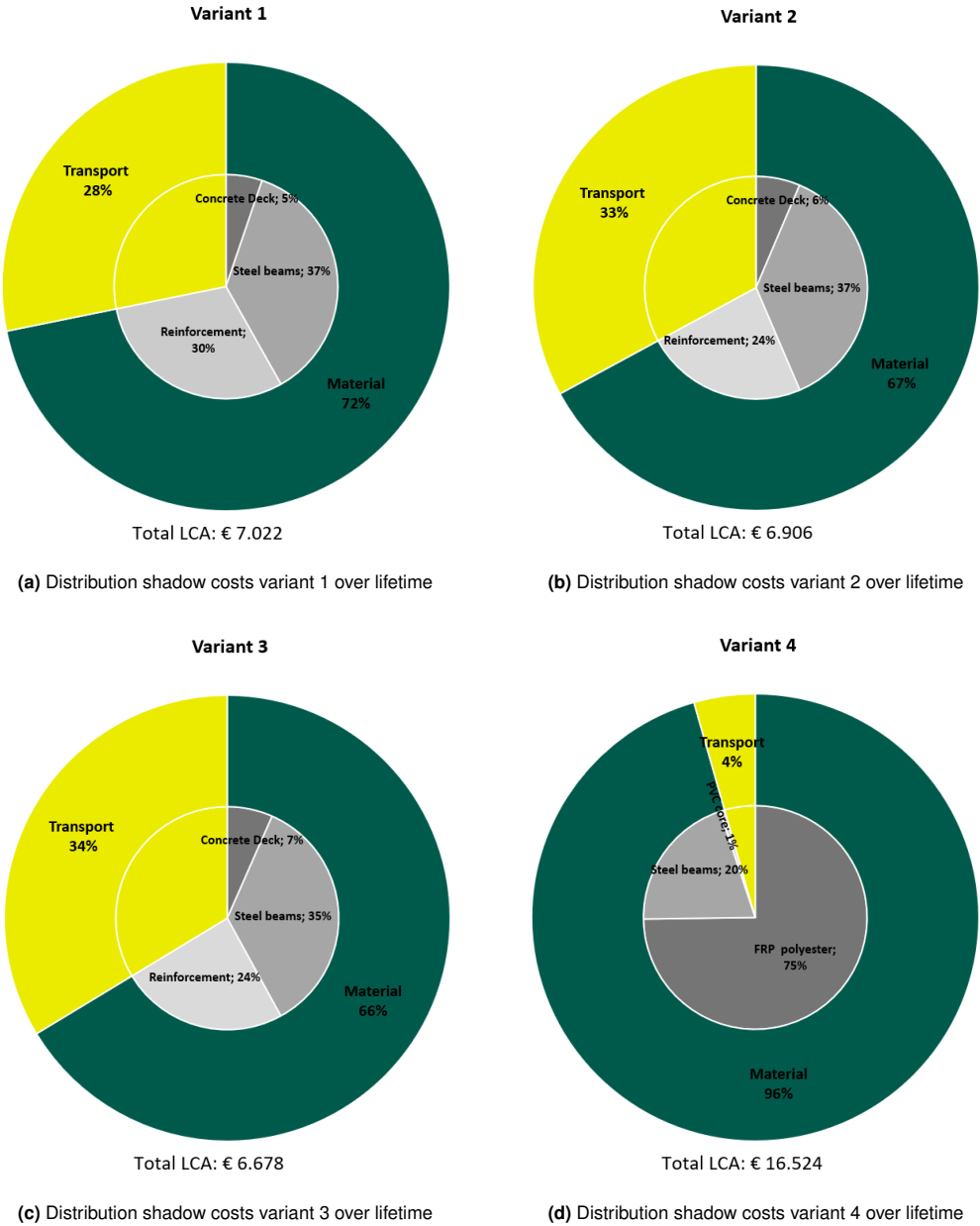


Figure 7.6: Distribution shadow costs all variants

7.5.2. Costs results

This section describes the results of the cost analysis. The costs of the traditional design and of the circular designs are displayed, showing the different distribution of costs. The full calculations of this cost analysis can be found in appendix D.

7.5.2.1. Traditional design

The traditional design, which is elaborated in Section 2.2.4 consists of the costs shown in Table 7.8.

Table 7.8: Overview financial costs traditional design

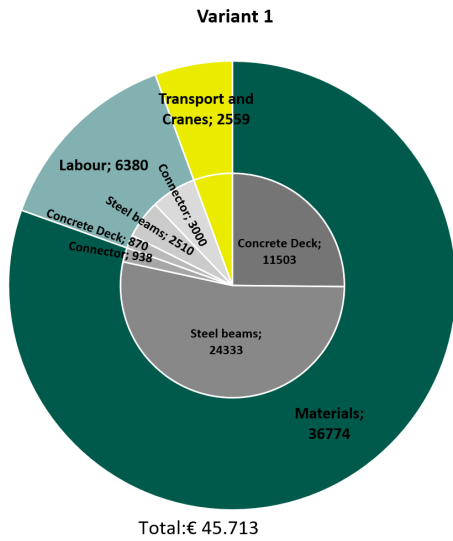
Financial costs traditional design		
Material Costs	Parts	€
Material Costs	Prefab Volstortliggers	21.000
	Prefab edge girder	2.576
	In-situ concrete (including reinforcement and pump)	10.110
	Formwork	325
Labour Costs	Placing prefab Volstortliggers	1.320
	Pouring in-situ concrete	1.080
Other costs	Crane placing prefab Volstortliggers	800
	Crane Framework	360
	Transport prefab Volstortliggers	1.600
Total		39.474

7.5.2.2. Circular design

In total, six different circular variants are developed using the parametric model (Section 7.2). In this section, all costs of these variants are explained more in detail. The results of the costs analysis is listed in Table 7.9, Figure 7.7 presents all results using pie charts. The left pie displays the costs to place the bridge one time, meanwhile, the right chart applies for the entire lifespan, in which the bridge is moved 10 times.

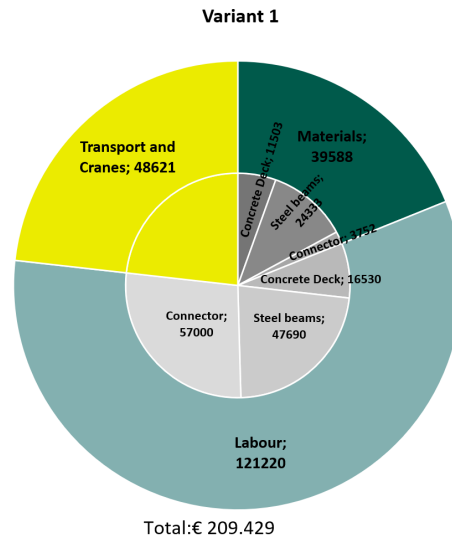
Table 7.9: Overview costs per design

Financial costs per design			
Design	Material Costs [€]	Mounting + Demounting Costs [€]	Total Costs (100 year) [€]
Traditional Design	35.540	7.860	434.000
Variant 1	45.712	18.159	209.143
Variant 2	44.415	18.279	208.926
Variant 3	43.310	18.907	213.473
Variant 4	90.043	24.197	307.816



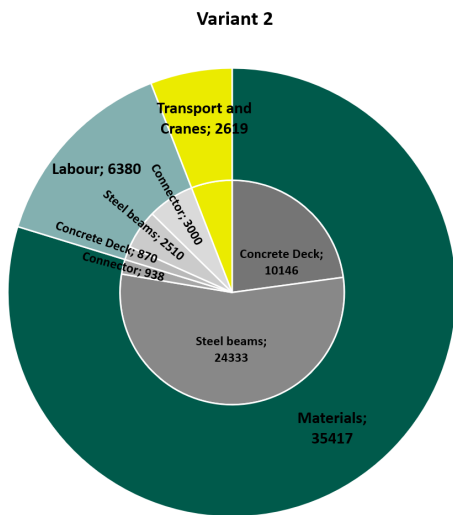
Total:€ 45.713

(a) Distribution costs variant 1



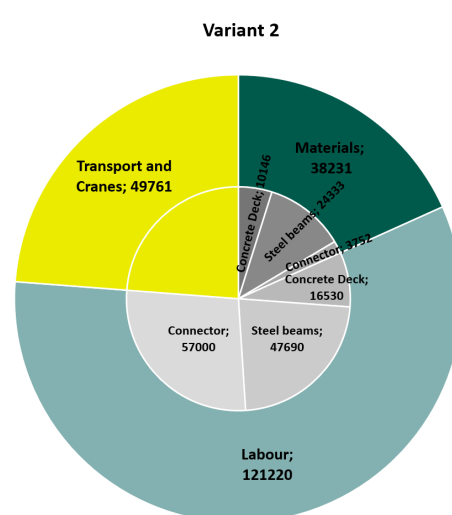
Total:€ 209.429

(b) Distribution costs variant 1 over lifetime



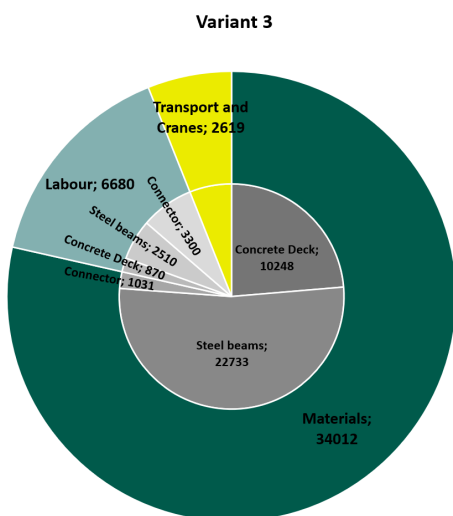
Total:€ 44.416

(c) Distribution costs variant 2



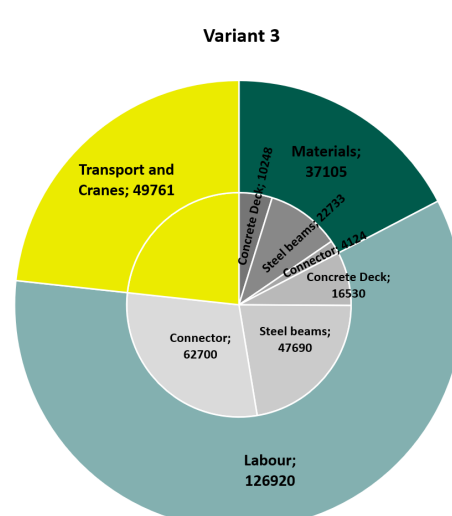
Total:€ 209.212

(d) Distribution costs variant 2 over lifetime



Total:€ 43.311

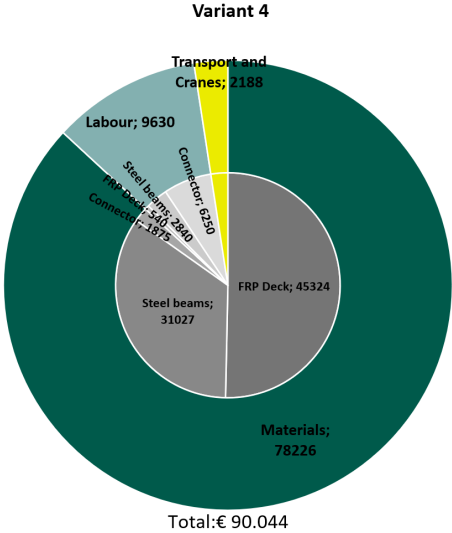
(e) Distribution costs variant 3



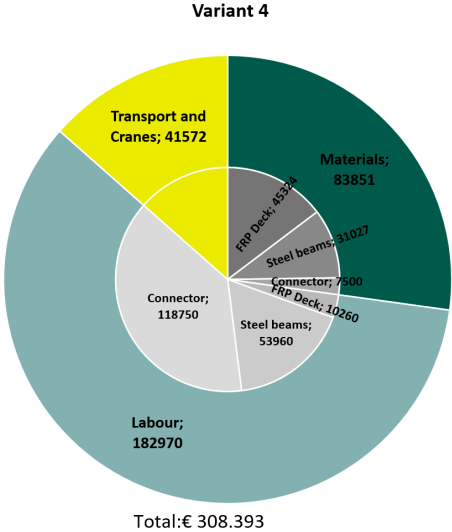
Total:€ 213.786

(f) Distribution costs variant 3 over lifetime

Figure 7.7: Distribution costs all variants



(g) Distribution costs variant 4



(h) Distribution costs variant 4 over lifetime

Figure 7.7: Distribution costs all variants

Graph 7.8 below displays the costs over lifetime of all variants and of the traditional design. As can be seen, the total cost of all variants is initially higher than that of the traditional design. However, the traditional design must be completely demolished at end of life. Because of this, circular designs are, based on costs, after about 2 reconstructions less expensive than the traditional design. Therefore,

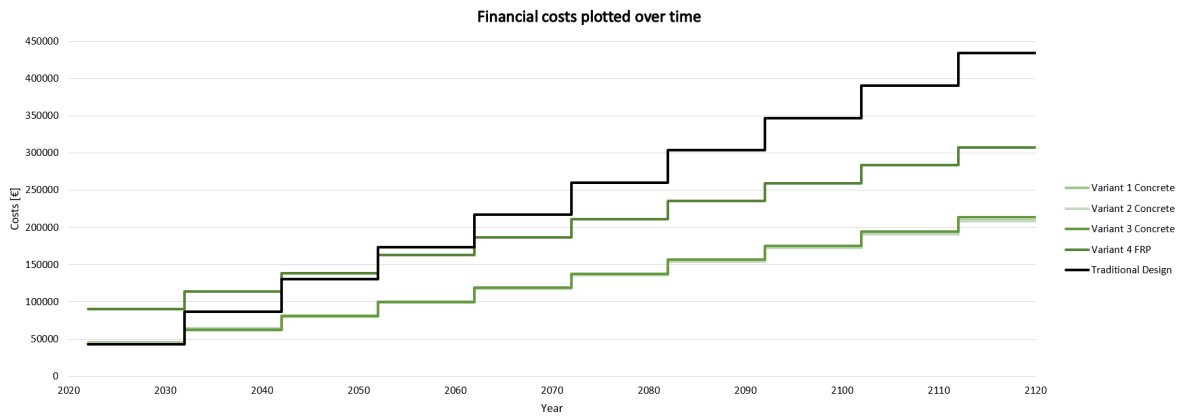


Figure 7.8: Costs over lifetime all variants

The following Table 7.10 shows how the costs of a variant are built up. The complete calculations can be found in Appendix D.

Table 7.10: Overview costs Variant 2

Financial costs variant 2		
Material Costs	Parts	€
Material Costs	Concrete Prefab slab	4.005
	Reinforcement prefab slab	6.141
	Steel Girder beams	20.114
	Steel Cross beams	4.219
	Injection Bolts	938
Labour Costs	Placing prefab deck	870
	Placing Steel beams	2.510
Other costs	Mounting injection bolts	3.000
	Crane placing prefab Deck	800
	Crane Steel beams	400
	Transport deck & beams	1.200
Total		44.197

7.5.3. Time to mound

In this section, Figure 7.9 displays the number of labour hours required per variant for assembling or disassembling of the structure. The bars are divided into labour time for mounting the deck, steel beams and shear connectors between the girder beams and the deck.

It is clear to see that the demountable connections have a major influence on the number of hours required. Compared to the traditional design, the variants require 4 to 6 times more labour hours for assembling and disassembling of the bridge structure.

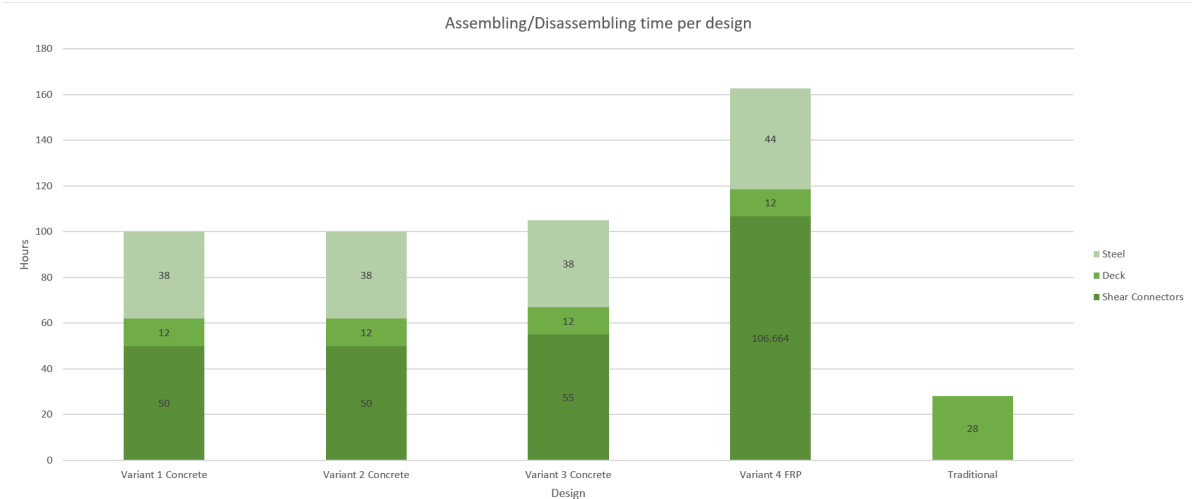


Figure 7.9: Labour hours per design

7.6. Final design

7.6.1. Result TOM

In Section 7.1, the performance indicators with corresponding weight factors of the Trade-Off Matrix were explained. This section displays the results of the analysis and literature study, which are combined into a trade-off. Appendix E displays and explains the TOM in detail. Table 7.11 displays the structural analysis results of all variants and table 7.12 displays the results of the TOM.

Table 7.11: Structural analysis results for variants

Variant	Mass [kg]	Costs [€]	LCA [€]	Deflection SLS [mm]	Construction height [m]	Number of connectors	max. Stress beams ULS [N/mm ²]
1	65.967	209.143	7.022	21.7	0.75	250	327
2	75.736	208.926	6.906	17.9	0.8	250	306
3	74.920	213.473	6.678	20.9	0.75	275	343
4	24.393	307.816	16.524	43.6	0.76	800	306

Table 7.12: Results TOM of all variants

Trade-Off Matrix						
Category	Performance indicator	Weight	V1	V2	V3	V4
Effective	Construction height	15	+	0	+	++
	Deflection	5	+	++	+	0
Shadow Costs		25	+	+	++	--
Demountability	Number of connections	15	++	++	+	--
	Complexity	10	-	-	-	+
Transportable	Weight	10	-	--	--	++
Costs		20	++	++	+	--
Total		100	73.75	68.75	68.75	35

As can be seen in Figure 7.12, variant 1 ultimately has the highest score and is the best design for a demountable bridge with a span of 12 meters. The TOM results show that these variants are common across all performance indicators. Furthermore, FRP sandwich panel deck has no advantage under the boundary conditions of this study over the variant with a concrete deck. The shadow costs and financial costs are higher for this type of deck than for a concrete deck, and these are performance indicators with a high weight.

IV

Results and final remarks

8

Discussion

This chapter describes the discussion on the presented results. Since this research covers a broad subject, it is inevitable to make assumptions and simplifications. Throughout this report, all these assumptions have been made with the relevant background theory in mind to obtain a balanced set of assumptions. Nevertheless, the assumptions will slightly influence the results. This is not a problem, as the focus of the research is on the general feasibility of demountable reusable superstructures as a replacement for the traditional design.

8.1. Discussion

8.1.1. Structural analysis

During this research, a variant study is done, where all variant studies are based on the parametric Grasshopper model. Because the geometry, materials and other properties (see Section 6.1.1.1) are generated parametrically, a wide variety of bridges can easily be modelled. Furthermore, a model in Rhinoceros has the advantage that it can be extended very easily by adding new components and parameters. However, there are also limitations to using Karamba3D. For example, Karamba3D is focussing especially on global analysis, containing less detailed aspects. As a result, the parametric model is especially suited for the preliminary design stage only, and further design should then use other FEM software that provides more accurate results on connection and composite behaviour. In this section, the consequences of this accuracy are discussed.

Simplification of details

Due to the fact that the analyzes are too global to properly design details, the required amount of shear connectors have been determined with hand calculations. As described in Section 6.1.2.2, the shear connections are modeled as a spring element with 0 lengths between the girder beam and the deck. These elements clearly influence the vertical deformations of the structure. However, the horizontal deformations are so limited that they cannot be properly determined by using the model.

8.1.2. Weight

Prior to this research, I thought that the weight would have an important influence on the transportability and on the ease of mounting and dismounting of the bridge. However, when calculating the costs, the difference in weight did not appear to have a major impact on the end result. For example, the cost of transporting a concrete deck is, with a 400 euros difference, twice as high as for an FRP deck. The difference in production costs of an FRP deck is about 90,000 euros more expensive so these transport costs can be almost neglected. The weight will mainly have a major influence on larger spans or movable bridges.

Substructure

Due to time limitations for this thesis research, it is necessary to maintain assumptions and limitations (see Section 1.2.4). Therefore, the entire substructure does not affect the results of this study. In retrospect, this has a more adverse effect on the variant with FRP deck than on the variant with concrete deck.

Since the total weight of the design with FRP deck is with 24.393 kilograms much lighter than the designs with a concrete deck, with a weight of 65.967 kilograms, a cheaper foundation can be used. This would mean that the final costs of both designs would come closer together, or that the FRP variant would even be financially more advantageous than the concrete design.

8.1.3. Maintenance

The life cycle costs were not included in this study. As described in Section 5.2, it has been shown that a concrete deck differs in maintenance from an FRP deck. Nystrom et al. [59] state that a bridge with FRP deck has 44% lower maintenance costs than a concrete deck. This not only affects the results of financial costs, but also affects the results of shadow costs.

8.1.4. ECI

Part of an LCA are modules C and D, end-of-life stages. These moduli were not included in this study, even though it can be established that the designed designs differ from each other with modules C and D. As described in Section 4.1.5, the residual value differs between the materials used; Steel, concrete and FRP. For example, steel can now be recycled 100%, which therefore has a higher residual value than concrete, which can only be crushed into aggregates after use, which is a very cost-intensive process.

9

Concluding remarks

This chapter presents the conclusions and recommendations of this thesis. In the first section, the conclusions are stated by answering the research questions. The conclusions are followed by recommendations for further research.

9.1. Conclusion

In order to answer the undermentioned research questions, a parametric model has been created with which, by means of optimization, a total of four different pre-design variants have been developed (Section 7.2). The variants were then weighed against each other by means of a TOM (Section 7.6.1), after which the best design could be designated. The conclusions described in this chapter are a summary of all the conclusions described during this study, leading to the answer to the main research question.

9.1.1. Answer to the sub-questions

The following sub-questions were answered in this thesis:

1. What are the specific limitations and challenges of a concrete or FRP deck?

A composite bridge is usually equipped with a concrete deck. Nowadays, it is increasingly common to opt for an FRP sandwich panel because of the advantage of, for example, saving on weight and maintenance costs.

In terms of strength and stiffness, an FRP sandwich panel is not inferior to a concrete deck (see calculations in Appendix A & B). Furthermore, due to the variations in the ratio of fibres to resin, geometry, and adhesion between the two constituents of the orientation of the fibres, the material can be easily optimized. However, when looking at the results in Section 7.5.1 & 7.5.2. The costs and shadow costs of FRP decks are many times higher than those of the concrete deck design. This is due to the material, but also because more shear connectors are required to transfer the same amount of shear force. Section 3.3.3 shows that the initial stiffness of demountable steel-concrete connections with 145.5 kN/mm versus 73.0 kN/mm for steel-FRP connections is much higher.

Since a concrete deck is much heavier than an FRP sandwich panel deck, an FRP deck is more economical in terms of transport and required crane capacity. This advantage is clearly visible in the calculations. However, it appears that under the boundary conditions of this study, the advantages of an FRP deck do not outweigh the disadvantages.

2. What are the most influential components during developing a demountable superstructure?

In order to answer this question, the following aspects must be considered: connections, weight & time to mound and dismount. After the various aspects have been described, this research question can be answered.

(a) Connections

In order to develop a demountable structure, it is necessary that the connections between the deck and the steel girder beams are demountable. These connections are important and ensure that the entire connection can be taken apart without any damage. The connection must be very stiff so that the different parts work well together and no permanent deformations will occur. On the other hand, the construction must be easily assembled and disassembled, which tends towards simple bolt connections. In this study, several existing connections have been investigated, eight different connection types can be used in combination with a concrete deck and 3 with an FRP deck. These connections are described in Section 3.3.3. The coupler connector in combination with steel reinforced injection bolts (Figure 3.32) will be used for the variants with a concrete deck and for the FRP deck resin injected coupler connectors are applied (Figure 3.45).

As described in Section 7.5.2, a large amount of the total financial costs consists of labour costs. According to ASK Romein Hillebrand's data, the total assembly time for a single bolt of this size is 8 minutes. For an injection bolt, this is even 12 minutes per bolt. This results in an amount of 11 euro labour costs per connector (including mixing the resin components and tightening the bolt). In total, the connections together with the material costs are 27 to 38 percent of the total costs of the variants (see Section 7.7).

(b) Weight

The results of the generated variants show that the variant with FRP deck, with a total weight of 24.393 kilos, is up to 67 percent lighter than the variants with a concrete deck, with 65.967 to 75.736 kilos. The choice of the material of which the deck consists of has the greatest influence on the total weight. Concrete slabs result in a much higher total construction weight than FRP sandwich panels.

With the assumptions and limitations of this study, the difference in weight influences the financial costs and shadow costs. These differences are described in Section 7.5 and are influenced by transport and required crane capacity. The FRP variant has an environmental impact of € 73 for a single transport compared to € 198 for the lightest variant with a concrete deck. The FRP variant has as financial costs for the necessary cranes and transports an amount of € 2188 compared to € 2559 for the lightest concrete variant. However, when looking at the end of the 100-year lifespan, the FRP variant does not score more favorably than the concrete variants on shadow costs and financial costs. Therefore, it can be concluded that under the assumptions and limitations of this study, the favorable weight of FRP has little influence on the results of the final design.

(c) Time to mound and dismount

Figure 7.9 in Section 7.5.3 shows the total amount of labour hours per design. As can be seen, all circular variants have an enormously high number of labour hours. As mentioned before, the mounting process of the demountable connectors takes a long time. The traditional time compared to the traditional design, the circular variants require almost 10 times more working hours. As described earlier, this is therefore also the biggest problem of a circular design.

3. What is the cost analysis per design?

The results of the cost analysis are presented in Section 7.5.2. Figures 7.7 display the cost distribution over the material, labour and transport & cranes. It can be concluded that at the end of the lifespan of 100 years, in which the superstructure has been moved 10 times, labour costs have the greatest influence on the total costs with up to 59 % of the total costs. Most of these labour costs are caused by the assembly and disassembly of the demountable shear connectors (with 39%) and of the steel girders and crossbars (with 17%). This is caused by the fact that bolts are very labour-intensive.

The costs plotted in time give more insight into the cost development of the circular variants over time, presented in Figure 9.1. As can be seen, it is in the long term very beneficial to be able to reuse the construction.

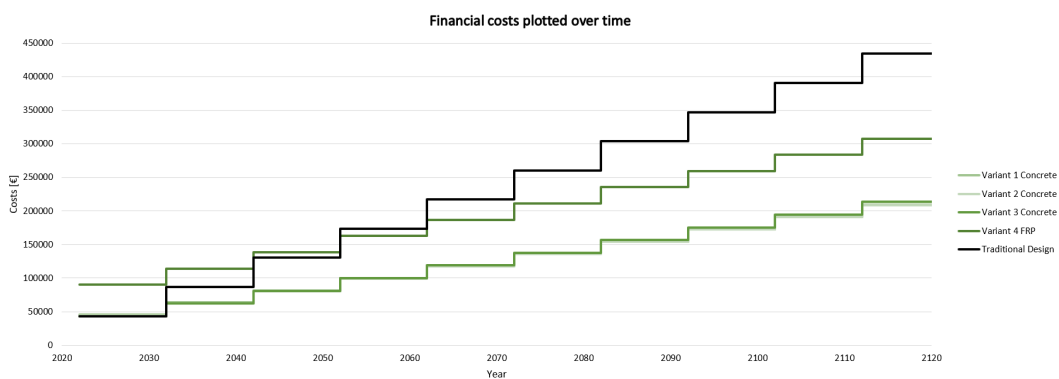


Figure 9.1: Financial costs plotted over time

4. What is the environmental impact of the developed superstructures?

(a) Which factors influence the quantification, and how can an objective comparison be obtained?

This research compared the shadow costs of the non-circular traditional superstructure, three circular steel-concrete composite superstructures and a circular steel-FRP composite superstructure. A lifespan of 100 years has been considered, with the design being moved a total of 10 times. With the boundary conditions and assumptions of this study, the results of Section 7.5.1 show that the environmental impact is mainly influenced by the composition of materials, where transport has only a small influence on the total. Figure 7.6 displays the shadow costs distribution per variant. Of the variants with a concrete deck, at least 28 % of the total shadow costs originate from transport. The lighter FRP variant has 63 % lower LCA transport costs. However, the FRP variant has at least 3.1 times higher LCA material costs than those with concrete decks. This leads to the conclusion that materials have the most influence on lower shadow costs

(b) What are the total shadow costs of the different designs?

The life cycle assessment results are presented in Section 7.5.1. The multiple figures (Figures 7.7, 7.5, 7.6) clearly show the differences between the circular variants and the traditional non-circular design. In the initial stage, after the designs have been built for the first time, the traditional design has a lower environmental impact than the circular designs. However, the shadow costs of the circular designs with a concrete deck become lower after about 1 move than the traditional design. And the circular design with FRP deck becomes lower after more than 5 moves. Therefore, it can be concluded that with the

boundary conditions and assumptions of this study, it becomes more beneficial with regard to financial charges when the superstructure is designed for less than 50 years. Since it appears that variants with an FRP deck have a significantly higher environmental impact, they become financially more attractive when the superstructure is designed for less than 25 years.

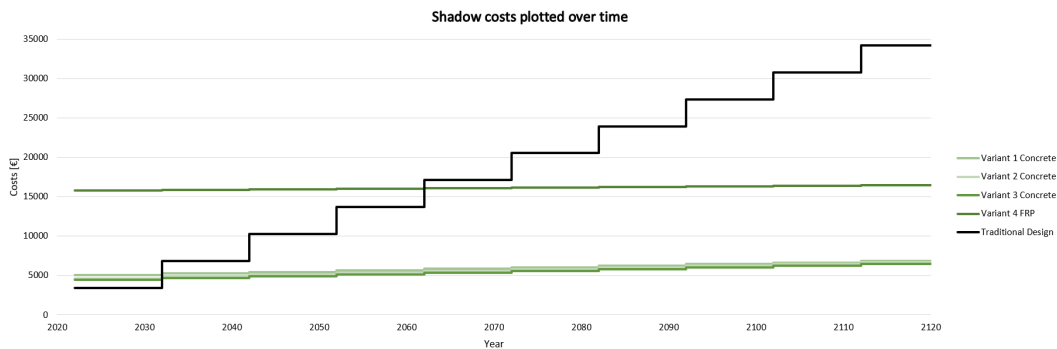


Figure 9.2: Shadow costs plotted over time

9.1.2. Answer to the main research question

Based on this research, the main research question as defined in Section 1.2.2 can be answered:

What is the optimal structure, in terms of shadow costs, mass and financial costs, for a modular superstructure?

This study concludes that it can be advantageous to replace the traditional design with a demountable design, with the assumed boundary conditions of this study. All developed variants have an advantage with regard to environmental impact and financial costs compared to the traditional design, assuming a lifespan of 100 years in which it is moved 10 times.

Since the developed variants with concrete deck differ little from each other. The difference is mainly between the concrete deck and FRP deck. In this research, the designs with concrete deck score better on the performance indicators of the TOM than the FRP deck. However, it should be noted that the limitations of this study are more disadvantageous for the FRP deck than for the concrete deck. Maintenance during lifetime is not included in this study and the foundation is not included, while the total weight of the developed design with FRP is 3 times lighter than with concrete deck.

Therefore, it is difficult to ultimately choose which design is the most optimal. This differs per situation and this study provides a good overview of how it can be determined for which situation the most optimal design can be developed.

9.2. Recommendations for further research

Due to the limited duration of thesis research, there are scope limitations and assumptions. For improvements and further research, the following recommendations are stated.

- Additional research on the entire bridge structure, including the substructure, would be insightful, and even important. This would result in a more objective comparison between an FRP deck and a concrete deck in follow-up research.
- Research on life cycle costs could result in more efficient results and could therefore be included in further research.
- Only module A of the LCA was included in this study. Because this research focuses on reusable bridges made of different types of materials, it would be an added value in future research to also include modules C and D, end of life stage in the research, also because research shows that the residual value of the materials used differs from each other.

References

- [1] Hoda Abuzied et al. *A review of advances in design for disassembly with active disassembly applications*. June 2020. DOI: [10.1016/j.jestch.2019.07.003](https://doi.org/10.1016/j.jestch.2019.07.003).
- [2] Luigi Ascione et al. *PROSPECT FOR NEW GUIDANCE IN THE DESIGN OF FRP STRUCTURES*. Tech. rep.
- [3] Amir Reza Ghiami Azad et al. "A technique for strengthening existing continuous non-composite steel girder bridges using post-installed shear connectors and inelastic moment redistribution". In: *IABSE Conference, Vancouver 2017: Engineering the Future - Report*. International Association for Bridge and Structural Engineering (IABSE), 2017, pp. 1217–1224. ISBN: 9783857481536. DOI: [10.2749/vancouver.2017.1217](https://doi.org/10.2749/vancouver.2017.1217).
- [4] R. Bjorhovde, A. Colson, and R. Zandonini. *Connections in steel structures III: Behaviour, strength and design*. 1996.
- [5] Johan Blaauwendraad. *Plates and FEM*. Tech. rep. URL: www.springer.com/series/6557.
- [6] Bouwen met Staal. "Duurzaamheid + staal". In: ().
- [7] Stewart Brand. *How buildings learn: What Happens After They're Built*. 1994.
- [8] *Circular Furniture*. URL: <https://circularfurniture-sawyer.eu/circular-economy/>.
- [9] *Classic Laminate Theory Tool*. URL: <https://delfttools.tudelft.nl/frp/>.
- [10] Consolis Spanbeton. *SJP FLEX 300-800*.
- [11] Fruzsina Csillag. *Demountable deck-to-girder connection of FRP-steel hybrid bridges*. Tech. rep. 2018. URL: <http://repository.tudelft.nl/>.
- [12] Sander De Bruyn et al. *Environmental Prices Handbook*. Tech. rep. 2018.
- [13] Ellen MacArthur Foundation. "Towards a circular economy business rationale for an accelerated transition". In: (2015).
- [14] *Eurocodeapplied Concrete design properties*.
- [15] *Eurocodeapplied Steel design properties*. URL: <https://eurocodeapplied.com/design/en1993/steel-design-properties>.
- [16] *Excel sheet Spanbeton of Dura Vermeer*.
- [17] *Frostburg state university*. URL: <https://www.frostburg.edu/programs/life-cycle-fac-management/Illustrated-Cradle-to-Grave-Process.php>.
- [18] C. C. Fu et al. "Field Performance of the Fiber-Reinforced Polymer Deck of a Truss Bridge". In: (2007).
- [19] N Gattesco and Giuriani E. *Experimental Study on Stud Shear Connectors Subjected to Cyclic Loading*. Tech. rep. 1. 1996, pp. 1–21.
- [20] Swaroop Gharde and Balasubramanian Kandasubramanian. *Mechanothermal and chemical recycling methodologies for the Fibre Reinforced Plastic (FRP)*. May 2019. DOI: [10.1016/j.eti.2019.01.005](https://doi.org/10.1016/j.eti.2019.01.005).
- [21] Ioan Andrei Gîrbacea. "Assessment of demountable steel-concrete composite flooring systems". PhD thesis. 2018.
- [22] *Guide-to-composites*. Tech. rep.
- [23] *Haitsma*. URL: <https://www.haitsma.eu/bridges-viaducts/hko>.
- [24] Rade Hajdin and Snezana Masovic. "Establishment of a Quality Control Plan-WG3". In: (2018). DOI: [10.13140/RG.2.2.28730.03526](https://doi.org/10.13140/RG.2.2.28730.03526). URL: <https://www.researchgate.net/publication/334122094>.

- [25] Shukur Abu Hassan. "Linear Static Finite Element Analysis of Composites Hat-Stiffened Laminated Plates". In: (2005). DOI: [10.13140/RG.2.1.3857.7368](https://doi.org/10.13140/RG.2.1.3857.7368). URL: <https://www.researchgate.net/publication/283121558>.
- [26] Neil M. Hawkins. "Strength in Shear and Tension of Cast-in-Place Anchor Bolts". In: (1987).
- [27] Jun He, Ahmed S.H. Suwaed, and George Vasdravellis. "Horizontal pushout tests and parametric analyses of a locking-bolt demountable shear connector". In: *Structures* 35 (Jan. 2022), pp. 667–683. ISSN: 23520124. DOI: [10.1016/j.istruc.2021.11.041](https://doi.org/10.1016/j.istruc.2021.11.041).
- [28] *Holcon BV*. URL: <https://www.holcon.com/16/producten/volstortliggers>.
- [29] Alexander Hollberg and Jürgen Ruth. "LCA in architectural design—a parametric approach". July 2016. DOI: [10.1007/s11367-016-1065-1](https://doi.org/10.1007/s11367-016-1065-1).
- [30] *Janson Bridging*. URL: <https://www.jansonbridging.nl/nl/oplossingen/bruggen/plaatliggerbrug-jsb>.
- [31] Henk M Jonkers. *Reader CIE4100 CEG-3MD-Materials & Environment-Sustainability Group*. Tech. rep.
- [32] Dae Sung Jung et al. "Demountable Bolted Shear Connector for Easy Deconstruction and Reconstruction of Concrete Slabs in Steel–Concrete Bridges". In: *Applied Sciences (Switzerland)* 12.3 (Feb. 2022). ISSN: 20763417. DOI: [10.3390/app12031508](https://doi.org/10.3390/app12031508).
- [33] Thomas Keller and Martin Schollmayer. "Plate bending behavior of a pultruded GFRP bridge deck system". In: *Composite Structures* 64.3-4 (June 2004), pp. 285–295. ISSN: 02638223. DOI: [10.1016/j.compstruct.2003.08.011](https://doi.org/10.1016/j.compstruct.2003.08.011).
- [34] Julian Kirchherr, Denise Reike, and Marko Hekkert. "Conceptualizing the Circular Economy: An Analysis of 114 Definitions". In: *SSRN Electronic Journal* (Sept. 2017). DOI: [10.2139/ssrn.3037579](https://doi.org/10.2139/ssrn.3037579).
- [35] Jan Knippers and Markus Gabler. *New Design Concepts for Advanced Composite Bridges-The Friedberg Bridge in Germany*. Tech. rep. 2006.
- [36] A. Kozma et al. "Push-out tests on demountable shear connectors of steel-concrete composite structures". In: *Structures* 21 (Oct. 2019), pp. 45–54. ISSN: 23520124. DOI: [10.1016/j.istruc.2019.05.011](https://doi.org/10.1016/j.istruc.2019.05.011).
- [37] M S J Kuijpers. *Circularity in the structural design*. Tech. rep.
- [38] Gunup Kwon, Michael D. Engelhardt, and Richard E. Klingner. "Behavior of post-installed shear connectors under static and fatigue loading". In: *Journal of Constructional Steel Research* 66.4 (Apr. 2010), pp. 532–541. ISSN: 0143974X. DOI: [10.1016/j.jcsr.2009.09.012](https://doi.org/10.1016/j.jcsr.2009.09.012).
- [39] Dennis Lam, Xianghe Dai, and Eleonora Saveri. "Behaviour of Demountable Shear Connectors in Steel-Concrete Composite Beams". In: (2013).
- [40] S van leeuwen et al. "TNO-2018-circulair bouwen in perspectief". In: (2018).
- [41] Qing Quan Liang. *Analysis and Design of Steel and Composite Structures*. CRC Press, 2015.
- [42] Valbona Mara, Reza Haghani, and Peter Harryson. "Bridge decks of fibre reinforced polymer (FRP): A sustainable solution". In: *Construction and Building Materials* 50 (2014), pp. 190–199. ISSN: 09500618. DOI: [10.1016/j.conbuildmat.2013.09.036](https://doi.org/10.1016/j.conbuildmat.2013.09.036).
- [43] W. T. Marshall, H. M. Nelson, and H. K. Banerjee. "An experiment study of the use of high-strength friction grip bolts as shear connectors in composite beams." In: (1971).
- [44] *Masterseries*. URL: <https://www.masterseries.com/blog/2019/calculating-the-shear-connection-of-a-composite-beam-to-eurocode-4>.
- [45] L Molenaar. *Design and optimization of FRP traffic decks considering uplift bolt forces Based on analytical and numerical approaches*. Tech. rep. URL: [http://repository.tudelft.nl/..](http://repository.tudelft.nl/)
- [46] Piero Morseletto. "Targets for a circular economy". Feb. 2020. DOI: [10.1016/j.resconrec.2019.104553](https://doi.org/10.1016/j.resconrec.2019.104553).
- [47] Jonathan P Moses et al. "Evaluation of Effective Width and Distribution Factors for GFRP Bridge Decks Supported on Steel Girders". In: (2006). DOI: [10.1061/ASCE1084-0702200611:4401](https://doi.org/10.1061/ASCE1084-0702200611:4401).

- [48] *Nederland circulair in 2050*. Tech. rep. 2016.
- [49] “NEN-EN 15804”. In: ().
- [50] “NEN-EN 1990”. In: ().
- [51] *NEN-EN 1991-2*. Tech. rep. 2021. URL: www.nen.nl.
- [52] “NEN-EN 1992-1-1”. In: ().
- [53] “NEN-EN 1994-1-1”. In: ().
- [54] M P Nijgh. *New Materials for Injected Bolted Connections A Feasibility Study for Demountable Connections*. Tech. rep. 2017.
- [55] Martin Paul Nijgh, Haohui Xin, and Milan Veljkovic. “Non-linear hybrid homogenization method for steel-reinforced resin”. In: *Construction and Building Materials* 182 (Sept. 2018), pp. 324–333. ISSN: 09500618. DOI: [10.1016/j.conbuildmat.2018.06.111](https://doi.org/10.1016/j.conbuildmat.2018.06.111).
- [56] R.P.L Nijssen. *Composieten Basiskennis*. 2e. 2013.
- [57] Itaru Nishizaki et al. *A Case Study of Life Cycle Cost based on a Real FRP Bridge*. Tech. rep. 2006.
- [58] Haico van Nunen, N. A. Hendriks, and Peter A. Erkelens. *Influence of service life on Life Cycle Assessments*. Tech. rep.
- [59] Halvard E Nystrom et al. “Financial Viability of Fiber-Reinforced Polymer “FRP... Bridges”. In: (2003). DOI: [10.1061/ASCE0742-597X200319:12](https://doi.org/10.1061/ASCE0742-597X200319:12).
- [60] G. Olivier and F. Csillag. “Bolted joints for FRP decks”. In: (2020).
- [61] Marko Pavlović et al. “Bolted shear connectors vs. headed studs behaviour in push-out tests”. In: *Journal of Constructional Steel Research* 88 (2013), pp. 134–149. ISSN: 0143974X. DOI: [10.1016/j.jcsr.2013.05.003](https://doi.org/10.1016/j.jcsr.2013.05.003).
- [62] Marko S Pavlović. *RESISTANCE OF BOLTED SHEAR CONNECTORS IN PREFABRICATED STEEL-CONCRETE COMPOSITE DECKS*. Tech. rep. 2013.
- [63] V Pillwein. *An Introduction to Finite Element Methods*. 2015.
- [64] Alessio Pipinato. *Innovative Bridge Design Handbook*. 2015.
- [65] José Potting et al. *CIRCULAR ECONOMY: MEASURING INNOVATION IN THE PRODUCT CHAIN*. Tech. rep. 2017.
- [66] Scott Reeve. “FRP bridge decking - 14 years and counting”. In: (2010).
- [67] *Retro Bridge*. URL: <https://www.gww-bouw.nl/tag/retro-bridge/>.
- [68] *Sarens Kraantabellen*. URL: <https://www.sarens.nl/kranen/kraangegevens.htm>.
- [69] Alkyoni Sarri. *Assessment of steel-concrete shear connector system with resin injected bolts*. Tech. rep. 2019. URL: [http://repository.tudelft.nl/..](http://repository.tudelft.nl/)
- [70] Sindu Satasivam et al. “Composite actions within steel-FRP composite beam systems with novel blind bolt shear connections”. In: *Engineering Structures* 138 (May 2017), pp. 63–73. ISSN: 18737323. DOI: [10.1016/j.engstruct.2017.01.068](https://doi.org/10.1016/j.engstruct.2017.01.068).
- [71] R.G. Slutter and John. W. Fisher. *Fatigue strength of shear connectors Fatigue Strength of Bridge Members View project*. Tech. rep. 1966. URL: <https://www.researchgate.net/publication/254634305>.
- [72] Joris Smits. “Fiber-Reinforced Polymer Bridge Design in the Netherlands: Architectural Challenges toward Innovative, Sustainable, and Durable Bridges”. In: *Engineering* 2.4 (2016), pp. 518–527. ISSN: 20958099. DOI: [10.1016/J.ENG.2016.04.004](https://doi.org/10.1016/J.ENG.2016.04.004).
- [73] Vivian W.Y. Tam. “Economic comparison of concrete recycling: A case study approach”. In: *Resources, Conservation and Recycling* 52.5 (Mar. 2008), pp. 821–828. ISSN: 09213449. DOI: [10.1016/j.resconrec.2007.12.001](https://doi.org/10.1016/j.resconrec.2007.12.001).
- [74] Cem Topkaya, Joseph A. Yura, and Eric B. Williamson. “Composite Shear Stud Strength at Early Concrete Ages”. In: *Journal of Structural Engineering* 130.6 (June 2004), pp. 952–960. ISSN: 0733-9445. DOI: [10.1061/\(asce\)0733-9445\(2004\)130:6\(952\)](https://doi.org/10.1061/(asce)0733-9445(2004)130:6(952)).

- [75] Fei Yang et al. "Shear performance of a novel demountable steel-concrete bolted connector under static push-out tests". In: *Engineering Structures* 160 (Apr. 2018), pp. 133–146. ISSN: 18737323. DOI: [10.1016/j.engstruct.2018.01.005](https://doi.org/10.1016/j.engstruct.2018.01.005).
- [76] Aixi Zhou. *Stiffness and strength of fiber reinforced polymer composite bridge deck systems Fire ember production from wildland and structural fuels View project Future of Firefighting and Career Training-Advancing Cognitive, Communication, and Decision Making Capabilities of Firefighters View project*. Tech. rep. 2002. URL: <https://www.researchgate.net/publication/238032748>.
- [77] Bin Zou et al. "Evaluation of effective flange width by shear lag model for orthotropic FRP bridge decks". In: *Composite Structures* 93.2 (Jan. 2011), pp. 474–482. ISSN: 02638223. DOI: [10.1016/j.compstruct.2010.08.033](https://doi.org/10.1016/j.compstruct.2010.08.033).

A

Hand calculations superstructure with concrete deck

A.1. Verification parametric model with concrete deck

The from Rhinoceros obtained results should be verified to be sure that there are no errors in the model. This is done by applying a simple uniform distributed load case on the superstructure and comparing the outcomes with hand calculations. This section describes an extensive elaboration of hand calculations.

A.1.1. General data

$L = 12 \text{ m}$

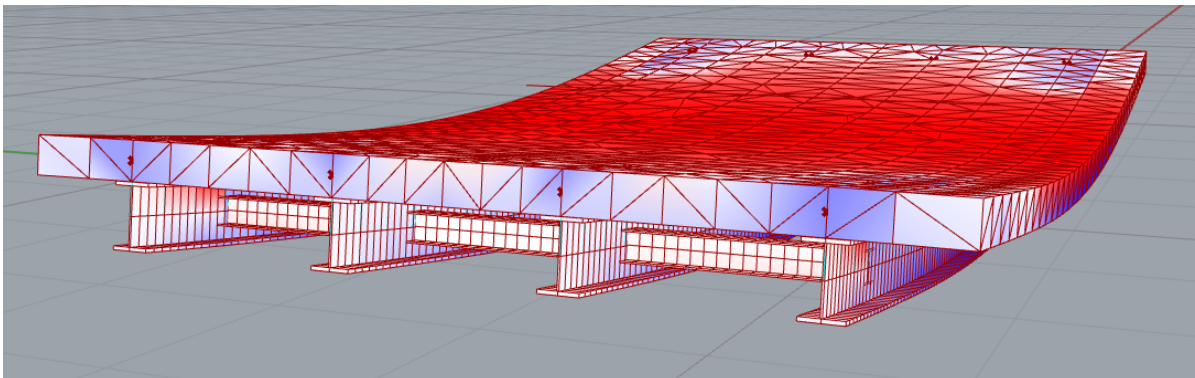


Figure A.1: Rhino structure verification

A.1.1.1. Steel Girders

The four girders consist of HEB500 profiles and have the following dimensions:

$$h_a = 500 \text{ mm}$$

$$b_f = 300 \text{ mm}$$

$$t_f = 28 \text{ mm}$$

$$t_w = 14.5 \text{ mm}$$

$$A_a = 23864 \text{ mm}^2$$

$$E_a = 210000 \text{ N/mm}^2$$

$$I_a = 107176 \cdot 10^4 \text{ mm}^4$$

$$\rho_a = 78.5 \text{ kN/m}^3$$

A.1.1.2. Concrete slab

On top of the girders is a concrete slab attached.

$$\begin{aligned} h_c &= 300 \text{ mm} \\ b_{\text{eff},c} &= \min(b_c, \frac{L}{4}) = 1750 \text{ mm} \\ f_{ck} &= 30 \text{ N/mm}^2 \\ E_c &= 32800 \text{ N/mm}^2 \\ I_c &= \frac{b_{\text{eff},c} h_c^3}{12} = 3.94 \cdot 10^9 \text{ mm}^4 \\ \rho_c &= 25 \text{ kN/m}^3 \end{aligned}$$

A.1.1.3. Bending stiffness

$$\begin{aligned} r_c &= \frac{h_c}{2} = 150 \text{ mm} \\ r_s &= \frac{h_a}{2} = 250 \text{ mm} \\ r &= r_c + r_s = 400 \text{ mm} \\ EI_0 &= E_a I_a + E_c I_c = 3.54 \cdot 10^{14} \text{ kNm}^2 \\ EI_{\text{inf}} &= EI_0 + \frac{E_a A_a \cdot E_c A_c}{E_a A_a + E_c A_c} \cdot r^2 = 9.75 \cdot 10^{14} \text{ kNm} \end{aligned}$$

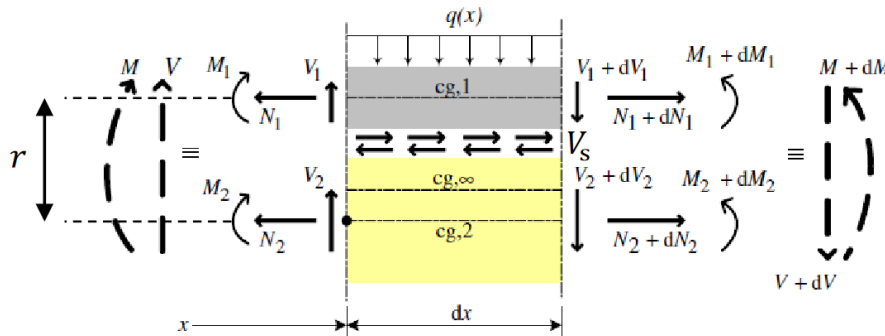
A.1.1.4. Differential equation

Figure A.2: Differential equation for composite interaction

$$\begin{aligned} \phi &= -\frac{dw}{dx} \\ \kappa &= \frac{d\phi}{dx} \\ M &= \frac{EI_{\text{inf}}}{\alpha^2} \left(\frac{dw}{dx^4} - \alpha^2 \cdot \frac{dw}{dx^2} - \frac{q}{EI_0} \right) \\ V &= \frac{dM}{dx} \\ N_1 &= \frac{\kappa \cdot EI_0 - M}{r} \\ r &= \frac{h_a}{2} + \frac{h_c}{2} \\ V_s &= \frac{dN_1}{dx} \\ s &= \left| \frac{V_1}{K} \right| \\ K &= 2 \cdot \frac{k_{sc}}{b_s} \\ \frac{dV}{dx} &= -q \quad \text{Vertical force equilibrium} \\ N_1 + N_2 &= 0 \quad \text{Horizontal force equilibrium} \\ M &= M_1 + M_2 - N_1 r \quad \text{Bending moment equilibrium} \\ V &= \frac{dM}{dx} \quad \text{Vertical shear force} \\ V_s &= K \cdot s = -\frac{dN_1}{dx} = \frac{dN_2}{dx} \quad \text{Longitudinal shear force flow} \end{aligned}$$

Differential equation for composite interaction:

$$w(x) = C_1 \frac{e^{\alpha x}}{\alpha^4} + C_2 \frac{e^{-\alpha x}}{\alpha^4} + C_3 x^3 + C_4 x^2 + C_5 x + C_6 + \frac{1}{24} \frac{qx^4}{EI_\infty}$$

A.1.1.5. Loads

In the parametric model, a uniform distributed load of 10 kN/m^2 is applied on the total bridge structure. Multiplying the load with the effective width leads to the following:

$$q = 1.75 \cdot 10 = 17.5 \text{ kN/m}$$

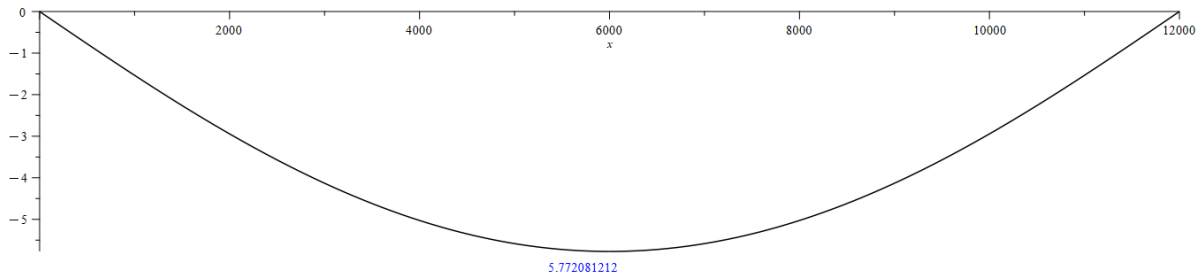


Figure A.3: Analytical deflection Concrete

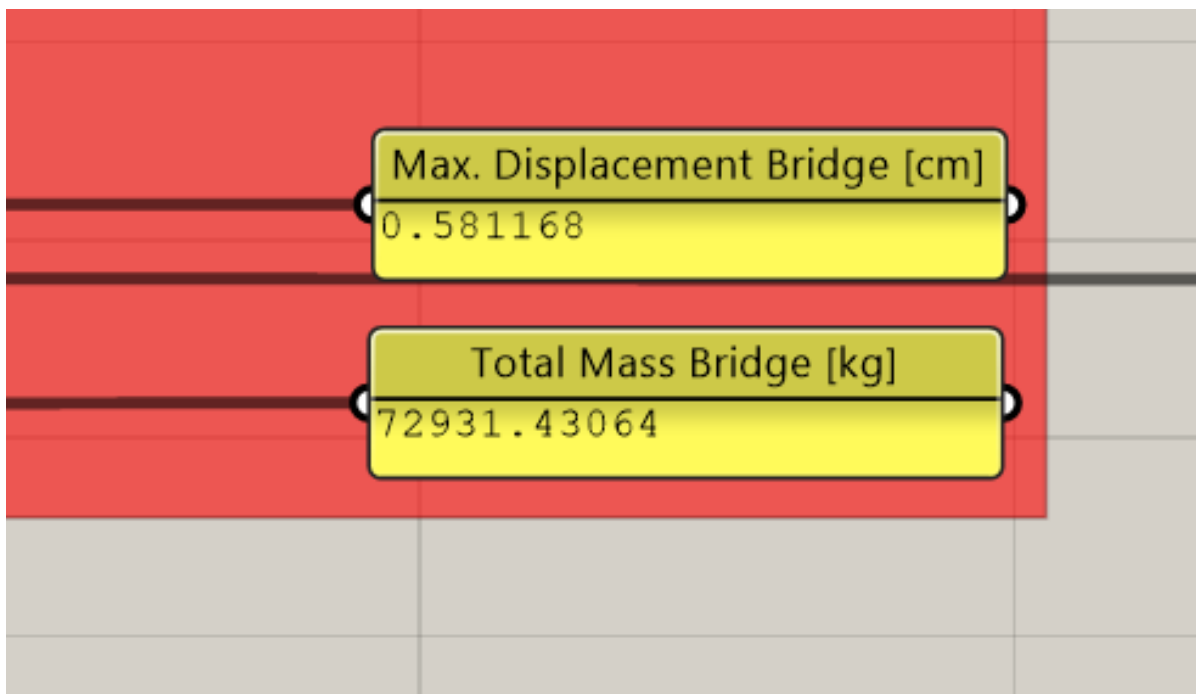


Figure A.4: Rhino deflection Concrete

Rhinoceros results in a deflection of 5.83 mm and the analytical hand calculations result in a deflection of 5.77 mm. This can verify that the results from Rhinoceros are correct.

A.2. Analytical approach variant 2

After the model has been analytically verified in Section A.1, in the following section, the results of variant 1 are approached analytically.

A.2.1. General data

$L = 12 \text{ m}$

Number of steel girder = 4

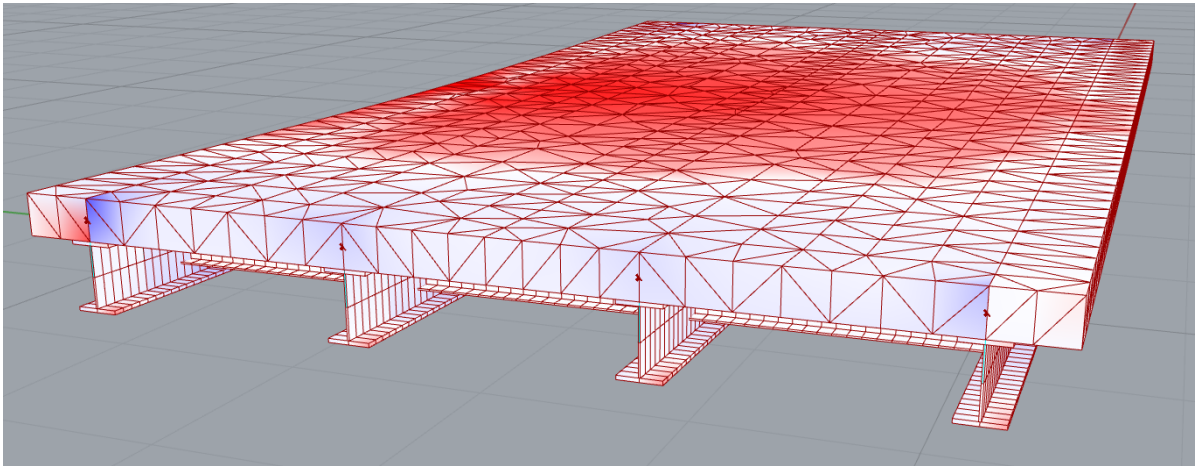


Figure A.5: Variant 2

A.2.1.1. Steel Girders

The four girders consist of HEB500 profiles and have the following dimensions:

$$h_a = 500 \text{ mm}$$

$$b_f = 300 \text{ mm}$$

$$t_f = 28 \text{ mm}$$

$$t_w = 14.5 \text{ mm}$$

$$A_a = 23864 \text{ mm}^2$$

$$E_a = 210000 \text{ N/mm}^2$$

$$I_a = 107176 \cdot 10^4 \text{ mm}^4$$

$$W_a = 4287 \cdot 10^3 \text{ mm}^3$$

$$\rho_a = 78.5 \text{ kN/m}^3$$

A.2.1.2. Concrete slab

On top of the girders is a concrete slab attached.

$$h_c = 300 \text{ mm}$$

$$b_{\text{eff},c} = 2000 \text{ mm}$$

$$f_{ck} = 30 \text{ N/mm}^2$$

$$E_c = 32800 \text{ N/mm}^2$$

$$I_c = \frac{b_{\text{eff},c} h_c^3}{12} = 4.5 \cdot 10^9 \text{ mm}^4$$

$$\rho_c = 25 \text{ kN/m}^3$$

A.2.1.3. Demountable connection

This variant will be executed with 2 Coupler SRR Connectors, which are placed with a center-to-center distance of 375 mm:

$$k_{sc} = 145.5 \text{ kN/mm}$$

$$b_s = 375 \text{ mm}$$

According table 3.9

Center-to-center distance connectors

A.2.1.4.Loads

LM1 (see Section 2.3.1.2) is the governing load model for variable loads and results in the following loads:

$$q = 18 \text{ kN/m}$$

$$F = 250 \text{ kN}$$

A.3. Deflection**A.3.1. Deflection Self Weight**

The self-weight of a single girder beam:

$$G_{\text{concrete}} = \rho_c * b_c * t_c = 15.0 \text{ kN/m} \quad \text{Self weight concrete}$$

$$G_{\text{steel}} = \rho_a * A_a = 1.87 \text{ kN/m} \quad \text{Self weight steel}$$

$$G_{\text{total}} = G_{\text{concrete}} + G_{\text{steel}} = 16.87 \text{ kN/m} \quad \text{Total self weight}$$

Due to the fact that after placing of the concrete slab, both materials are not connected to each other yet. The total self-weight has to be taken by the steel Girder beam.

$$w = \frac{5}{384} \cdot \frac{q_{SLS} \cdot l^4}{EI_a}$$

Where:

$$l = 12000 \text{ mm}$$

$$q_{SLS} = G_{\text{total}} = 16.87 \text{ kN/m}$$

$$EI_a = E_a \cdot I_a = 2.25 \cdot 10^{14} \text{ Nmm}^4$$

The total deflection of the girder beam due to the self-weight is:

$$w = \frac{5}{384} \cdot \frac{q_{SLS} \cdot l^4}{EI_a} = 20.2 \text{ mm}$$

A.3.2. Deflection Variable loads

As mentioned before, traffic load model 1 creates a uniform distributed load of 19.17 kN/m and a point load at midspan of 250 kN.

A.3.2.1.Bending stiffness

$$r_c = \frac{h_c}{2} = 150 \text{ mm}$$

$$r_s = \frac{h_a}{2} = 250 \text{ mm}$$

$$r = r_c + r_s = 400 \text{ mm}$$

$$EI_0 = E_a I_a + E_c I_c = 3.73 \cdot 10^{14} \text{ kNm}^2$$

$$EI_{\text{inf}} = EI_0 + \frac{E_a A_a \cdot E_c A_c}{E_a A_a + E_c A_c} \cdot r^2 = 1.01 \cdot 10^{15} \text{ kNm}$$

A.3.2.2. Differential equation

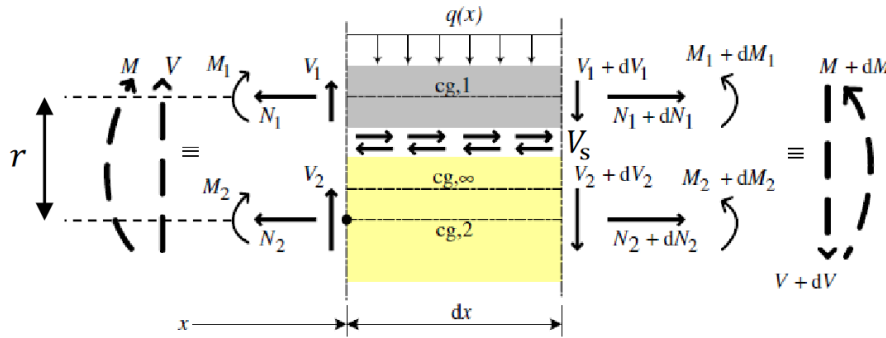


Figure A.6: Differential equation for composite interaction

$$\phi = -\frac{dw}{dx}$$

$$\kappa = \frac{d\phi}{dx}$$

$$M = \frac{EI_{ref}}{\alpha^2} \left(\frac{dw}{dx^4} - \alpha^2 \cdot \frac{dw}{dx^2} - \frac{q}{EI_0} \right)$$

$$V = \frac{dM}{dx}$$

$$N_1 = \frac{\kappa \cdot EI_0 - M}{r}$$

$$r = \frac{h_a}{2} + \frac{h_c}{2}$$

$$V_s = \frac{dN_1}{dx}$$

$$s = \left| \frac{V_1}{K} \right|$$

$$K = 2 \cdot \frac{k_{sc}}{b_s}$$

$$\frac{dV}{dx} = -q \quad \text{Vertical force equilibrium}$$

$$N_1 + N_2 = 0 \quad \text{Horizontal force equilibrium}$$

$$M = M_1 + M_2 - N_1 r \quad \text{Bending moment equilibrium}$$

$$V = \frac{dM}{dx} \quad \text{Vertical shear force}$$

$$V_s = K \cdot s = -\frac{dN_1}{dx} = \frac{dN_2}{dx} \quad \text{Longitudinal shear force flow}$$

Differential equation for composite interaction:

$$w(x) = C_1 \frac{e^{\alpha x}}{\alpha^4} + C_2 \frac{e^{-\alpha x}}{\alpha^4} + C_3 x^3 + C_4 x^2 + C_5 x + C_6 + \frac{1}{24} \frac{qx^4}{EI_\infty}$$

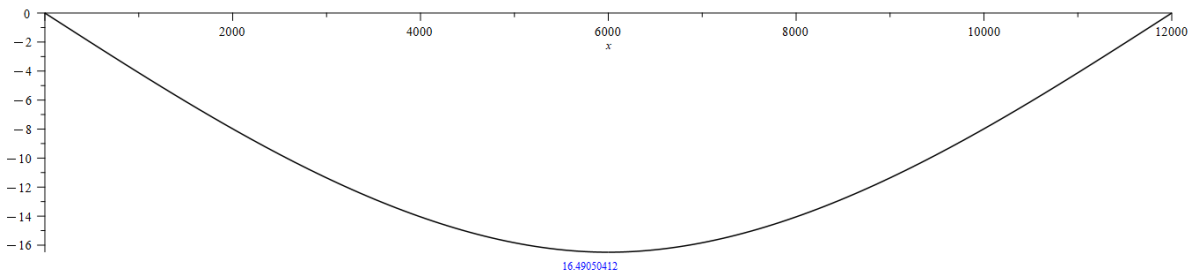


Figure A.7: Deflection SLS due to variable load

As can be seen in Figure A.7, the governing deflection is 16.5 mm.

A.3.3. Total deflection

The total deflection according the deflection due to the self weight and the deflection due to the variable loads is:

$$w_{total} = w_{sw} + w_{vl} = 36.7mm$$

Unity Check:

$$U.C. = \frac{36.7}{0.004 \cdot 12000} = 0.76$$

The Rhino model results in a deformation of 38.4 mm.

A.4. Verification Structure

A.4.1. Bending moment resistance

A.4.1.1. Self weight

The verification of the structure is when ULS is applied:

$$q_{ULS} = 1.2 \cdot G_{total} = 20.24 \text{ kN/m}$$

$$\sigma_a = \frac{M}{W_a}$$

$$M = \frac{1}{8} \cdot q_{ULS} \cdot l^2 = 364.4 \text{ kNm}$$

$$\sigma_{SW} = \frac{M}{W_a} = 85 \text{ N/mm}^2$$

A.4.1.2. Variable loads

The verification of the structure is when ULS is applied:

$$q_{ULS} = 1.5 \cdot Q = 27 \text{ kN/m}$$

$$F_{ULS} = 1.5 \cdot F = 375 \text{ kN}$$

These variable loads results in the following deflection:

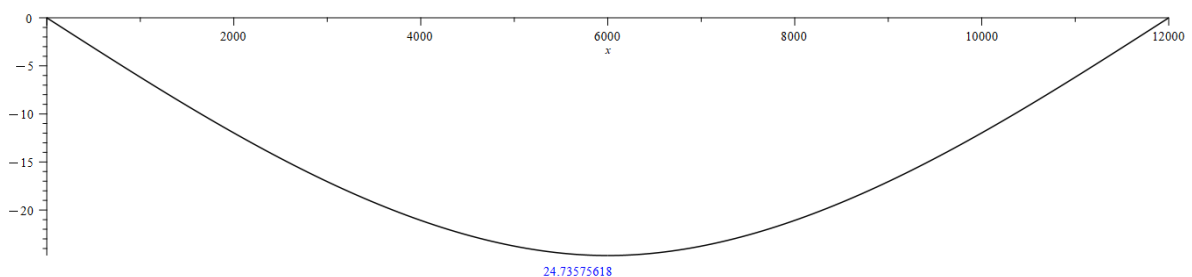


Figure A.8: Deflection ULS

As can be seen in Figure A.8 is the maximal deflection at ULS 24.7 mm.

A.4.1.2.1 Moment distribution

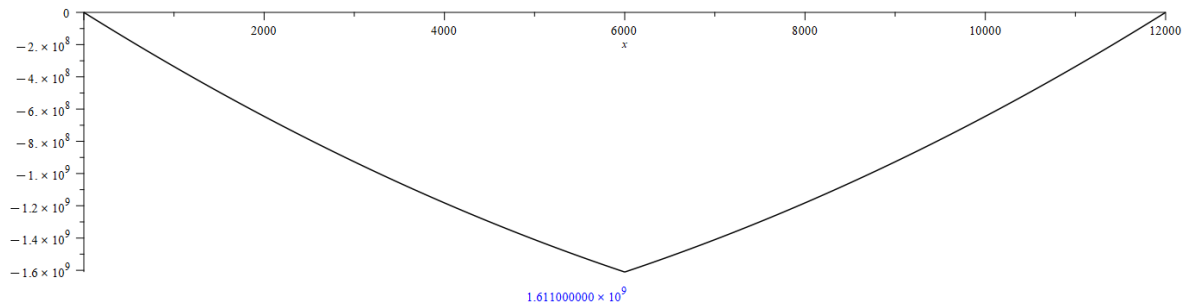


Figure A.9: Moment distribution ULS

Figure A.9 shows the moment distribution of the steel-concrete composite bridge. The governing moment force is 1611 kNm and acts at midspan

A.4.1.2.2 Normal force distribution

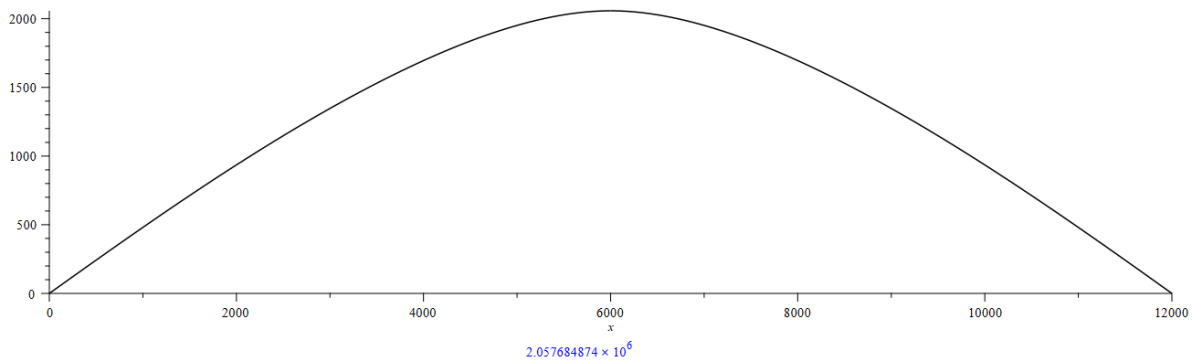


Figure A.10: Normal force ULS

Figure A.10 displays a maximal normal force of 2057.7 kN. The maximum stress in the concrete deck can be calculated according to the following formula:

$$\sigma_c = \frac{N}{e_{t0} \cdot b_{eff}}$$

$$A_{c,Tr} = \frac{b_{eff}}{n} \cdot h_c = \frac{2000}{32.8} * 300 = 93714 \text{ mm}^2 \quad \text{Transformed concrete area}$$

$$e_{t0} = \frac{A_{cTr} + 0.5 \cdot h_c + A_s \cdot (h_c + 0.5 \cdot h_a)}{A_{c,Tr} + A_s} = 231.2 \text{ mm} \quad \text{Height neutral axis from top of concrete}$$

$$\sigma_c = \frac{N}{e_{t0} \cdot b_{eff}} = 4.45 \text{ N/mm}^2$$

Unity Check:

$$U.C. = \frac{\sigma_c}{f_{cd}} = 0.28$$

Together with the maximal moment force displayed in Figure A.9, the governing bending stress can be calculated.

$$\sigma_s = \frac{M \cdot 0.5 h_a}{I_s} \frac{N_1}{A_s} = 197.2 \text{ N/mm}^2$$

A.4.1.3. Total Bending stress

The total bending stress in the steel girder beam is:

$$\sigma_{total} = \sigma_{sw} + \sigma_{vl} = 282.2 \text{ N/mm}^2$$

Unity Check:

$$U.C. = \frac{282.2}{355} = 0.80$$

The Rhino model results in maximum bending stress of 306.0 N/mm².

A.4.2. Slip deformation

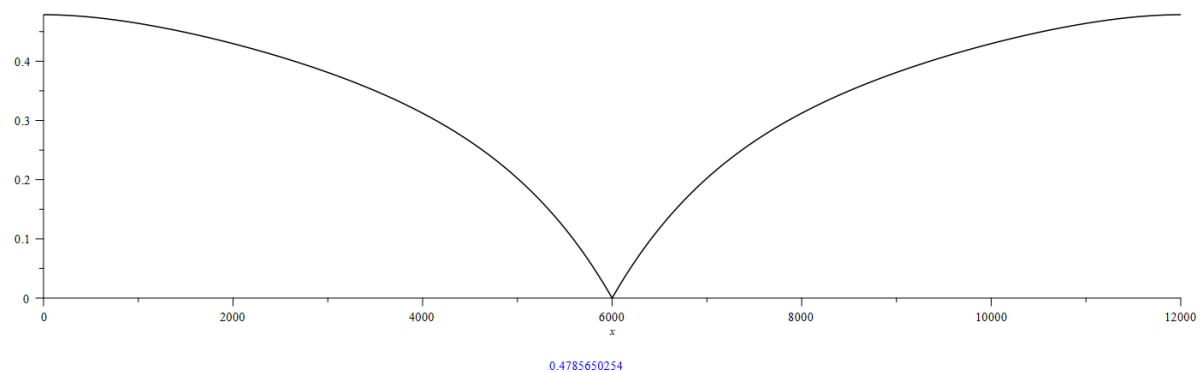


Figure A.11: Slip deformation

As shown in Figure A.11, the slip at the supports at L=0 and L=12m is 0.49 mm. Which is low enough to avoid plastic deformation.

A.5. Concrete Deck

The maximum reinforcement bar length is 12 meters.

A.5.1. Concrete cover

Whole section is according NEN-EN 1992-1-1 [52].

Because the deck is cyclically wet and dry and exposed to spray containing chlorides, the deck has the following environment exposure class.

Environment exposure class: = XD3

$$c_{nom} = c_{min} + \Delta c_{dev}$$

According to Table 4.3 of NEN-EN 1992-1-1 [52], the structural classification has to increase by 2 class due to Design Working Life of 100 years. However, because the bridge deck has a slab geometry and is ensured of special quality control during production, the construction class is reduced by 2 classes. As a result, the final structural classification is S4 and, in combination with XD3, this results in a $c_{min} = 45 \text{ mm}$.

According to NEN-En 1992-1-1 [52], the value $\Delta c_{dev} = 10$ mm. However, since this concrete deck is fabricated where fabrication is subjected to a quality assurance system, the allowance in design for deviation may be reduced: $\Delta c_{dev} = 5$ mm.

This results in the following concrete cover:

$$c_{nom} = 45 + 5 = 50 \text{ mm}$$

A.5.2. Main Reinforcement

The main reinforcement of the concrete deck is in the transverse direction. The secondary reinforcement is placed in the longitudinal direction of the span of the bridge.

A.5.2.1. Reinforcement Transverse direction

General information

$$h_c = 300 \text{ mm}$$

$$c = 50 \text{ mm}$$

$$f_{cd} = 435 \text{ N/mm}^2 \quad f_{ck} = 30 \text{ N/mm}^2$$

Governing moment forces

From Rhinoceros:

$$M_{y,sag} = 54.4 \text{ kNm/m}$$

$$M_{y,hog} = 55.3 \text{ kNm/m}$$

Reinforcement bottom bars

$$\varnothing_{bar} = 10 \text{ mm}$$

$$d_{bot} = h_c - c - \frac{\varnothing_{bar}}{2} = 239 \text{ mm} \quad \text{Effective depth}$$

$$A_{sl,bot} = \frac{M_{y,sag}}{0.9 \cdot f_{cd} \cdot d} = 518.4 \text{ mm}^2/\text{m}$$

$$A_{bar} = \frac{1}{4} \cdot \varnothing_{bar}^2 \cdot \pi = 78.5 \text{ mm}^2$$

$$ctc = \frac{A_{sl}}{A_{bar}} = 7.4 \quad \text{So, c.t.c distance of 125}$$

Reinforcement transverse direction bottom:

$$\varnothing 10 - 125 \text{ mm}$$

Reinforcement top bars

$$\varnothing_{bar} = 10 \text{ mm}$$

$$d_{top} = h_c - c - \frac{\varnothing_{bar}}{2} = 239 \text{ mm} \quad \text{Effective depth}$$

$$A_{sl,top} = \frac{M_{y,sag}}{0.9 \cdot f_{cd} \cdot d} = 591.0 \text{ mm}^2/\text{m}$$

$$A_{bar} = \frac{1}{4} \cdot \varnothing_{bar}^2 \cdot \pi = 78.5 \text{ mm}^2$$

$$ctc = \frac{A_{sl}}{A_{bar}} = 7.5 \quad \text{So, c.t.c distance of 125}$$

Reinforcement transverse direction top:

$$\varnothing 10 - 125 \text{ mm}$$

A.5.2.2. Reinforcement longitudinal direction

General information

Governing moment forces

From Rhinoceros:

$$M_{x,sag} = 156.5 \text{ kNm/m}$$

$$M_{x,hog} = 8.23 \text{ kNm/m}$$

Reinforcement bottom bars

$$\begin{aligned} \varnothing_{\text{bar}} &= 16 \text{ mm} \\ d_{\text{bot}} &= h_c - c - \varnothing - \frac{\varnothing_{\text{bar}}}{2} = 226 \text{ mm} \quad \text{Effective depth} \\ A_{\text{sl,bot}} &= \frac{M_{x,\text{sag}}}{0.9 \cdot f_{\text{cd}} \cdot d} = 1768.8 \text{ mm}^2/\text{m} \\ A_{\text{bar}} &= \frac{1}{4} \cdot \varnothing_{\text{bar}}^2 \cdot \pi = 201 \text{ mm}^2 \\ \text{ctc} &= \frac{A_{\text{sl}}}{A_{\text{bar}}} = 8.8 \quad \text{So, c.t.c. distance is 110 mm} \end{aligned}$$

Reinforcement longitudinal direction bottom:

$$\varnothing 16 - 110 \text{ mm}$$

Reinforcement top bars

$$\begin{aligned} \varnothing_{\text{bar}} &= 6 \text{ mm} \\ d_{\text{top}} &= h_c - c - \varnothing - \frac{\varnothing_{\text{bar}}}{2} = 231 \text{ mm} \quad \text{Effective depth} \\ A_{\text{sl,top}} &= \frac{M_{x,\text{sag}}}{0.9 \cdot f_{\text{cd}} \cdot d} = 91.0 \text{ mm}^2/\text{m} \\ A_{\text{bar}} &= \frac{1}{4} \cdot \varnothing_{\text{bar}}^2 \cdot \pi = 28.3 \text{ mm}^2 \\ \text{ctc} &= \frac{A_{\text{sl}}}{A_{\text{bar}}} = 3.2 \quad \text{So, c.t.c. distance is 250 mm} \end{aligned}$$

Reinforcement longitudinal direction top:

$$\varnothing 6 - 250 \text{ mm}$$

A.5.3. Shear reinforcement

$$\begin{aligned} V_{\text{Ed}} &= 175.2 \text{ kN} \\ v_{\text{Ed}} &= \frac{V_{\text{Ed}}}{b \cdot d} = 0.74 \\ k &= 1 + \sqrt{\frac{200}{d}} \leq 2.0 = 2.0 \\ v_{\text{min}} &= 0.035 \cdot k^{\frac{3}{2}} \cdot \sqrt{f_{\text{ck}}} = 0.51 \\ v_{\text{Ed}} &> v_{\text{min}} \quad \text{So, shear reinforcement is necessary} \end{aligned}$$

The center to center distance of stirrups $s = 110 \text{ mm}$ & $\epsilon = 45$ results in:

$$A_{\text{sw}} = \frac{V_{\text{Ed}} \cdot b \cdot s}{0.9 \cdot f_{\text{yd}} \cdot \cot \epsilon} = 208.6 \text{ mm}^2$$

$$\varnothing 6$$

$$A_{\text{bar}} = \frac{1}{4} \cdot \varnothing_{\text{bar}}^2 \cdot \pi = 28.3 \text{ mm}^2$$

$$\frac{1000}{125} \cdot A_{\text{bar}} = 226.4 \text{ mm}^2 > A_{\text{sw}} = 208 \text{ mm}^2$$

A.5.4. Crack width**A.5.4.1. Material properties**

Concrete strength class :C30/37

$$\text{Design value of concrete compressive strength : } f_{\text{cd}} = \frac{f_{\text{ck}}}{\gamma_c} = \frac{30}{1.5} = 20 \text{ N/mm}^2$$

$$\text{Mean axial tensile strength of concrete : } f_{\text{ctm}} = 2.90 \text{ N/mm}^2$$

$$\text{Modulus of elasticity of concrete (long term) : } E_{\text{cm}(\infty)} = 17000 \text{ N/mm}^2$$

$$\text{Diameter reinforcement: } \varnothing = 16 \text{ mm}$$

$$\text{effective depth: } d = 300 - 50 - \frac{10}{2} = 245 \text{ mm}$$

$$\text{Design yield strength of reinforcement : } f_{\text{yd}} = \frac{500}{1.15} = 435 \text{ N/mm}^2$$

$$\text{Modulus of elasticity of reinforcing steel : } E_s = 200000 \text{ N/mm}^2$$

$$\text{Ratio } \frac{E_s}{E_{\text{cm}}} = \alpha_e = 6.1$$

$$\text{Crack width limit : } w_{\text{max}} = 0.3 \text{ mm}$$

$$\text{Partial material factors : } \gamma_c = 1.5$$

$$\text{: } \gamma_s = 1.15$$

Governing bending moment in SLS (According from Rhino in ULS):

$$M_{\text{Eqp}} = 113.8 \text{ kNm}$$

Calculating of the height of the compressive zone in the SLS:

$$\frac{x}{d} = -\alpha_e \cdot \rho_l + \sqrt{(\alpha_e \cdot \rho_l)^2 + 2\alpha_e \cdot \rho_l}$$

Reinforcement ratio provided:

$$\rho_l = \frac{A_s}{b \cdot d} = \frac{1608}{1000 \cdot 192} = 0.84\%$$

$$\frac{x}{192} = -11.8 \cdot 0.0084 + \sqrt{(11.8 \cdot 0.0084)^2 + 2 \cdot 11.8 \cdot 0.0084} = 0.36$$

$$x = 68.4 \text{ mm}$$

Steel stress in SLS:

$$\sigma_s = \frac{M_{EqP}}{A_{s,prov} \left(d - \frac{1}{3}x\right)} = \frac{113.8 \cdot 10^6}{1608 \cdot \left(192 - \frac{1}{3} \cdot 68.4\right)} = 279 \text{ N/mm}^2$$

Verification of the type of crack pattern

Height of the tensile member

$$h_{c,eff} = 2.5(h - d) \leq \frac{h - x}{3}$$

$$h_{c,eff} = 2.5(h - d) = 2.5 \cdot (250 - 192) = 145 \text{ mm}$$

$$h_{c,eff} \leq \frac{h - x}{3} = \frac{250 - 68.4}{3} = 60.5 \text{ mm}$$

To be used: $h_{c,eff} = 60.5 \text{ mm}$.

Reinforcement ratio of the "hidden" tensile member:

$$\rho_{p,eff} = \frac{A_s}{h_{eff} \cdot b} = \frac{1608}{60.5 \cdot 1000} = 0.027$$

The cracking force of the "hidden" tensile member:

$$N_{cr} = A_{c,eff} f_{ctm} (1 + \alpha_e \rho_{p,eff})$$

$$N_r = 64.8 \cdot 1000 \cdot 2.9 \cdot (1 + 11.8 \cdot 0.027) = 230.4 \cdot 10^3 \text{ N}$$

Steel stress after cracking of the "hidden" tensile member:

$$\sigma_{sr} = \frac{N_r}{A_s} = \frac{230.4 \cdot 10^3}{1608} = 143.3 \text{ N/mm}^2$$

Calculation of the crack width

$$\varepsilon_{cr} = \varepsilon_{sm} - \varepsilon_{cm} = \frac{\sigma_s - k_t \frac{f_{ct,eff}}{\rho_{p,eff}} (1 + \alpha_e \rho_{p,eff})}{E_s} \geq 0.6 \frac{\sigma_s}{E_s}$$

$$\varepsilon_{cr} = 0.00094 > 0.00081$$

$$w_k = s_{r,max} \varepsilon_{cr}$$

$$\text{Maximum crack spacing: } s_{r,max} = k_3 c + k_1 k_2 k_4 \frac{\sigma_s}{\rho_{p,eff}}$$

where:

$$k_1 = 0.8$$

$$k_2 = 0.5$$

$$k_3 = 3.4$$

$$k_4 = 0.425$$

$$s_{r,\max} = 281.2$$
$$\text{Ratio } \frac{E_s}{E_{cm}} = \alpha_e = 6.1$$
$$w_k = 0.26 \text{ mm}$$

The maximum crack width has to be limited to 0.3 mm according to Eurocode 2 Table 7.1 [52].
Conclusion: The crack width requirement is met.

B

FRP properties

B.1. Material properties

Fibre reinforced polymer material is built up of multiple plies. Each ply consists of fibers and resin which is made in a certain composition. The first subsection [B.1.1](#) will describe the material properties of the fibres, after which the second subsection [B.2](#) will describe the material properties of the resin. The subsequent subsection will describe the structure of a Unidirectional (UD) ply, after which the laminate theory will be elaborated (Subsections [B.3.1](#) & [B.3.2](#)).

B.1.1. Fibre properties

In the construction world, E-glass and R-glass fibres are used. The most common type of glass is the E-glass fibres, that is why only these characteristics are displayed in table [B.1](#) [2]. To demonstrate the differences in properties between glass and carbon fibres, the table also shows the characteristics of High Strength (HS) carbon fibre. However, as mentioned before, carbon fibres are hardly used in Building engineering.

Table B.1: Characteristic E-glass and High strength carbon material properties [2]

	Material Characteristic	Symbol	E-glass	Carbon (HS)	Unit
Tension in fibre direction	Poisson ratio	ν_f	0.24	0.3	-
	Young's Modulus	E_{f1}	73100	238000	N/mm ²
	Strain limit	ε_{f1}	3.8	1.5	%
	Strength	f_{f1}	2750	3600	N/mm ²
Tension perpendicular fibre direction	Poisson's ratio	ν_f	0.24	0.02	-
	Young's modulus	E_{f2}	73100	15000	N/mm ²
	Strain limit	ε_{f2}	2.4	0.9	N/mm ²
	Strength	σ_{12}	1750	2140	N/mm ²
Compression in fibre direction	Strain limit	ε_1	2.4	0.9	%
	Strength	σ_{11}	1750	135	N/mm ²
Shear	Modulus	G_f	30000	50000	N/mm ²
	Strain limit	γ_{12}	5.6	2.4	%
	Strength	τ_{12}	1700	1200	N/mm ²
Density		ρ	2570	1790	kg/m ³
Thermal expansion		α	5.0	-0.4	10 ⁻⁶ /°C]

B.2. Resin properties

The most common resins are polyester, vinyl ester and epoxy [2]. Epoxy shrinks less but is the most expensive (see table B.2).

Table B.2: Characteristic resin material properties [2]

	Symbol	Polyester	Vinyl ester	Epoxy	Unit
Density	ρ_r	1200	1100	1250	kg/m ³
Poisson's ratio	ν_r	0.38	0.26	0.39	-
Glass transition temperature	T_g	approx. 60	approx. 100	approx. 80-150	°C
Tensile or compression strength	f_r	55	75	75	N/mm ²
Young's modulus in tension	E_r	3550	3350	3100	N/mm ²
Strain limit in tension or compression	ε_r	1.8	2.2	2.5	%
In-plane shear modulus	G_r	1350	1400	1500	N/mm ²
Shear strength	τ_r	approx. 50	approx. 65	approx. 80	N/mm ²
Shear strain limit	γ_r	3.8	3.7	5	%
Thermal expansion coefficient	α_r	50-120	50-75	45-65	10 ⁻⁶ /°C

B.3. Core material properties

As mentioned before, the bridge deck can be constructed with or without a foam core. Generally speaking, three types of cores form the central part of sandwich panels: solid cores, foam cores, and honeycomb cores. Manufacturing of the foam cores exceed that of the other structural sandwiches due

to their favourable strength and stiffness-to-weight ratios together with their relatively low price. Typically the rigid, closed-cell foam core materials are used for structural applications, with a core density of 32 to 300 kg/m³ [22]. A trade-off should select good core material between mechanical properties, weight and price.

Table B.3 describes the properties of the most used core materials; Polyvinylchloride (PVC), Polyurethane (PUR), and PMI.

Table B.3: Characteristic core material properties [2]

	Symbol	PUR	PVC	PMI	Unit				
Density	ρ_r	50	100	40	80	80	30	70	kg/m ³
Compression strength	f_r	0.3 - 0.5	0.6 - 1.0	0.5 - 0.8	1.2 - 2.0	approx. 0.9	approx. 0.5	approx. 1.5	N/mm ²
Elasticity modulus	E_r	6 - 10	approx. 30	20 - 30	60 - 90	approx. 50	approx. 30	approx. 90	N/mm ²
In-plane shear modulus	G_r	4 - 5	approx. 10	approx. 10	20 - 30	20	approx. 15	approx. 30	N/mm ²
Shear strength	τ_r	approx. 0.2	0.3 - 0.5	0.3 - 0.4	0.7 - 1.0	0.5 - 1.0	approx. 0.3	approx. 1.0	N/mm ²

B.3.1. UD-plyies

Below is an example of calculating the characteristic stiffness properties of an UD-ply with 40% E-glass and polyester resin. All different fibre volume percentages results in table B.4. The calculations below are done according [2].

$$E_1 = [E_r + (E_{f1} - E_r) * V_f] * \phi_{UD} \quad (\text{In plane E-modulus in material main direction 1})$$

Where:

$$E_r = 3550 \text{ N/mm}^2 \quad (\text{E-modulus of resin})$$

$$E_{f1} = 73100 \text{ N/mm}^2 \quad (\text{E-modulus of fibres in main fibre direction 1})$$

$$V_f = 40\% \quad (\text{Fibre volume percentage of ply})$$

$$\phi_{UD} = 0.97 \quad (\text{Emperical reduction factor})$$

Results in:

$$E_1 = 30400 \text{ N/mm}^2$$

$$E_2 = \left[\frac{1 + \xi_2 \eta_2 V_f}{1 - \eta_2 V_f} * E_r \right] * \phi_{UD} \quad (\text{In plane E-modulus in material main direction 2})$$

Where:

$$\eta_2 = \frac{\left(\frac{E_{f2}}{E_R} - 1 \right)}{\left(\frac{E_{f2}}{E_R} + \xi_2 \right)}$$

In which:

$$\xi_2 = 2$$

$$E_{f2} = 73100 \text{ N/mm}^2 \quad (\text{E-modulus of fibres in main fibre direction 2})$$

Gives:

$$\eta_2 = 0.87$$

Results in:

$$E_2 = 8900 \text{ N/mm}^2$$

$$G_{12} = \left[\frac{1 + \xi_G \eta_G V_f}{1 - \eta_G V_f} * G_r^{[1]} \right] * \phi_{UD} \quad (\text{In plane shear modulus})$$

Where:

$$\eta_G = \frac{\left(\frac{G_f}{G_R} - 1 \right)}{\left(\frac{G_f}{G_R} + \xi_G \right)}$$

$$\xi_G = 1$$

In which:

$$G_f = 30000 \text{ N/mm}^2$$

$$G_R = 1350 \text{ N/mm}^2 \quad (\text{Shear modulus of resin})$$

Gives:

$$\eta_G = 0.91$$

Results in:

$$G_{12} = 2700 \text{ N/mm}^2$$

$$v_{12} = v_r - (v_r - v_f) * V_f \quad (\text{in plane poisson ratio in material main directions 1 and 2})$$

In which:

$$v_r = 0.38 \quad (\text{In plane Poisson ratio resin})$$

$$v_f = 0.24 \quad (\text{In plane Poisson ratio of fibre})$$

Results in:

$$v_{12} = 0.30$$

The same calculations are done for the other fibre volume compositions with E-glass and polyester resin. Which results in the following characteristic stiffness properties:

Table B.4: Characteristic stiffness properties of UD-plyies with E-glass and polyester resin

V_f	E_1 [kN/mm ²]	E_2 [kN/mm ²]	G_{12} [kN/cm ²]	v_{12}
40%	30.4	8.9	2.7	0.30
50%	37.2	11.4	3.4	0.29
60%	43.9	14.6	4.3	0.27
70%	50.7	19.4	5.8	0.26

B.3.2. Laminate theory

After the characteristic stiffness properties are known, the material properties can be calculated. The FRP material is built up of several layers, whereby it is possible to determine which properties the material must meet. The facings that will be used will be made from a different laminate composition than the webs. This is due to the facings are mainly loaded in the longitudinal direction and the webs mainly with shear forces.

Facings

In sandwich panels, the common anisotropic GFRP laminate proportion for the facings is [55%/15%/15%/15%] in orientations [0°/+45°/90°/-45°]. The laminate properties of this material are calculated below according to [2].

The ABD matrices will be used to calculate the laminate properties. These matrices are obtained using the online classic laminate theory tool [9]. Figure x displayed the input for an 40% laminate and figure B.2 shows the corresponding ABD matrices.

(a) Input online tool, materials facings

Materials: Base Material

E_{11} : 30.4 GPa E_{22} : 8.9 GPa G_{12} : 2.7 GPa ν_{12} : 0.30

Layers: [Empty]

ABD Matrix: [Empty]

(b) Input online tool, layers facings

Materials: [Empty]

Layers:

- Layer 1: Thickness 5.5 mm, Direction 0°, Material Base Material
- Layer 2: Thickness 1.5 mm, Direction 45°, Material Base Material
- Layer 3: Thickness 1.5 mm, Direction 90°, Material Base Material
- Layer 4: Thickness 1.5 mm, Direction -45°, Material Base Material

ABD Matrix: [Empty]

Figure B.1: Input online tool

Materials		4.56	0.91	0.00	$\cdot 10^5 \text{ N/mm}$
	A	0.91	2.79	0.00	
		0.00	0.00	0.90	
Layers		0.00	0.00	0.00	
ABD Matrix	B	0.00	0.00	0.00	N
		0.00	0.00	0.00	
Loads		1.97	0.21	0.02	$\cdot 10^7 \text{ Nmm}$
	D	0.21	0.67	0.02	
		0.02	0.02	0.21	
Conditions					

Figure B.2: ABD matrices tool facings

Now the matrices are known, the properties of the facing laminates can be determined. The under-mentioned formulas are used according to [2]:

$$\mathbf{A}^{-1} = \mathbf{a} = \begin{bmatrix} a_{11} & a_{12} & a_{16} \\ a_{21} & a_{22} & a_{26} \\ a_{61} & a_{62} & a_{66} \end{bmatrix} \quad (\text{B.1})$$

$$E_{1,f} = \frac{1}{t_f} \cdot \left(A_{11,f} - \frac{A_{12,f}^2}{A_{22,f}} \right) = 21.3 \text{ GPa} \quad (\text{B.2})$$

$$E_{2,f} = \frac{1}{t_f} \cdot \left(A_{22,f} - \frac{A_{12,f}^2}{A_{11,f}} \right) = 13.0 \text{ GPa} \quad (\text{B.3})$$

$$G_{xy,f} = \frac{1}{t_f} \cdot A_{66,f} = 4.5 \text{ GPa} \quad (\text{B.4})$$

$$v_{12,f} = \frac{A_{12,f}}{A_{22,f}} = 0.33 \quad v_{21,f} = \frac{A_{12,f}}{A_{11,f}} = 0.20 \quad (\text{B.5})$$

To calculate the strength properties the 1.2% and 1.6% failure strain criteria for the axial and shear stresses, respectively according to [2] are used.

$$\sigma_{1,f} = E_{1,f} \cdot 1.2\% = 256 \text{ MPa} \quad (\text{B.6})$$

$$\sigma_{2,f} = E_{2,f} \cdot 1.2\% = 157 \text{ MPa} \quad (\text{B.7})$$

$$\tau_{12,f} = G_{12,f} \cdot 1.6\% = 72 \text{ MPa} \quad (\text{B.8})$$

The abovementioned calculations (equation B.1 to equation B.8) results in the following laminate properties:

Table B.5: Laminate properties facings

V_f	E_x [kN/mm ²]	E_y [kN/mm ²]	G_{xy} [kN/cm ²]	ν_{xy}	σ_1 [N/mm ²]	σ_2 [N/mm ²]	τ_{xy} [N/mm ²]	α_x [·10 ⁻⁶ K ⁻¹]	α_y [·10 ⁻⁶ K ⁻¹]	ρ [kg/m ³]
40%	21.3	13.0	4.5	0.33	256	157	72	15.4	25.2	1748
50%	26.3	16.3	5.6	0.32	315	196	89.6	12.7	20.5	1885
60%	31.3	20.0	6.9	0.31	376	240	110.4	10.9	17.0	2022
70%	37.1	25.0	8.7	0.30	445	300	139.2	9.3	13.9	2159

Webs

For the webs an quasi-isotropic laminate proportions [25%/25%/25%/25%] in orientations [0°/+45°/90°/-45°] is applied. In this way the material is equal in strength in both directions.

Below the matrices obtained with the online tool B.2 are displayed. According to the same equations as used for the facings (equation B.1 to equation B.8), the laminate properties (Table B.6) are calculated for the webs.

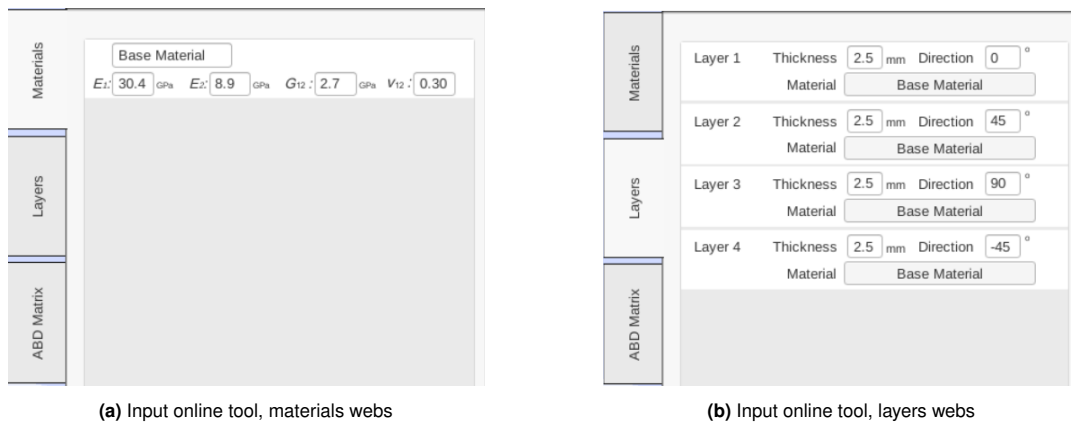


Figure B.3: Input online tool

Materials	A	3.43	1.15	0.00	$\cdot 10^5 \text{ N/mm}$
Layers		1.15	3.43	0.00	
		0.00	0.00	1.14	
ABD Matrix	B	0.00	0.00	0.00	N
Loads	D	1.57	0.31	0.10	$\cdot 10^7 \text{ Nmm}$
		0.31	0.88	0.10	
		0.10	0.10	0.31	
INS					

Figure B.4: ABD matrices tool webs

Table B.6: Laminate properties webs

V_f	E_x [kN/mm ²]	E_y [kN/mm ²]	G_{xy} [kN/cm ²]	ν_{xy}	σ_1 [N/mm ²]	σ_2 [N/mm ²]	τ_{xy} [N/mm ²]	α_x [$\cdot 10^{-6} \text{K}^{-1}$]	α_y [$\cdot 10^{-6} \text{K}^{-1}$]	ρ [kg/m ³]
40%	15.2	15.2	5.7	0.33	183	183	91.2	21.5	21.5	1748
50%	18.9	18.9	7.1	0.33	227	227	113.6	17.7	17.7	1885
60%	22.9	22.9	8.7	0.33	275	275	138.4	14.8	14.8	2022
70%	28.0	28.0	10.6	0.32	336	336	169.6	12.4	12.4	2159

B.4. Verification parametric model with FRP deck

The from Rhinoceros obtained results should be verified to be sure that there are no errors in the model. This is done by applying a simple uniform distributed load case on the superstructure and comparing the outcomes with hand calculations. This section describes an extensive elaboration of hand calculations.

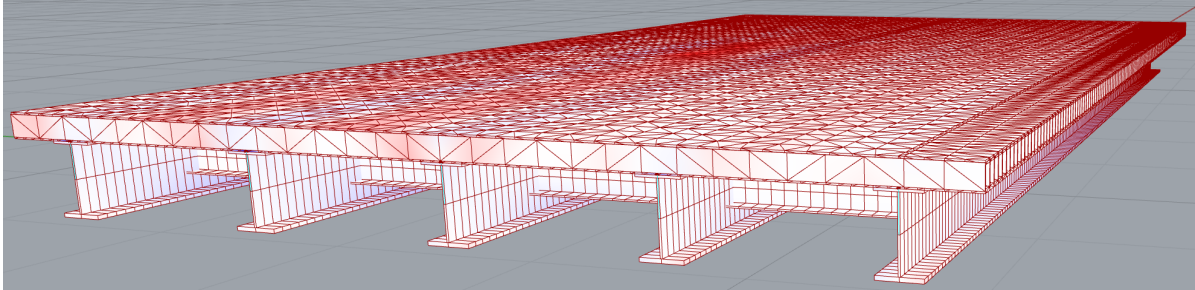


Figure B.5: FRP variant

B.4.1. FRP material properties

This chosen FRP deck has a fibre volume percentage of 50 % and has the following properties below (which have been explained earlier):

Flanges - Anisotropic FRP laminate

$$E_{1,f} = 26.3 \text{ GPa}$$

$$E_{2,f} = 16.3 \text{ GPa}$$

$$G_{12,f} = 5.6 \text{ GPa}$$

$$\nu_{12,f} = 0.32$$

$$\sigma_{1t,f} = 315 \text{ MPa} \quad \sigma_{2t,f} = 196 \text{ MPa} \quad \tau_{12f} := 89.6 \text{ MPa}$$

$$\sigma_{1c,f} = 315 \text{ MPa} \quad \sigma_{c2,f} = 196 \text{ MPa} \quad \tau_{ILSS,f} = 30 \text{ MPa}$$

Web-Quasi-isotropic FRP laminate

$$E_{1,w} = 18.9 \text{ GPa}$$

$$E_{2,w} = 18.9 \text{ GPa}$$

$$G_{12,w} = 7.1 \text{ GPa}$$

$$\nu_{12,w} = 0.33$$

$$\sigma_{1t,w} = 227 \text{ MPa} \quad \sigma_{2t,w} = 227 \text{ MPa} \quad \tau_{12,w} = 113.6 \text{ MPa}$$

$$\sigma_{1c,w} = 227 \text{ MPa} \quad \sigma_{c2,w} = 227 \text{ MPa} \quad \tau_{ILSS,w} = 30 \text{ MPa}$$

FRP Geometry

$$\text{Width of FRP panel: } L_{sp} = 1400 \text{ mm}$$

$$\text{Thickness of the facing: } t_f = 25 \text{ mm}$$

$$\text{Web/core height: } h_c = 135 \text{ mm}$$

$$\text{Height of sandwich panel: } h_d = 2 \cdot t_f + h_c = 185 \text{ mm}$$

$$\text{Web thickness: } t_w = 15 \text{ mm}$$

$$\text{Spacing of the webs: } s_w = 100 \text{ mm}$$

Steel beam properties

The steel profile is an HEB 550, with the following properties:

$$\begin{aligned}
 f_y &= 355 \text{ MPa} \\
 E_a &= 210 \text{ GPa} \\
 b_{f,a} &= 300 \text{ mm} \\
 t_{f,a} &= 29 \text{ mm} \\
 h_{w,a} &= 492 \text{ mm} \\
 t_{w,a} &= 15 \text{ mm}
 \end{aligned}$$

B.4.2. Effective bending stiffness

To verify Rhino's FEM results, the effective bending stiffness must be calculated. As can be seen in Figure B.6, the cross section is divided into three parts; top facing (Region 1), bottom facing (Region 2) and the steel girder (Region 3).

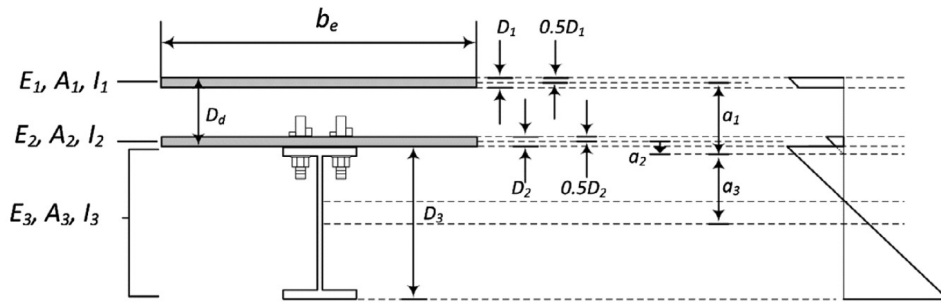


Figure B.6: Cross section of sandwich panel deck, with steel girder beam (Adapter from [70])

$$L_{beam} = 12000 \text{ mm}$$

Top facing - Region 1

$$b_1 = L_{sp} = 1.5 \text{ m}$$

$$h_1 = t_f = 25 \text{ mm}$$

Eurocode 4 part 1 concrete-steel girders is used to get an initial approximation of the effective width:

Distance between outstand shear connectors $b_0 = 200 \text{ mm}$

Effective width of the FRP flange on each side of the web: $b_{e1} = \frac{L_{beam}}{8}$

$b_{eff} = b_0 + 2 \cdot b_{e1} = 3200 \text{ mm}$

Effective width: $b_{1,eff} = \min(b_{eff}, L_{span}) = 1400 \text{ mm}$

$E_1 = E_{2,f} = 16.3 \text{ GPa}$

$A_1 = b_{1,eff} \cdot h_1 = 3.5 \times 10^4 \text{ mm}^2$

$I_1 = \frac{b_{1,eff} \cdot h_1^3}{12} = 1.823 \times 10^6 \text{ mm}^4$

In-plane shear stiffness of the FRP deck is taken from Gürter (2004) as the shear stiffness of a DuraSpan deck

$$G_{xz,Duraspan} = 3.3 \text{ MPa}$$

$$k_1 = G_{xz,Duraspan} \cdot \frac{1}{h_d} = 17.8 \times 10^{-3} \text{ N/mm}^3$$

$$K_1 = b_{1,eff} \cdot k_1 = 24.97$$

$$\gamma_1 = \frac{1}{1 + \frac{\pi^2 \cdot E_1 \cdot A_1}{K_1 \cdot L_{beam}^2}} = 0.39$$

Bottom facing - Region 2

$$b_{2,\text{eff}} = 1400 \text{ mm}$$

$$h_2 = t_f = 25 \text{ mm}$$

$$E_2 = E_{2,f} = 16.3 \text{ GPa}$$

$$A_2 = b_{2,\text{eff}} \cdot h_2 = 3.5 \times 10^4 \text{ mm}^2$$

$$I_2 = \frac{b_{2,\text{eff}} \cdot h_2^3}{12} = 1.823 \times 10^6 \text{ mm}^4$$

$$\gamma_2 = 1$$

Steel section-Region 3

$$h_3 = h_{w,a} + 2 \cdot t_{f,a} = 550 \text{ mm}$$

$$E_2 = E_n = 210 \text{ GPa}$$

$$A_2 = A_n = 25406 \text{ mm}^2$$

$$I_3 = I_a = 1.37 \times 10^9 \text{ mm}^4$$

$$k_3 = 73 \text{ kN/mm} \quad - \text{ initial connection stiffness (according to [11])} \quad K_3 = 2 \cdot k_3 = 146 \text{ kN/mm}^2 \text{ bolts per row}$$

$$c_w = 200 \text{ mm} \quad \text{stud spacing}$$

$$\gamma_3 = \frac{1}{1 + \frac{\pi^2 \cdot E_3 \cdot A_3 \cdot c_w}{K_3 \cdot L_{\text{beam}}^2}} = 0.66$$

Distance from the region's geometrical centroid to its neutral axis:

$$a_2 := \frac{\gamma_1 \cdot E_1 \cdot A_1 \cdot (h_1 + h_2) - \gamma_3 \cdot E_3 \cdot A_3 \cdot (h_2 + h_3)}{2 \cdot (\gamma_1 \cdot E_1 \cdot A_1 + \gamma_2 \cdot E_2 \cdot A_2 + \gamma_3 \cdot E_3 \cdot A_3)} = -0.234 \text{ m}$$

$$a_1 := - \left(h_d - \frac{h_1}{2} - \frac{h_2}{2} - a_2 \right) = -0.394 \text{ m}$$

$$a_3 := \frac{h_2}{2} + \frac{h_3}{2} + a_2 = 0.54 \text{ m}$$

Effective bending stiffness:

$$E_{\text{eff}} = (E_1 \cdot I_1 + \gamma_1 \cdot E_1 \cdot A_1 \cdot a_1^2) + (E_2 \cdot I_2 + \gamma_2 \cdot E_2 \cdot A_2 \cdot a_2^2) + (E_3 \cdot I_3 + \gamma_3 \cdot E_3 \cdot A_3 \cdot a_3^2)$$

$$E_{\text{eff}} = 3.630 \times 10^{14} \text{ Nmm}^2$$

Steel beam bending stiffness:

$$E_a \cdot I_a = 2.87 \times 10^{14} \text{ Nmm}^2$$

B.4.3. Displacements

Loads

In the parametric model, a uniform distributed load of 10 kN/m^2 is applied on the total bridge structure. Multiplying the load with the effective width leads to the following:

$$q = 1.4 \cdot 10 = 14 \text{ kN/m}$$

Analytically

$$G_a = \frac{E_a}{2 \cdot (1 + 0.3)} = 8.077 \times 10^4 \text{ MPa}$$

$$A_{a,w} = t_{w,a} \cdot h_{w,a} = 8250 \text{ mm}^2$$

$$k_a = \frac{A_{a,w}}{A_a} = 0.32$$

$$w = \frac{1}{48} \cdot \frac{F \cdot L_{\text{beam}}^3}{E_{\text{eff}}} + \frac{1}{8} \cdot \frac{q \cdot b_1 \cdot L_{\text{beam}}^2}{k_a \cdot G_a \cdot A_a} = 13.6 \text{ mm}$$

Rhinoceros FEA

The parametric model gives the following deflection:

$$w, \text{ rhino} = 15.3 \text{ mm}$$

$$\frac{15.3}{13.6} = 1.125$$

As can be seen, the Rhinoceros results obtained correspond to the hand calculations.

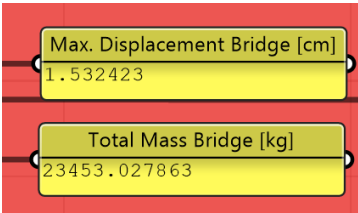


Figure B.7: Displacement Rhino

C

LCA

Table C.1: Environmental impact values

Shadow prize (Euro) per kg	Abiotic depletion	Global warming	Ozone layer depletion	Human toxicity	Fresh water aquatic ecotox.	Marine aquatic ecotoxicity	Terrestrial ecotoxicity	Photochemical oxidation	Acidification	Eutrophication	€/Unit
Unit	kg Sb eq	kg CO2 eq	kg CFC-11 eq	kg 1,4-DB eq	kg 1,4-DB eq	kg 1,4-DB eq	kg 1,4-DB eq	kg C2H4	kg SO2 eq	kg PO4 eq	
Materials	bioitic depletion	Global warming	Ozone layer depletion	Human toxicity	Fresh water aquatic ecotox.	Marine aquatic ecotoxicity	Terrestrial ecotoxicity	Photochemical oxidation	Acidification	Eutrophication	
Steel	1.54E-02	1.79E+00	7.17E-08	3.81E+00	1.49E+00	1.32E+03	3.18E-02	9.27E-04	7.38E-03	1.34E-03	0.25
Concrete (CEM III)	2.71E-04	9.33E-02	4.42E-09	1.03E-02	2.17E-03	3.57E+00	1.81E-04	7.40E-06	2.22E-04	3.94E-05	0.0073
Concrete (CEM III)	2.76E-04	9.45E-02	4.50E-09	1.04E-02	2.20E-03	3.63E+00	1.83E-04	7.53E-06	2.26E-04	4.02E-05	0.0074
Concrete (CEM III)	2.79E-04	9.55E-02	4.58E-09	1.05E-02	2.19E-03	3.64E+00	1.85E-04	7.62E-06	2.29E-04	4.06E-05	0.0075
Concrete (CEM I-CEM III)	3.05E-04	1.07E-01	4.88E-09	1.12E-02	2.28E-03	3.80E+00	2.01E-04	8.24E-06	2.44E-04	4.29E-05	0.0082
Concrete (CEM I-CEM III)	3.31E-04	1.18E-01	5.19E-09	1.19E-02	2.37E-03	3.96E+00	2.17E-04	8.86E-06	2.60E-04	4.53E-05	0.0090
Steel Reinforcement	1.54E-02	1.79E+00	7.17E-08	3.81E+00	1.49E+00	1.32E+03	3.18E-02	9.27E-04	7.38E-03	1.34E-03	0.66
FRP epoxy	3.59E-02	4.42E+00	4.53E-07	7.41E+00	2.60E+00	4.06E+02	4.09E-02	8.93E-04	2.51E-02	2.84E-03	1.14
FRP polyester	3.43E-02	4.65E+00	7.54E-07	8.71E+00	2.80E-01	5.36E+02	4.04E-02	1.10E-03	1.92E-02	2.15E-03	1.18
FRP vinylster	3.19E-02	3.44E+00	2.06E-07	5.73E+00	1.56E-01	2.83E+02	2.54E-02	7.68E-04	1.32E-02	1.02E-03	0.79
PVC Core	2.26E-02	1.96E+00	2.95E-09	5.93E-01	1.53E-01	4.09E+01	6.84E-03	3.13E-04	5.35E-03	7.60E-04	0.19
Lorry >26 kg/tkm	1.01E-03	1.36E-01	2.26E-08	2.84E-02	6.31E-03	1.13E-03	3.02E-04	2.62E-05	7.18E-04	1.53E-04	0.014

Variant 1		
Concrete slab		
Width	7	m
Length	12	m
Height	0.25	m
Volume	21	m ³
Weight Concrete	2500	kg/m ³
Total Weight concrete	52500	kg
Reinforcement	152	kg/m ³
Total Weight reinforcement	3192	kg
Steel		
Girders	HEB500	
Number of Girders	4	
Weight	191	kg/m
Cross beams	HEA240	
Number of cross beams	3	
Length	6	m
Weight	61.5	kg/m
Weight Girders	9168	kg
Weight Cross beams	1107	kg
Total Weight Steel	10275	kg
Total Weight	65967	kg
Shadow Costs		
Material	€/kg	Total
Concrete	0.007	367.50
Steel reinforcement	0.66	2106.72
Steel beams	0.25	2568.75
Total		5042.97
	€/tkm	km
Transport	0.015	200
Results		
Material		€ 5,042.97
Transport		€ 197.90

Variant 2		
Concrete slab		
Width	7	m
Length	12	m
Height	0.3	m
Volume	25.2	m ³
Weight Concrete	2500	kg/m ³
Total Weight concrete	63000	kg
Reinforcement	97.66	kg/m ³
Total Weight reinforcement	2461.032	kg
Steel		
Girders	HEB500	
Number of Girders	4	
Weight	191	kg/m
Cross beams	HEA240	
Number of cross beams	3	
Length	6	m
Weight	61.5	kg/m
Weight Girders	9168	kg
Weight Cross beams	1107	kg
Total Weight Steel	10275	kg
Total Weight	75736.032	kg
Shadow Costs		
Material	€/kg	Total
Concrete	0.007	441.00
Steel reinforcement	0.66	1624.28
Steel beams	0.25	2568.75
Total		4634.03
	€/tkm	km
Transport	0.015	200
Results		
Material		€ 4,634.03
Transport		€ 227.21

Variant 3		
Concrete slab		
Width	7	m
Length	12	m
Height	0.3	m
Volume	25.2	m ³
Weight Concrete		
	2500	kg/m ³
Total Weight concrete	63000	kg
Reinforcement		
	97.66	kg/m ³
Total Weight reinforcement	2461.032	kg
Steel		
Girders	HEB450	
Number of Girders	4	
Weight	174	kg/m
Cross beams		
	HEA240	
Number of cross beams	3	
Length	6	m
Weight	61.5	kg/m
Weight Girders		
	8352	kg
Weight Cross beams		
	1107	kg
Total Weight Steel		
	9459	kg
Total Weight		
	74920.032	kg
Shadow Costs		
Material	€/kg	Total
Concrete	0.007	441.00
Steel reinforcement	0.66	1624.28
Steel beams	0.25	2364.75
		4430.03
	€/tkm	km
Transport	0.015	200
Results		
Material	€ 4,430.03	
Transport	€ 224.76	

Variant 4		
FRP deck		
Fibre Volume	50	%
Total Weight	10471.55	kg
Weight Fibres	7138.432	kg
Weight Resin	3333.12	kg
Core	604.25	kg
Steel		
Girders	HEB550	
Number of Girders	5	
Weight	203	kg/m
Length	12	m
Cross beams		
	HEA240	
Number of cross beams	12	
Length	1.5	m
Weight	61.5	kg/m
Weight Girders		
	12180	kg
Weight Cross beams		
	1107	kg
Total Weight Steel		
	13287	kg
Total Weight		
	24362.802	kg
Shadow Costs		
Material	€/kg	Total
FRP polyester	1.18	12356.43
Core	0.19	114.81
Steel beams	0.25	3321.75
Total		15792.99
	€/tkm	km
Transport	0.015	200
Results		
Material	€ 15,792.99	
Transport	€ 73.09	

D

Costs

Variant 1		4x HEB500, 25 cm dik dek			
Materiaal		4			
		HVH	EEH	PPE	Prijs
Prefab platen exc. Wapening		C45/55 3x7x0,25 m			
Betonmortel					
	Leverantie	5.25	m3	€ 119.00	€ 624.75
	Arbeid	1.575	mu	€ 45.00	€ 70.88
	Materieel/pomp	0.525	uur	€ 90.00	€ 47.25
Kist					
	Afschrijving	26	m2	€ 7.00	€ 182.00
	Arbeid	0.6006	mu	€ 45.00	€ 27.03
	Materieel/kraan	0.2	kru	€ 60.00	€ 12.00
					€ 963.90
					€ 183.60 /m3
Wapening prefab platen		Aanname		152 kg/m ³	
	Leverantie	798	kg	€ 1.00	€ 798.00
	Arbeid	798	kg	€ 1.00	€ 798.00
	Materieel	0.798	kru	€ 60.00	€ 47.88
	Bouten	63	st	€ 4.25	€ 267.75
					€ 1,911.63
					€ 2.40 /kg
Stalen dek					
Stalen balken hoofdligger		HEB550 12m			
	Leverantie	2292	kg	€ 1.50	€ 3,438.00
	Samenstellen	2292	kg	€ 0.25	€ 573.00
	Coating	25.44	m2	€ 40.00	€ 1,017.60
					€ 5,028.60
					€ 2.19 /kg
Stalen balken dwarsbalk		HEA240		2 m	
	Leverantie Balk	123	kg	€ 1.25	€ 153.75
	Leverantie kopplaat	20	kg	€ 1.75	€ 35.00
	Samenstellen	143	kg	€ 1.00	€ 143.00
	Coating	2.74	m2	€ 50.00	€ 137.00
					€ 468.75
					€ 312.50 /m
Bouten		M20 injectie bout			
	Leverantie	1	st	€ 3.75	€ 3.75
					€ 3.75
					€ 3.75 /st
Montage		HVH	EEH	PPE	Prijs
Prefab platen					
	Kraan	4	kru	€ 120.00	€ 480.00
	Arbeid	12	mu	€ 55.00	€ 660.00
	Materiaal	84	m2	€ 2.50	€ 210.00
	Transport	2	p	€ 400.00	€ 800.00
					€ 2,150.00
					€ 25.60 /m2
Staalwerk		Dek 12x7 m			
	Kraan	9.5	kru	€ 92.50	€ 878.75
	Arbeid	38	mu	€ 55.00	€ 2,090.00
	Materiaal	84	m2	€ 5.00	€ 420.00
	Transport	1	p	€ 400.00	€ 400.00
					€ 3,788.75
					€ 45.10 /m2
Bouten					
	Arbeid	0.2	mu	€ 55.00	€ 11.00
	Materiaal	1	st	€ 1.00	€ 1.00
					€ 12.00
					€ 12.00 /st

Variant 2		4x HEB500, 30 cm dik dek				
Materiaal		4				
	HVH	EEH	PPE	Prijs		
Prefab platen exc. Wapening		C30/37 3x7x0,30 m				
Betonmortel						
	Leverantie	6.3	m3	€ 100.00	€ 630.00	
	Arbeid	1.89	mu	€ 45.00	€ 85.05	
	Materieel/pomp	0.63	uur	€ 90.00	€ 56.70	
Kist						
	Afschrijving	27	m2	€ 7.00	€ 189.00	
	Arbeid	0.6237	mu	€ 45.00	€ 28.07	
	Materieel/kraan	0.207692	kru	€ 60.00	€ 12.46	
					€ 1,001.28	€ 158.93 /m3
Wapening prefab platen		Aanname 97.66 kg/m ³				
	Leverantie	615.258	kg	€ 1.00	€ 615.26	
	Arbeid	615.258	kg	€ 1.00	€ 615.26	
	Materieel	0.615258	kru	€ 60.00	€ 36.92	
	Bouten	63	st	€ 4.25	€ 267.75	
					€ 1,535.18	€ 2.50 /kg
Stalen dek		Stalen balken hoofdligger HEB500 12m				
	Leverantie	2292	kg	€ 1.50	€ 3,438.00	
	Samenstellen	2292	kg	€ 0.25	€ 573.00	
	Coating	25.44	m2	€ 40.00	€ 1,017.60	
					€ 5,028.60	€ 2.19 /kg
Stalen balken dwarsbalk		HEA240 2 m				
	Leverantie Balk	123	kg	€ 1.25	€ 153.75	
	Leverantie kopplaat	20	kg	€ 1.75	€ 35.00	
	Samenstellen	143	kg	€ 1.00	€ 143.00	
	Coating	2.74	m2	€ 50.00	€ 137.00	
					€ 468.75	€ 312.50 /m
Bouten		M20 injectie bout				
	Leverantie	1	st	€ 3.75	€ 3.75	
					€ 3.75	€ 3.75 /st
Montage		HVH	EEH	PPE	Prijs	
Prefab platen						
	Kraan	4	kru	€ 135.00	€ 540.00	
	Arbeid	12	mu	€ 55.00	€ 660.00	
	Materiaal	84	m2	€ 2.50	€ 210.00	
	Transport	2	p	€ 400.00	€ 800.00	
					€ 2,210.00	€ 26.31 /m2
Staalwerk		Dek 12x7 m				
	Kraan	9.5	kru	€ 92.50	€ 878.75	
	Arbeid	38	mu	€ 55.00	€ 2,090.00	
	Materiaal	84	m2	€ 5.00	€ 420.00	
	Transport	1	p	€ 400.00	€ 400.00	
					€ 3,788.75	€ 45.10 /m2
Bouten						
	Arbeid	0.2	mu	€ 55.00	€ 11.00	
	Materiaal	1	st	€ 1.00	€ 1.00	
					€ 12.00	€ 12.00 /st

Variant 3		4x HEB450, 30 cm dik dek			
Materiaal		4			
	HVH	EEH	PPE	Prijs	
Prefab platen exc. Wapening		C30/37 3x7x0,25 m			
Betonmortel					
Leverantie	6.3	m3	€ 100.00	€ 630.00	
Arbeid	1.89	mu	€ 45.00	€ 85.05	
Materieel/pomp	0.63	uur	€ 90.00	€ 56.70	
Kist					
Afschrijving	27	m2	€ 7.00	€ 189.00	
Arbeid	0.6237	mu	€ 45.00	€ 28.07	
Materieel/kraan	0.207692	kru	€ 60.00	€ 12.46	
				€ 1,001.28	€ 158.93 /m3
Wapening prefab platen		Aanname		97.66 kg/m ³	
Leverantie	615.258	kg	€ 1.00	€ 615.26	
Arbeid	615.258	kg	€ 1.00	€ 615.26	
Materieel	0.615258	kru	€ 60.00	€ 36.92	
Bouten	69	st	€ 4.25	€ 293.25	
				€ 1,560.68	€ 2.54 /kg
Stalen dek					
Stalen balken hoofdlijger		HEB450 12m			
Leverantie	2088	kg	€ 1.50	€ 3,132.00	
Samenstellen	2088	kg	€ 0.25	€ 522.00	
Coating	24.36	m2	€ 40.00	€ 974.40	
				€ 4,628.40	€ 2.22 /kg
Stalen balken dwarsbalk		HEA240		2 m	
Leverantie Balk	123	kg	€ 1.25	€ 153.75	
Leverantie kopplaat	20	kg	€ 1.75	€ 35.00	
Samenstellen	143	kg	€ 1.00	€ 143.00	
Coating	2.74	m2	€ 50.00	€ 137.00	
				€ 468.75	€ 312.50 /m
Bouten		M20 injectie bout			
Leverantie	1	st	€ 3.75	€ 3.75	
				€ 3.75	€ 3.75 /st
Montage		HVH	EEH	PPE	Prijs
Prefab platen					
Kraan	4	kru	€ 135.00	€ 540.00	
Arbeid	12	mu	€ 55.00	€ 660.00	
Materiaal	84	m2	€ 2.50	€ 210.00	
Transport	2	p	€ 400.00	€ 800.00	
				€ 2,210.00	€ 26.31 /m2
Staalwerk		Dek 12x7 m			
Kraan	9.5	kru	€ 92.50	€ 878.75	
Arbeid	38	mu	€ 55.00	€ 2,090.00	
Materiaal	84	m2	€ 5.00	€ 420.00	
Transport	1	p	€ 400.00	€ 400.00	
				€ 3,788.75	€ 45.10 /m2
Bouten					
Arbeid	0.2	mu	€ 55.00	€ 11.00	
Materiaal	1	st	€ 1.00	€ 1.00	
				€ 12.00	€ 12.00 /st

Variant 4		5x HEB550, 160 mm dik dek FRP			
Materiaal		5			
FRP Deck					
Dimensions					
Height deck	185	mm			
Facings	25	mm			
Webs	10	mm			
CTC Webs	100	mm			
Fiber Volume	50	%			
Material FRP Deck					
	Glass Fibers	7138.432	kg	€ 3.00	€ 21,415.30
	Resin	3333.12	kg	€ 3.70	€ 12,332.54
	Foam	604.25	kg	€ 11.40	€ 6,888.45
	Bouten	750	st	€ 6.25	€ 4,687.50
		11075.8		€ 45,323.79	€ 4.09 /kg
Stalen dek					
Stalen bakken hoofdligger		HEB550 12m			
	Leverantie	2436	kg	€ 1.50	€ 3,654.00
	Samenstellen	2436	kg	€ 0.25	€ 609.00
	Coating	26.64	m2	€ 40.00	€ 1,065.60
				€ 5,328.60	€ 2.19 /kg
Stalen bakken dwarsbalk		HEA240 1.5 m			
	Leverantie Balk	92.25	kg	€ 1.25	€ 115.31
	Leverantie kopplaat	20	kg	€ 1.75	€ 35.00
	Samenstellen	112.25	kg	€ 1.00	€ 112.25
	Coating	2.055	m2	€ 50.00	€ 102.75
				€ 365.31	€ 243.54 /m
Bouten		M20 bout			
	Leverantie	1	st	€ 2.50	€ 2.50
				€ 2.50	€ 2.50 /st
Montage					
		HVH	EEH	PPE	Prijs
FRP Deck					
	Kraan	4	kru	€ 92.50	€ 370.00
	Arbeid	6	mu	€ 55.00	€ 330.00
	Materiaal	84	m2	€ 2.50	€ 210.00
	Transport	1	p	€ 400.00	€ 400.00
				€ 1,310.00	€ 15.60 /m2
Staalwerk		Dek 12x7 m			
	Kraan	11	kru	€ 92.50	€ 1,017.50
	Arbeid	44	mu	€ 55.00	€ 2,420.00
	Materiaal	84	m2	€ 5.00	€ 420.00
	Transport	1	p	€ 400.00	€ 400.00
				€ 4,257.50	€ 50.68 /m2
Bouten					
	Arbeid	0.13333	mu	€ 55.00	€ 7.33
	Materiaal	1	st	€ 1.00	€ 1.00
				€ 8.33	€ 8.33 /st

Variant 1		4x HEB500	Dek Concrete	25 cm	Liggers	50 cm	
Omschrijving		HVH	EEH	PPE	Prijs		
Staalwerk	Leverantie hoofd liggers	4	st	€ 5,029	€ 20,114		
	Leverantie dwarsligger	9	st	€ 469	€ 4,219		
	Leveratie bouten	250	st	€ 4	€ 938		
	Montage stalen liggers	84	m2	€ 45	€ 3,789		
	Montage bouten	250	st	€ 12	€ 3,000		
Betonwerk	Wapening prefab platen	3192	kg	€ 2	€ 7,647		
	Beton prefab platen	21	m3	€ 184	€ 3,856		
	Montage prefab platen	84	m2	€ 26	€ 2,150		
				Materiaal	€ 35,835	€ 427 /m2	
				Montage	€ 9,876	€ 18,159	
				Totaal	€ 45,712		

Variant 2		4x HEB500	Dek Concrete	30 cm	Liggers	50 cm	
Omschrijving		HVH	EEH	PPE	Prijs		
Beton prefab platen							
Staalwerk	Leverantie stalen liggers	4	st	€ 5,029	€ 20,114		
	Leverantie dwarsligger	9	st	€ 469	€ 4,219		
	Montage stalen liggers	84	m2	€ 45	€ 3,789		
	Leveratie bouten	250	st	€ 4	€ 938		
	Montage bouten	250	st	€ 12	€ 3,000		
Betonwerk	Wapening prefab platen	2461.032	kg	€ 2	€ 6,141		
	Beton prefab platen	25.2	m3	€ 159	€ 4,005		
	Montage prefab platen	84	m2	€ 26	€ 2,210		
				Materiaal	€ 34,479	€ 410 /m2	
				Montage	€ 9,936	€ 18,279	
				Totaal	€ 44,415		

Variant 3		4x HEB450	Dek Concrete	30 cm	Liggers	45 cm	
Omschrijving		HVH	EEH	PPE	Prijs		
Staalwerk	Leverantie stalen liggers		4 st	€ 4,628	€ 18,514		
	Leverantie dwarsligger		9 st	€ 469	€ 4,219		
	Leveratie bouten		275 st	€ 4	€ 1,031		
	Montage stalen liggers		84 m2	€ 45	€ 3,789		
	Montage bouten		275 st	€ 12	€ 3,300		
Betonwerk	Wapening prefab platen	2461.032	kg	€ 3	€ 6,243		
	Beton prefab platen	25.2	m3	€ 159	€ 4,005		
	Montage prefab platen	84	m2	€ 26	€ 2,210		
				Materiaal	€ 32,980	€ 393 /m2	
				Montage	€ 10,330	€ 18,907	
				Totaal	€ 43,310		

Variant 4		5x HEB550	Dek FRP	185 mm	Liggers	55 cm	
Omschrijving		HVH	EEH	PPE	Prijs		
Staalwerk	Leverantie stalen liggers		5 st	€ 5,329	€ 26,643		
	Leverantie dwarsligger		12 st	€ 365	€ 4,384		
	Leveratie bouten		750 st	€ 3	€ 1,875		
	Montage stalen liggers		84 m2	€ 51	€ 4,258		
	Montage bouten		750 st	€ 8	€ 6,250		
FRP Deck	Kosten deck	11075.80	kg	€ 4	€ 45,324		
	Montage sandwich panel deck	84	m2	€ 16	€ 1,310		
				Materiaal	€ 76,351	€ 908.94 /m2	
				Montage	€ 13,692	€ 24,197	
				Totaal	€ 90,043		

E

Trade-Off Matrix analysis

E.1. Structural analysis

Table E.1: Structural analysis results for variants

Variant	Mass [kg]	Costs [€]	LCA [€]	Deflection SLS [mm]	Construction height [m]	Number of connectors	max. Stress beams ULS [N/mm ²]
1	65.967	209.143	7.022	21.7	0.75	250	327
2	75.736	208.926	6.906	17.9	0.8	250	306
3	74.920	213.473	6.678	20.9	0.75	275	343
4	24.393	307.816	16.524	43.6	0.76	800	306

E.2. Trade-off matrix

E.2.1. Explanation of scoring

Table E.2: Score TOM on effective strategy: construction height

Construction height	[m]	15
V1	0.75	+
V2	0.8	0
V3	0.75	+
V4	0.735	++

Table E.3: Score TOM on effective strategy: deflection SLS

Deflection SLS	[mm]	5
V1	21.7	+
V2	17.9	++
V3	20.9	+
V4	43.6	0

Table E.4: Score TOM on shadow costs

Shadow costs	[€]	20
V1	7.022	+
V2	6.906	+
V3	6.678	++
V4	16.524	--

Table E.5: Score TOM on demountability strategy: number of connections

Number of connections		15
V1	250	++
V2	250	++
V3	275	+
V4	750	--

Table E.6: Score TOM on demountability strategy: Complexity

Complexity		10
V1		-
V2		-
V3		-
V4		+

Table E.7: Score TOM on transportable strategy: weight

Weight	Mass	10
V1	65.967	-
V2	75.736	--
V3	74.920	--
V4	24.393	++

Table E.8: Score TOM on costs

Costs	[€]	20
V1	209.143	++
V2	208.926	++
V3	213.473	+
V4	307.816	--